NTNU

Norwegian University of
Science and Technology

Strength assessment of transversal T-beam webs in cruise ships

Mikhail Pudovkin

Maritime Engineering
Submission date: July 2017
Supervisor: Bernt Johan Leira, IMT
Co-supervisor: Jani Romanoff, Aalto University
Ari Niemelä, Meyer Turku Shipyard Oy
Aleksi Laakso, Meyer Turku Shipyard Oy

Norwegian University of Science and Technology
Department of Marine Technology

Abstract

Shipyards are increasing production efficiency. The main means to achieve higher efficiency are reducing the number of structural parts and increasing manufacturing automation. Potential target for the improvements would be design of transversal T-beams webs.

This thesis presents strength assessment method for evaluation transversal T-beam webs in cruise ships. The method is based on nonlinear finite element method. Generic loading is applied to T-beams to evaluate capacity using buckling, yielding and ultimate limit state criteria. The main realistic loadings were presented: global still water and wave loads, local deck pressure and block lifting. Realistic loading is compared against strength obtained by generic load.

The method is applied to a two case studies. Case study one compares the effect of the tripping brackets. It is discovered that strength is not increased significantly in case of 0; 1 and 2 tripping brackets. However, the presence of the tripping brackets significantly increase post buckling capacity of the T-beams. Case study two shows the cumulative production load from transportation, welding, blocks balancing, block lifting etc. The magnitude of production loads is found to be significantly higher than combined contribution from global and local loads.

Keywords Ship structural design, buckling, strength assessment, web plate, T-beam, Finite Element Method

Acknowledgement

This thesis was written for the Department of Applied Mechanics of Aalto University and Department of Marine Technology of Norwegian University of Science and Technology. Research was carried out in Meyer Turku shipyard. Financial support provided by Meyer Werft is greatly appreciated.

The author would also like to thank supervisors of the thesis Professors Jani Romanoff, Professor Bernt Johan Leira and instructors, Aleksi Laakso, Ari Niemelä for their guidance and comments during the process. Additional thanks to hull basic design department for provided help and scientific literature for the thesis.

Finally, I would like to thank my family and friends for their support during my studies.

Turku, 25 July 2017

Mikhail Pudovkin

Contents

Abstract i
Acknowledgement ii
List of figures v
List of tables vii
Nomenclature viii
Abbreviations ix
1 Introduction 1
1.1 Background 1
1.2 Buckling and effect of web openings 3
1.3 Methods for strength assessment 6
1.4 Research objective 7
1.5 Limitations 7
2 Strength assessment of T-beam under generic loading 8
2.1 Generic loading 9
2.2 Nonlinear response by FEM 13
2.3 Stress (yielding) criteria 18
2.4 Buckling and post buckling criteria 21
3 Realistic loads of a cruise ship 22
3.1 Global still water and wave loads 22
3.2 Global response 25
3.3 Local deck pressure 29
3.4 Local response 30
3.5 Production loads: Block lifting 32
3.6 Block lifting response 34
4 Case study 1: Effect of the tripping brackets 36
4.1 Studied geometry 36
4.2 Strength results 38
4.3 Post buckling 43
5 Case study 2: Magnitude of production loads 45
5.1 Cumulative production load 45
5.2 Studied geometry 46
5.3 Results 47
6 Design safety against realistic loads 50
7 Discussion 52
8 Conclusion 53
References 54

Appendix A: Sensitivity analysis for nonlinear finite element analysis ..... A - 1
Appendix B: Moment diagrams ..... B - 1
Appendix C: Post buckling behavior and ULS ..... C - 1
Appendix D: Increase in capacity with wider flange ..... D - 1

List of figures

Figure 1.1: Typical configuration of T-beam web frame. 1
Figure 1.2: Failure buckling modes by (Paik & Kim, 2002). 3
Figure 1.3: Stress ratio ψ from 1 (uniform compression) with an increment of 0.5 to -1 (pure bending) (Sweedan & El-Sawy, 2011). 3
Figure 1.4: Buckling locations in web with rounded and square openings (Serror, et al., 2016). 4
Figure 1.5: Buckling deformation in (a) tripping of T-bar stiffener without attached plate, (b) plate tripping and plate buckling with rigid web, (c) simultaneously buckling of web and plate in tripping of T-bar (Rahbar-Ranji, 2012). 5
Figure 1.6: Critical Euler stress for case (c). (Rahbar-Ranji, 2012). 5
Figure 1.7: Load, geometry and boundary conditions of the web plate with cut-outs (DNV GL AS, 2016). 6
Figure 2.1: Simple outline of the steps for strength assessment. 8
Figure 2.2: Ultimate capacity curve. 8
Figure 2.3: Generic loading. 9
Figure 2.4: Boundary conditions. 9
Figure 2.5: Study of axial compression and tension and opposite sign rotation in hogging and sagging. 10
Figure 2.6: Study of clockwise and counterclockwise rotation. 10
Figure 2.7: Study of axial compression and tension and rotation clockwise and counterclockwise. 11
Figure 2.8: Loading vectors for non-linear modeling (load type 1, Quadrant III). 11
Figure 2.9: Enforced displacement and corresponding rotation for ULS analysis. 12
Figure 2.10: Shell element (CQUAD4) geometry system (NX Nastran 10, 2014). 13
Figure 2.11: Shell element (CTRIA3) geometry system (NX Nastran 10, 2014). 13
Figure 2.12: Defect of 4-moded element defect (Mathisen, 2016). 14
Figure 2.13: Offset beam element (CBEAM) geometry system (NX Nastran 10, 2014). 14
Figure 2.14: Elements in FE-models. 14
Figure 2.15: Material curve steel S355. 15
Figure 2.16: Newton-Raphson method (NAFEMS, 1992). 15
Figure 2.17: Typical instabilities of a system under load control - snap-through (a), displacement control - snap-back (b) and bifurcation behavior (c) (Leahu-Aluas & Abed-Meraim, 2011). 16
Figure 2.18: Schematic comparison between Newton-Rapson with displacement control and arc-length methods. 16
Figure 2.19: Failure criterion surface (von Mises - red curve, Tresca - black curve) (Abrate, 2008). 18
Figure 2.20: Yielding in the web plate: relevant and irrelevant cases. 19
Figure 2.21: First yielding in the flange. 20
Figure 2.22: Buckling concept of load-deflection curve (Brubak, 2016). 21
Figure 2.23: Post buckling point at maximum loading. 21
Figure 3.1: Location of investigated T-beam webs. 22
Figure 3.2: Typical bending moment distribution. 22
Figure 3.3: Global FE-model. 22
Figure 3.4: Global deformation in hogging and sagging conditions. 23
Figure 3.5: Section deformations in hogging (left) and sagging (right). 23
Figure 3.6: Racking induced deformation. 23
Figure 3.7: Section deformations in racking. 24
Figure 3.8: Node's locations. 25

Figure 3.9: Global loads plotted in load type 1 figure. 27
Figure 3.10: Global loads plotted in load type 2 figure. 27
Figure 3.11: Global loads plotted in load type 3 figure. 28
Figure 3.12: Intermediate bulkhead in the middle of the web frame. 28
Figure 3.13: Modeling of the deck pressure (green arrows pointed down). 29
Figure 3.14: Boundary condition for a deck pressure load (bottom fixed). 29
Figure 3.15: Local loads plotted in load type 1 figure. 30
Figure 3.16: Local loads plotted in load type 2 figure. 31
Figure 3.17: Local loads plotted in load type 3 figure. 31
Figure 3.18: Case A: boundary conditions for block lifting load. 32
Figure 3.19: Case A: undeformed (left) and deformed (right) block lifting model in FEM. ... 33
Figure 3.20 Case B: undeformed (left) and deformed (right) block lifting model in FEM. 33
Figure 3.21: Block lifting plotted in load type 1 figure. 34
Figure 3.22: Block lifting plotted in load type 2 figure. 34
Figure 3.23: Block lifting plotted in load type 3 figure. 35
Figure 4.1: Dimensions of the web configuration without tripping brackets. 36
Figure 4.2: FE model of T-beam web without tripping brackets. 36
Figure 4.3: Dimensions of web configuration with 2 tripping brackets (left), tripping bracket dimensions (right). 36
Figure 4.4: FE model of a T-beam web with 2 tripping brackets (red). 37
Figure 4.5: Dimensions of the web configuration with 1 tripping bracket (left), tripping bracket dimensions (right). 37
Figure 4.6: FE model of a T-beam web with 1 tripping bracket (red). 37
Figure 4.7: First yield in linear and nonlinear analysis plotted in load type 1 figure. 38
Figure 4.8: First yield in linear and nonlinear analysis plotted in load type 2 figure. 39
Figure 4.9: First yield in linear and nonlinear analysis plotted in load type 3 figure. 39
Figure 4.10: ULS, first yielding in web and flange plotted in load type 1 figure. 41
Figure 4.11: ULS, first yielding in web and flange plotted in load type 2 figure. 42
Figure 4.12: ULS, first yielding in web and flange plotted in load type 3 figure. 42
Figure 4.13: Ultimate limit state and post buckling parameter. 43
Figure 5.1: Production phase: defects in T-beams. 45
Figure 5.2: Dimensions of the web configuration with 2 tripping brackets (left), tripping bracket dimensions (right). 46
Figure 5.3: FE model of a T-beam web with 2 tripping brackets (red) and flange 150x10 mm (yellow). 46
Figure 5.4: Capacity of T-beams with flanges 100x10 and 150x10 plotted in load type 1 figure. 47
Figure 5.5: Capacity of T-beams with flanges 100x10 and 150x10 plotted in load type 2 figure. 48
Figure 5.6: Capacity of T-beams with flanges 100x10 and 150x10 plotted in load type 3 figure. 48
Figure 6.1: Realistic load and load-carrying capacity plotted in load type 1 figure. 50
Figure 6.2: Realistic load and load-carrying capacity plotted in load type 2 figure. 51
Figure 6.3: Realistic load and load-carrying capacity plotted in load type 3 figure. 51
Figure 7.1: Tripping mode of a stiffener with tee profile (Fujikubo & Yao, 1999). 52

List of tables

Table 2.1: Numerical data for load vectors. 12
Table 2.2: Enforced displacement and rotation based on web dimensions. 12
Table 3.1: Algorithm for global response. 26
Table 3.2: Block main dimensions. 32
Table 4.1: Average difference in ultimate limit state and post buckling between cases with 0, 1 and 2 TB. 43
Table 4.2: Overall average difference in ULS and post buckling capacity between cases with 0, 1 and 2 TB. 44
Table 5.1: Average difference in ultimate limit state and post buckling capacities in case of wider flange 150x10 mm. 49
Table 5.2: Overall average difference in ULS and post buckling capacity between the cases with flanges 100x10 mm and 150x10mm. 49

Nomenclature

E	Young's Modulus
K_{T0}^{n}	Tangential stiffness matrix
$R_x, R_y R_z$	Rotations along axis
$T_x, T_y T_z$	Translations along axis
x, y, z	Coordinate
f^n	Applied load
r_1^n	Residual forces
h	Height
ν	Poisson's ratio
σ	Normal stress
τ	Shear stress
ψ	Stress ratio
δd_0^n	Iterative displacement

Abbreviations

BC	Boundary Conditions
CFM	Closed Form Method
DEG	Degrees
DNV	Det Norske Veritas
DOF	Degree of freedom
FEA	Finite Element Analysis
FEM	Finite Element Method
GL	Germanischer Lloyd
GT	Gross tonnage
HP	Holland Profile
IACS	International Association of Classification Societies
ISSCI	International Ship structures Congress
NAFEMS	Association of the Engineering Modelling, Analysis and Simulation Community
RAD	Radians
RBE2	Rigid body element, type 2
TAN	Tangent
TB	Tripping Bracket
ULS	Ultimate limit state

1 Introduction

1.1 Background

Production efficiency is a cornerstone that defines shipyard's success in shipbuilding process (Hellgren, et al., 2017; Pires, et al., 2009) . Due to that, Meyer Turku Shipyard has been constantly making investments in production line facilities. According to the press release from August 26, 2016, 75 million of euros were provided for upgrading the old facilities and increasing the overall productivity and quality level (Meyer Turku Media, 2016).

One effective way to enhance the production efficiency is to increase manufacturing automation. By replacing the most of the manual work with automated technology, shipyards are aiming to improve the speed, quality and cost of the production (The MediTelegraph , 2016).

Another aspect to improve the production efficiency is to decrease the number of structural connections. Every steel member requires welding in assembly processes. The welding workload can be significantly reduced by decreasing the number of parts in production process (Hellgren, et al., 2017).

The T-beam web is a load carrying structure welded to a steel deck plate. The structure is commonly used part of the ship's hull and superstructure. Automated production of T-beams can significantly increase the production efficiency at the shipyard. Traditionally (Rockey, 1957), vertical stiffeners also known as tripping brackets have been required when web plates have a great height to plate thickness ratio. Typical configuration of a web in cruise ship superstructure, Figure 1.1, includes several openings and a couple of tripping brackets.

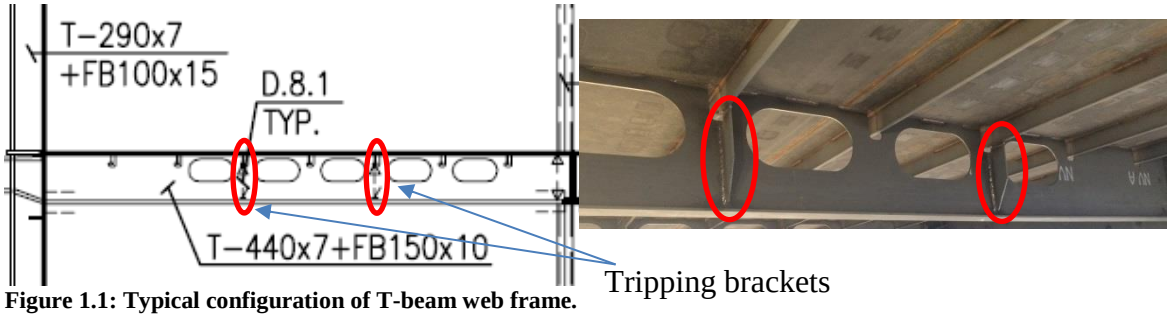

Figure 1.1: Typical configuration of T-beam web frame.

Tripping Brackets (TBs) are commonly used in transversally oriented beams. The presence of the TB ensures correct buckling hierarchy. The failure sequence starts with unstiffened deck, next deck's stiffeners, and then the whole T-beam. Such hierarchy ensures that there is still load carrying capacity left when one of the members has failed (Shama, 2013).

The superstructure of the cruise ship may accommodate over 3000 transverse web-frames, i.e. over 6000 tripping brackets. The transverse webs usually do not experience heavy loading conditions on cruise ships; however tripping brackets are still used for strengthening and preventing torsional buckling.

Automated production of T-beams is complicated from the technological viewpoint. The plate sides should remain flat to be able to pass through vertical rollers. All additional protrusions except of the flange are welded manually after passing T-beam robotic welding. The process increases the manual work, cost and performance time. In order to introduce fully automated T-beam welded system, it is beneficial to minimize the number of reinforcing stiffeners / tripping brackets.

In order to improve current design of transversal T-beams, it is required to understand the background physics of the problem, reasoning for plate strengthening and critical failure modes of the structure. Additionally, external loads acting on the T-beams should be studied.

1.2 Buckling and effect of web openings

One demanding issue in strength assessment of a T-beam web is defining its buckling capacity. Many studies have been trying to address the buckling problem. Over the years, analytical, numerical and experimental approaches were developed for panels under the compressive loads (Guedes Soares & Soreide, 1983; Guedes Soares & Gordo, 1997; Paik & Kim, 2002). Paik and Kim suggested five most typical failure buckling modes depending on the collapse pattern that are presented in Figure 1.2: (1) overall collapse after overall buckling of the plating and stiffeners as a unit, (2) plate-induced failure by yielding at the corners of plating between stiffeners, (3) plate-induced failure by yielding of stiffeners attached with plating at mid-span, (4) stiffener induced failure by local buckling of stiffener web, and (5) stiffener-induced failure by lateral-torsional buckling (i.e. tripping) of stiffeners.

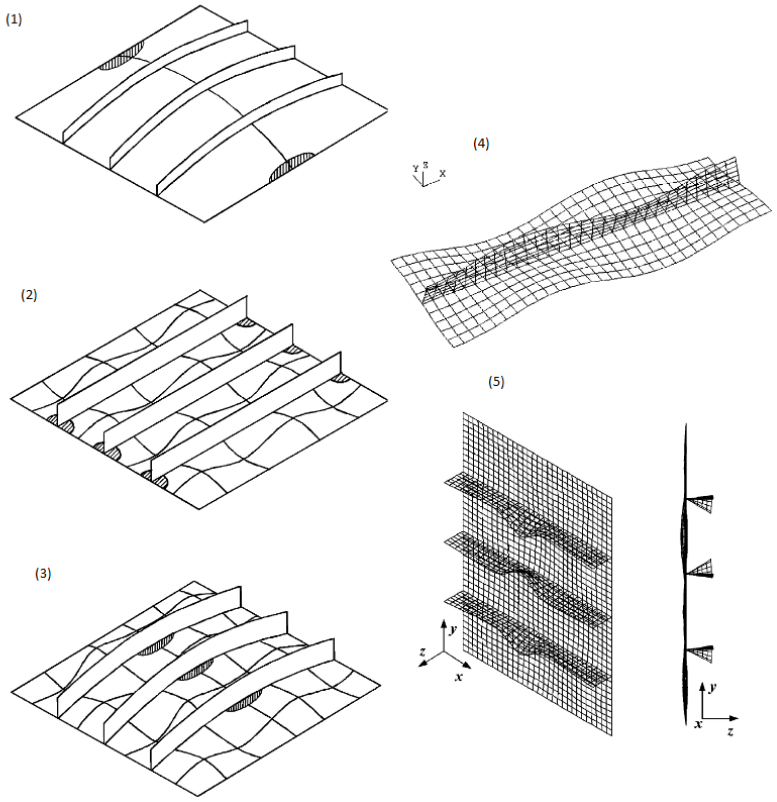

Figure 1.2: Failure buckling modes by (Paik & Kim, 2002).

The buckling of investigated T-beam webs is complicated due to the presence of the web openings and tripping brackets. Recently, numerical and experimental approaches have been developed to understand behavior of the perforated and solid plates under various loading and boundary conditions, Figure 1.3. The developed solution is presented in terms of design formulas, design charts and closed-form expressions (Serror, et al., 2016).

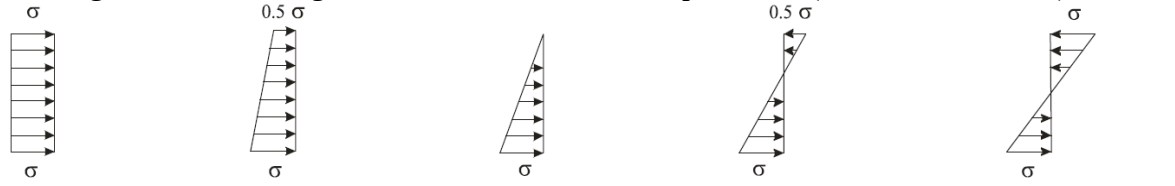

Figure 1.3: Stress ratio ψ from 1 (uniform compression) with an increment of 0.5 to -1 (pure bending) (Sweedan & El-Sawy, 2011).

Moen and Schafer developed a closed-form formulation that considers effect from individual and set of openings on critical elastic buckling stress for rectangular plates. They found that the presence of opening can either improve or decrease elastic buckling capacity of the plate depending on opening geometry and spacing (Moen & Schafer, 2009). Evidently, good design of the openings changes buckling half-wave not to match natural half-wavelength, leading to increase of critical buckling stress (Timoshenko & Gere, 1961).

Plate under the compression-tension stresses with bigger openings was found to be more stable compared to smaller openings configuration. However, the relative stability of a plate should be considered pertaining to fact that ultimate capacity of the plate is reducing simultaneously due to reduction of solid material in a cross-section. (Sweedan & El-Sawy, 2011)

Numerous researches were dedicated to investigation of elastic buckling (Shanmugam, et al., 1999; Komur & Sönmez, 2008) and inelastic buckling (El-Sawy, et al., 2004; Chow & Narayanan, 1984) of perforated plates. Typical buckling locations can be categorized in Figure 1.4 as following: (1) plate between the openings, (2) longitudinal strips that are stretched below and above the openings and (3) plate-opening border, and (Serror, et al., 2016).

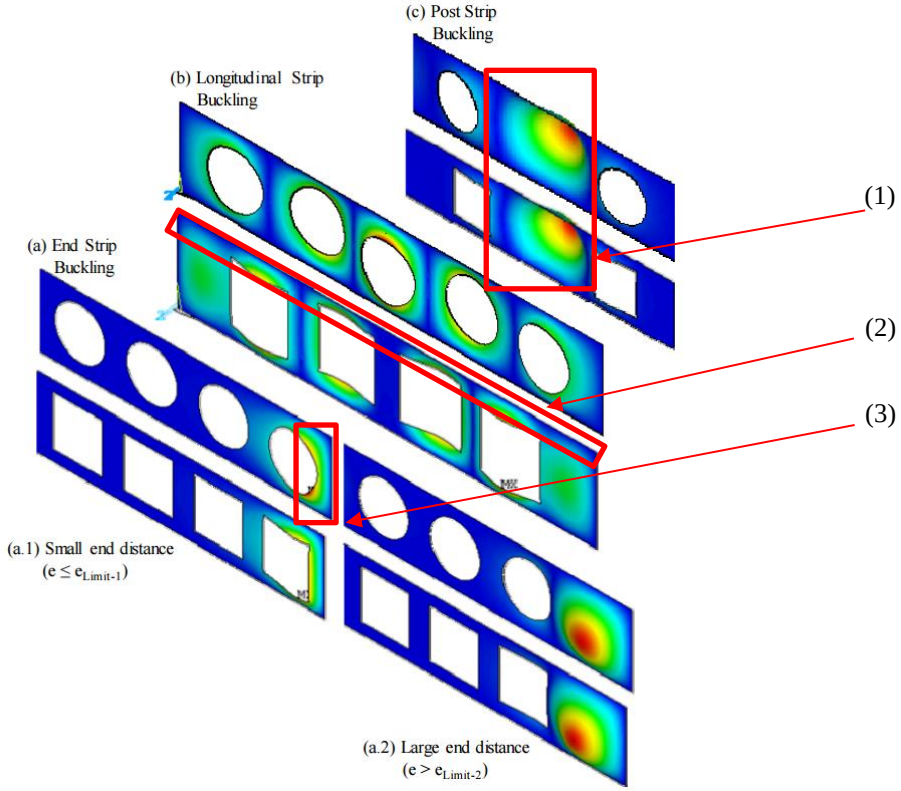

Figure 1.4: Buckling locations in web with rounded and square openings (Serror, et al., 2016).

According to (Serror, et al., 2016) web opening may change the buckling mode of the beam from tripping mode to local, but not the vice versa. Yet, several failure patterns can happen at once, but usually each of them is investigated separately. Then, minimum strength obtained with all separate collapse modes is defined as buckling capacity of the member (Gaspar, et al., 2011).

It is worth noting that coupled buckling modes generally lead to lower critical strength in comparison to a single mode. According to reports, combined column and tripping modes can reduce the critical buckling compared to the pure column buckling (Euler load) by 30% (Ostapenko & Yoo, 1988).

In several design codes, the presence of adjusted structural elements is taken into account by rotational springs (Paik & Thayamballi, 2000; Hughes, et al., 2004; Paik, et al., 1998). The study by (Rahbar-Ranji, 2012) was devoted to a comparison between the rule based and literature formulations for buckling capacity of T-bar stiffened plate under variety of buckling modes. The investigated buckling modes and their interactions, Figure 1.5, can be categorized as following: (a) torsional buckling of stiffener without attached plate, (b) torsional buckling of stiffeners, web buckling of stiffener, plate buckling, (c) coupled buckling of web and plate in a tripping mode.

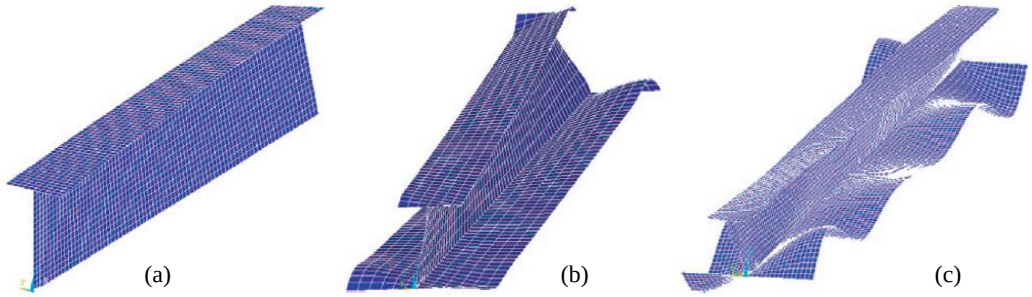

Figure 1.5: Buckling deformation in (a) tripping of T-bar stiffener without attached plate, (b) plate tripping and plate buckling with rigid web, (c) simultaneously buckling of web and plate in tripping of T-bar (Rahbar-Ranji, 2012).

The formulation of critical Euler stress was revised for each buckling mode separately (Fujikubo & Yao, 1999). It was determined that in case of coupling of all modes (c) the rule book formulation (DNV, 2009), (Zheng & Hu, 2005) and (Hughes, 1983) are giving wrong estimate of elastic buckling capacity of T-bars, whereas FEM and (Fujikubo & Yao, 1999) give almost similar results, Figure 1.6. However, rule formula is found to give acceptable results for a tripping buckling mode when attached plate is not loaded.

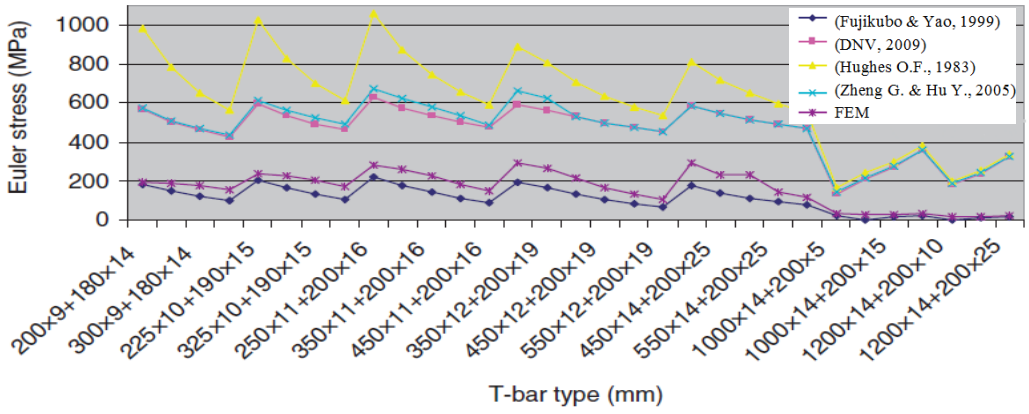

Figure 1.6: Critical Euler stress for case (c). (Rahbar-Ranji, 2012).

The buckling capacity of the structure is affected by geometry, material properties, initial defects and boundary conditions. Thus, DNV GL rules introduce the allowable buckling utilization factor. Utilization factor is a safety measure that accounts for the influence of neglected factors in the buckling expressions, such as compressive stress, shear stress, lateral pressure, etc. (Gaspar, et al., 2011) .

1.3 Methods for strength assessment

Nonlinear finite element analysis is applied in order to consider nonlinear behavior of the material and geometry. However, the analysis requires a great amount of computational time for large and complicated structures (Yao, et al., 2006). The results from nonlinear finite element method are greatly affected by the modelling technique. The effects of boundary conditions, mesh density, geometrical imperfections, residual stress, etc. should be wisely considered during analysis (Paik, et al., 2009).

Possible alternative for nonlinear FEM would be Closed Form Method (CFM) by (DNV GL AS, 2016). CFM uses semi-empirical approach whereas nonlinear FEM provides numerical solution. The capacity of the structure is different depending on chosen method for the analysis. The difference in end result is shown in (DNV GL AS, 2016) study for a girder with cut-outs under the pure axial load, Figure 1.7. The comparison between two methods shows that ultimate limit state obtained with nonlinear FE analysis is 140 MPa while the result obtained with CFM is 48% smaller, resulting in 94 MPa.

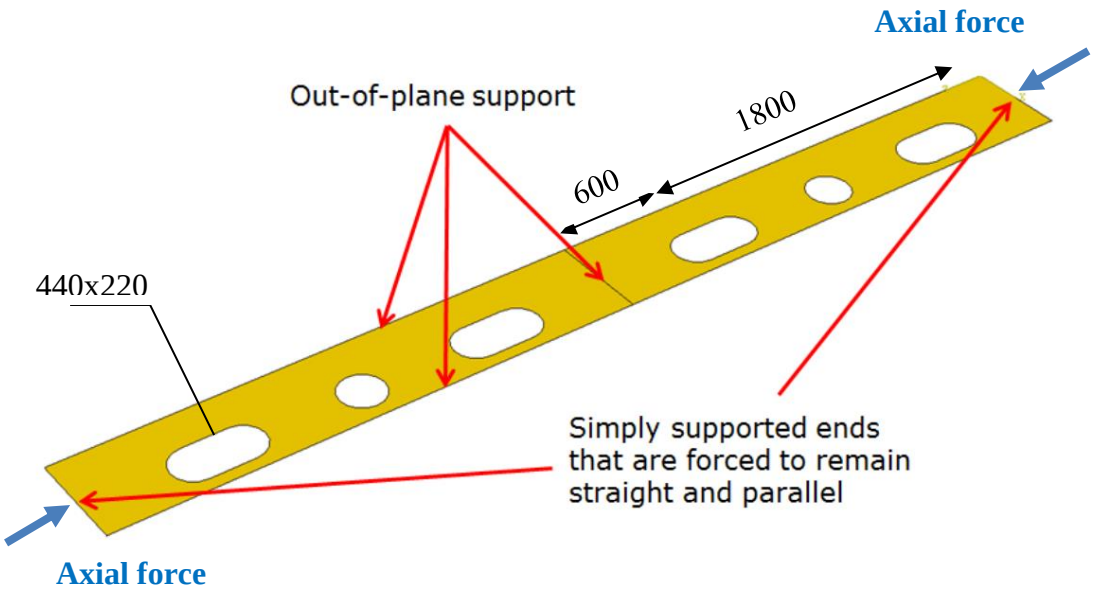

Figure 1.7: Load, geometry and boundary conditions of the web plate with cut-outs (DNV GL AS, 2016).

Based on the results it is clear that nonlinear finite element investigation is significantly more accurate compared to semi-empirical formulations of CFM. Despite the fact that nonlinear calculations are more time consuming, modern computers have enough computational power to carry out nonlinear FEM calculations. Thus, it is decided to use nonlinear FEM as a main tool for the thesis.

1.4 Research objective

The main goal of the study is to establish reliable method for strength assessment of T-beams. Main failure mechanisms of T-beam web structure under the applied load will be studied. Additionally, the thesis studies three main groups of loading: global, local and production loads. The strength criteria are calculated and compared with actual response levels.

1.5 Limitations

The research is limited to a general external loading. Specific loading cases with extensive point loads such as car deck, machinery deck, etc. are left out of the work. The residual stresses are not considered in the analysis.

Fatigue is not considered in the study. In passenger ships, transverse elements usually do not experience low- and high-cycle fatigue. Unlike merchant ships, where fully loaded departure condition is followed by ballast condition resulting in constant compression-tension pattern for decks; cruise ships are not subjected to constant fluctuations in still water bending moment (Webb Institute of Naval Architecture, 1973).

2 Strength assessment of T-beam under generic loading

The strength assessment overview can be seen in Figure 2.1. When the web configuration and material properties have been chosen, the response of the T-beams is calculated with nonlinear FEA. The load carrying capacity is evaluated by applying generic loading. Then strength criteria and ultimate limit state capacity are calculated and compared to realistic load.

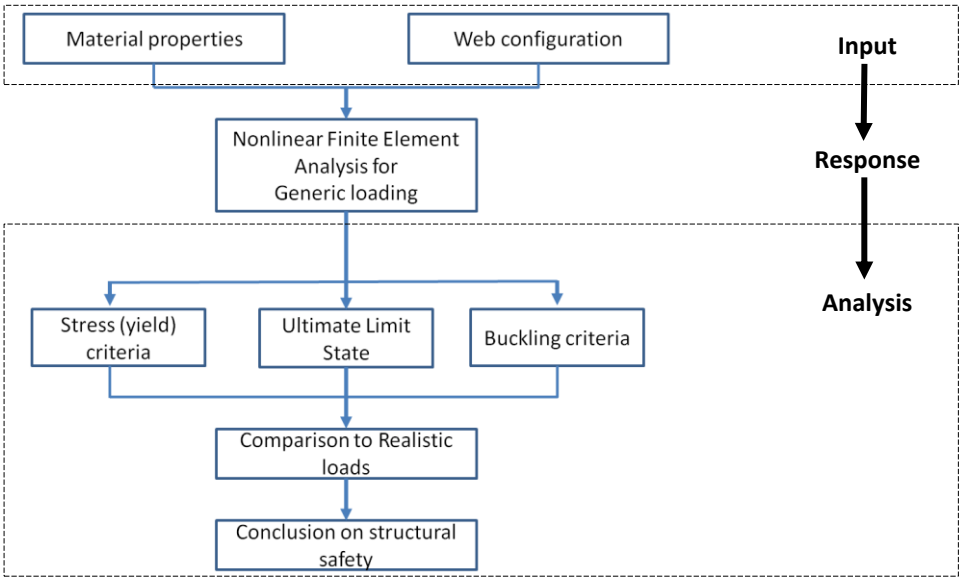

Figure 2.1: Simple outline of the steps for strength assessment.

Generally, in ship design stress level is compared to strength criteria in order to verify structural integrity and safety. Based on variety of sources (Yong Hur, et al., 2004; Brubak & Hellesland, 2008; Garbatov, et al., 2015) it is possible to distinguish four major structural failure modes in strength assessment: yielding, buckling, high- and low-cycled fatigue. This chapter defines yielding and buckling criteria for T-beam webs.

Criteria for yielding and buckling are developed in order to prevent failure. The criteria define the maxima loading that can be applied without risking structural integrity. Additionally, ultimate limit state is calculated to evaluate load carrying capacity after introduced strength criteria are exceeded. The method defines the applied load combination and capacity of the structure. The area inside the curve in Figure 2.2 represents tolerable actual stress under any combination of two applied loads.

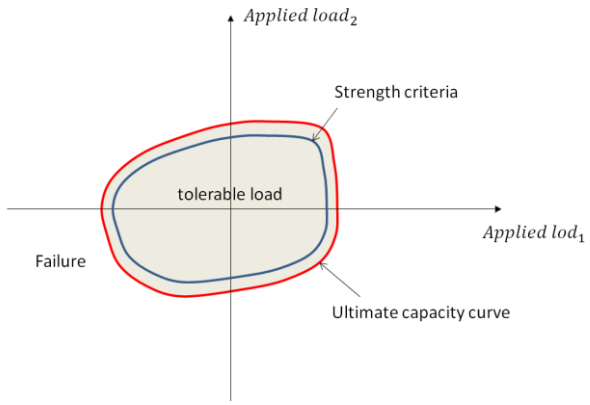

Figure 2.2: Ultimate capacity curve.

2.1 Generic loading

The ultimate limit state (ULS) is analyzed for several loading cases presented in Figure 2.3: axial compression and tension, bending in sagging (downwards) and hogging (upwards) and finally bending when both ends of the web rotate same direction clockwise (positive) and counterclockwise (negative). Loading is applied as enforced displacement, and enforced rotation.

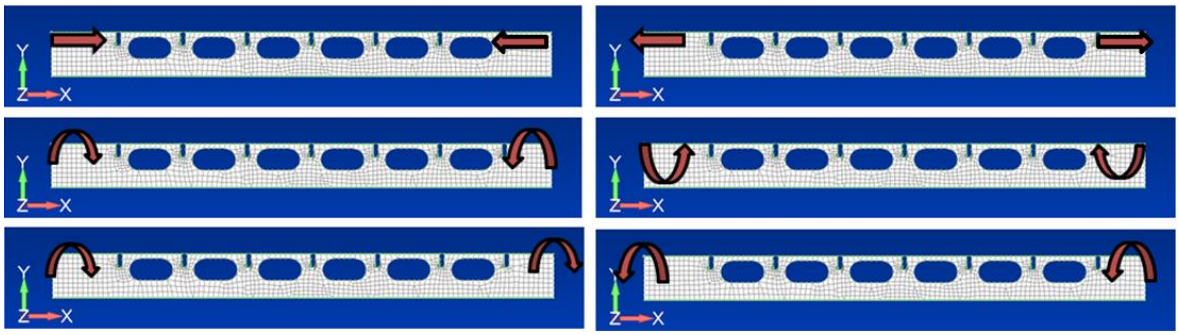

Figure 2.3: Generic loading.

Both ends of the web are modeled using rigid elements in finite element software FEMAP. In this way, the applied load is evenly distributed along the web ends that model the beam kinematics used in coarse mesh global model. The condition guarantees the compatibility between two models. All loads are applied as enforced displacements and rotations in the rigid elements of the web. The boundary conditions can be seen in Figure 2.4.

It should be noted that Boundary Conditions (BC) at web-frame ends in a real structure are neither entirely fixed nor simply supported. Simply supported BCs are usually used for analytical or semi-analytical design methods to simplifying algebraic calculations (Paik & Seo, 2009). For the purposes of this study it is essential to have fixed BCs due to the fact that loading is controlled by enforced displacements and rotations.

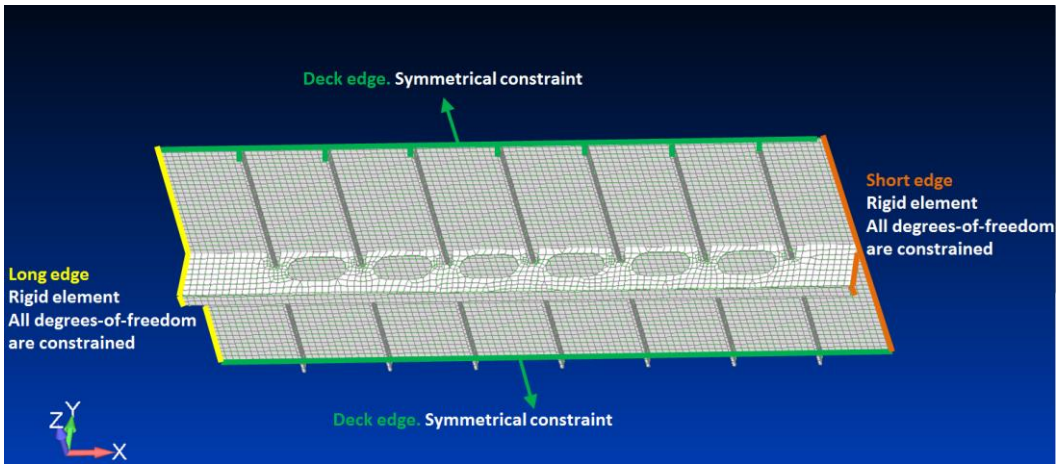

Figure 2.4: Boundary conditions.

The generic loading for obtaining ULS is divided into three separate types of combined loading:

1. Axial compression / tension and equal rotations in opposite directions.
2. Independent rotations at the ends.
3. Axial compression / tension and equal rotations in the same direction.

Load type 1, Figure 2.5, includes a case where bending induced by axial displacement is equal to applied rotations, i.e. the constraint moments at the edges are almost zero. The described case is matching the simply supported BC. Thus, the studied load type includes the whole range between simply supported and entirely fixed BC.

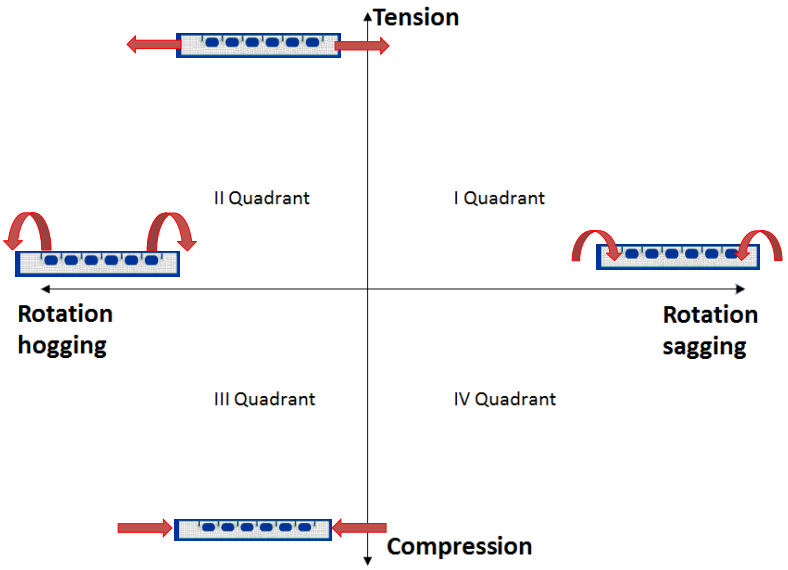

Figure 2.5: Study of axial compression and tension and opposite sign rotation in hogging and sagging.

In load type 2, Figure 2.6, uneven rotations are applied at web edges. Due to that the location of maximum bending moment and shear load shifts along the web. Thus, the load type 2 covers the shear loads.

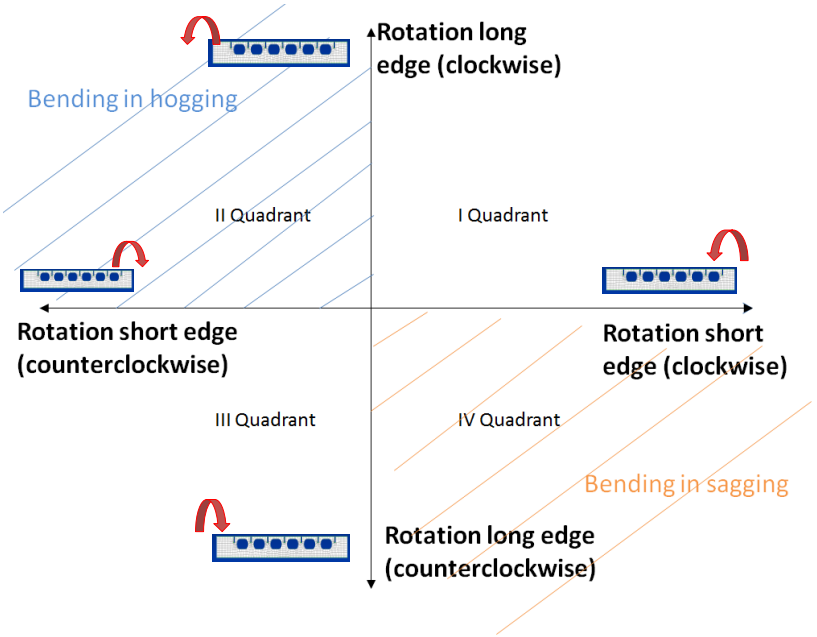

Figure 2.6: Study of clockwise and counterclockwise rotation.

Load type 3, Figure 2.7, covers the combined effects of axial and shear loads.

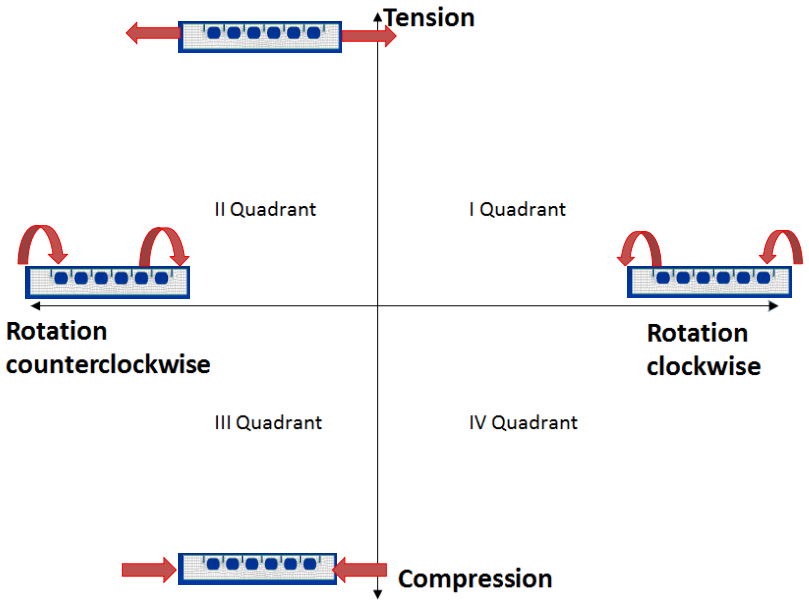

Figure 2.7: Study of axial compression and tension and rotation clockwise and counterclockwise.

The strategy for individual load case is described for load type 1; other loading types are studied with the same approach.

In load type 1 series of calculations involving variety of loads between the compression, tension and rotation are performed. In Quadrant III the applied load combinations are based on established load vectors, Figure 2.8. Blue points represent the load when maximum axial compression is applied while rotation in hogging is varied from 0% - 100% (with step of 20%) of maximum rotation. The red points represent the load when compression is varied from 0% - 100% (with step of 20%) from maximum axial compression while applied rotation load in hogging is kept as a maximum.

The arrows, Figure 2.8, represent selected load vectors for the analysis. Numerical data for presented vectors can be found in Table 2.1.

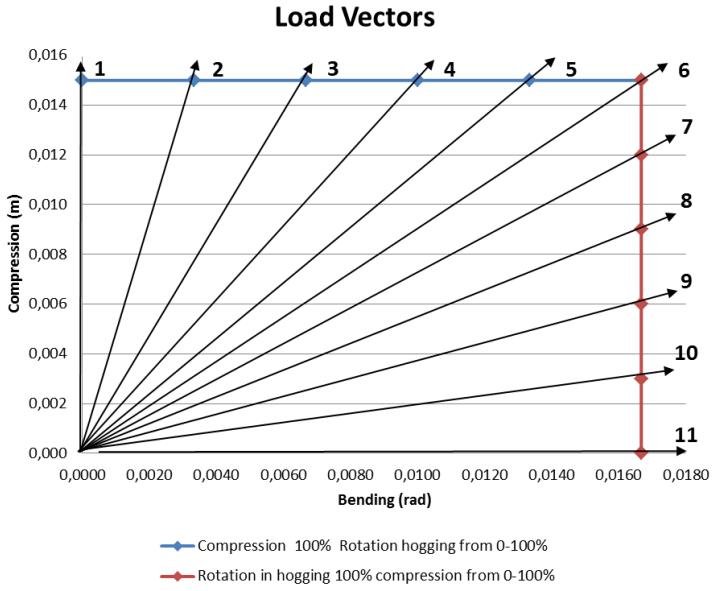

Figure 2.8: Loading vectors for non-linear modeling (load type 1, Quadrant III).

Table 2.1: Numerical data for load vectors.

Load Vectors							
Compression 100% Rotation in hogging from 0-100%				Rotation in hogging 100% compression from 0-100%			
Vector	Compression (m)	Rotation (rad)	Rotation (%)	Vector	Rotation (rad)	Rotation (m)	Compression (%)
6	0,015	0,01667	1,00	6	0,01667	0,015	1,00
5	0,015	0,01334	0,80	7	0,01667	0,012	0,80
4	0,015	0,01000	0,60	8	0,01667	0,009	0,60
3	0,015	0,00667	0,40	9	0,01667	0,006	0,40
2	0,015	0,00333	0,20	10	0,01667	0,003	0,20
1	0,015	0,00000	0,00	11	0,01667	0,000	0,00

The similar procedure is repeated for all 4 quadrants of analysis field. The total number of load vectors for study of load type 1 is 40. Thus, in order obtain the ULS curve for all three load types the required number of vectors is 120.

The magnitude of applied load for rotation, tension and compression is decided based on the web plate dimensions and physical properties. The yield strain of the steel can be found as a ratio between Young's modulus and yield stress, Table 2.2. The applied enforced displacement should be significantly higher than yield strain in order to observe post buckling behavior of the structure.

The enforced displacement is chosen as 0.3% of the total length of the web. The resulting strain occurred to be 74% higher than yield strain. For consistency of the analysis, enforced rotations are calculated based on enforced displacement value.

The rotations required to cause enforced displacement of 0.3% of the total web length are applied, Figure 2.9. The obtained total angle is evenly divided between two edges of the web, Table 2.2. In Figure 2.9 blue rectangles represent the web plate, applied displacement is 0,015 meters and the corresponding rotation is 0,01667 radians. The plate dimensions and calculated loads can be found in Table 2.2.

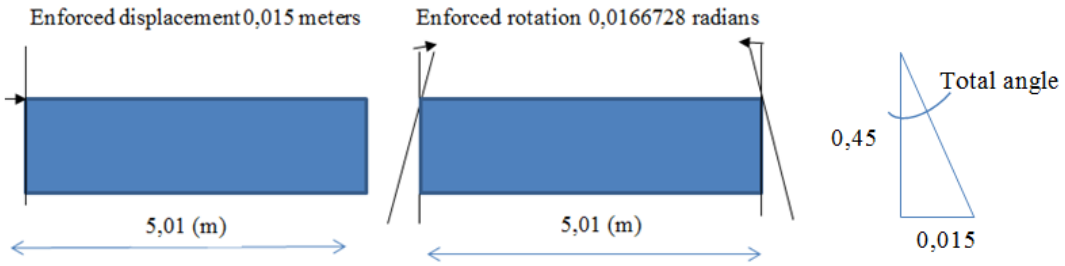

Figure 2.9: Enforced displacement and corresponding rotation for ULS analysis.

Table 2.2: Enforced displacement and rotation based on web dimensions.

Parameter	Value	Parameter	Value
Length (m)	5,01	Web height (m)	0,44
Young's modulus (MPa)	206000	Flange height (m)	0,01
Yield stress (MPa)	355	Web + Flange (m)	0,45
Yield strain (m)	0,0017233	TAN (Applied Displacement/ Web + Flange)	0,03333
Applied stress (MPa)	616,77	Total angle for two angles (RAD)	0,03335
Applied displacement (m)	0,015	Total angle for two angles (DEG)	1,91057
Applied strain %	0,3	Angle at one end (RAD)	0,01667
Angle to one end (DEG)	0,9552836	-	-

2.2 Nonlinear response by FEM

The structure is explicitly modeled in FEMAP using elements from NX Nastran's element library. The deck and deck's stiffeners are modeled using 4-node quadrilateral shell elements CQUAD4, Figure 2.10. The T-beam web is modeled with CQUAD4 elements; however, in some locations next to the openings for longitudinal stiffeners 3-node triangular elements CTRIA3 are used, Figure 2.11. Deck's stiffener bulbs are modeled with beam elements CBEAM, Figure 2.13.

CQUAD4 and CTRIA3 are isoparametric elements with optional coupling of bending and membrane stiffness. The formulations of the elements are based on the Mindlin-Reissner shell theory. The elements include in-plane bending and transverse shear behavior. Elements do not give direct elastic stiffness for the rotational degrees-of-freedom (dof) which are normal to the surface of the element (NX Nastran 10, 2014).

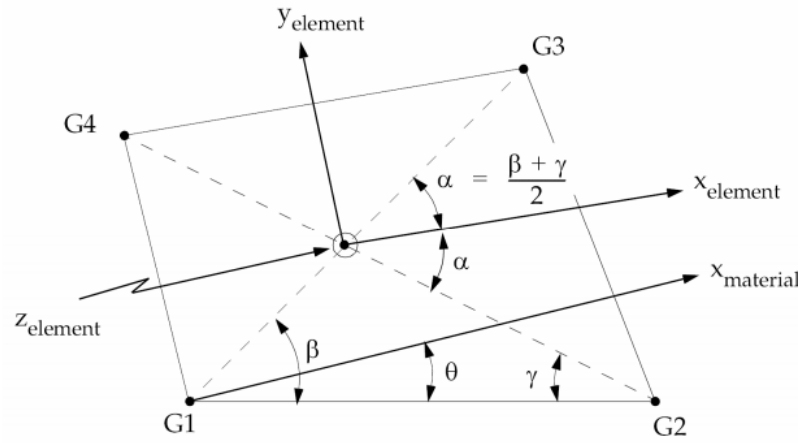

Figure 2.10: Shell element (CQUAD4) geometry system (NX Nastran 10, 2014).

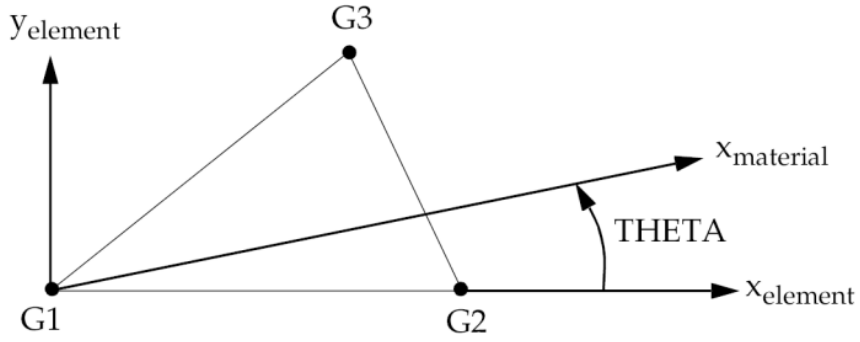

Figure 2.11: Shell element (CTRIA3) geometry system (NX Nastran 10, 2014).

It should be noted that 4-node quadrilateral elements are over stiff in pure bending, because it cannot generate correct displacement mode, Figure 2.12. Under the pure bending the top and bottom sides of the element remain straight resulting only in horizontal translations in the nodes. Similarly, 3-node triangular elements cannot provide exhibit pure bending, due to parasitic shear absorbing strain energy (Mathisen, 2016).

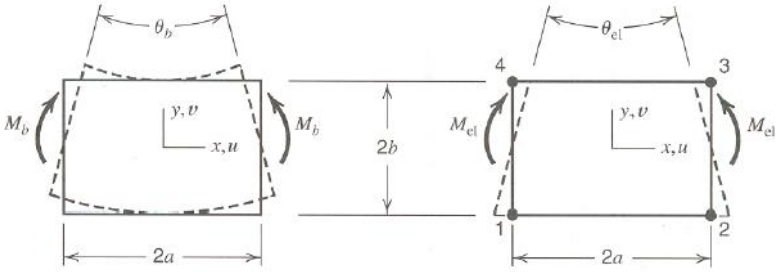

Figure 2.12: Defect of 4-moded element defect (Mathisen, 2016).

The CBEAM beam element, Figure 2.13, includes extension, torsion, bending in two perpendicular planes, and shear response.

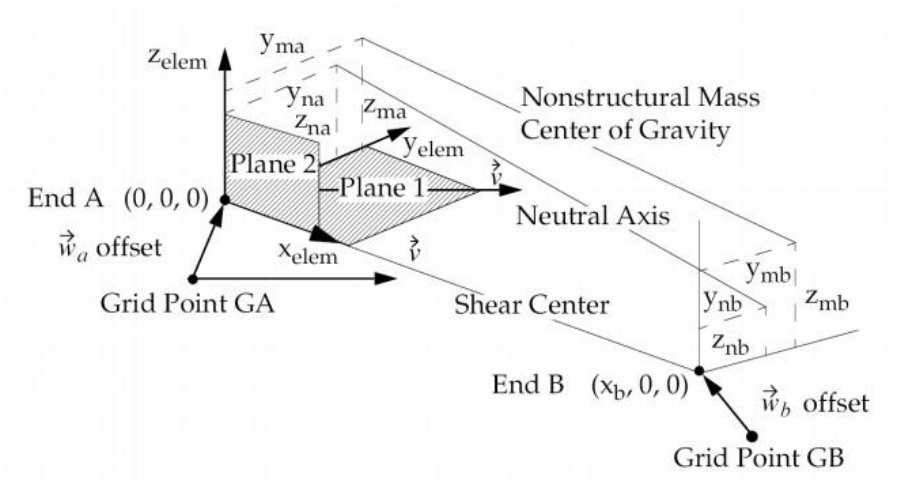

Figure 2.13: Offset beam element (CBEAM) geometry system (NX Nastran 10, 2014).

Both ends of the web are modeled using rigid elements RBE2. Each edge has one node with independent degrees-of-freedom. The rest of the grid points at the edge assigned with depended dof. i.e. same component numbers as independent dof. Thus, RBE2 elements couple the motion of depended and independent degrees of freedom. Typical mesh of elements presented in Figure 2.14.

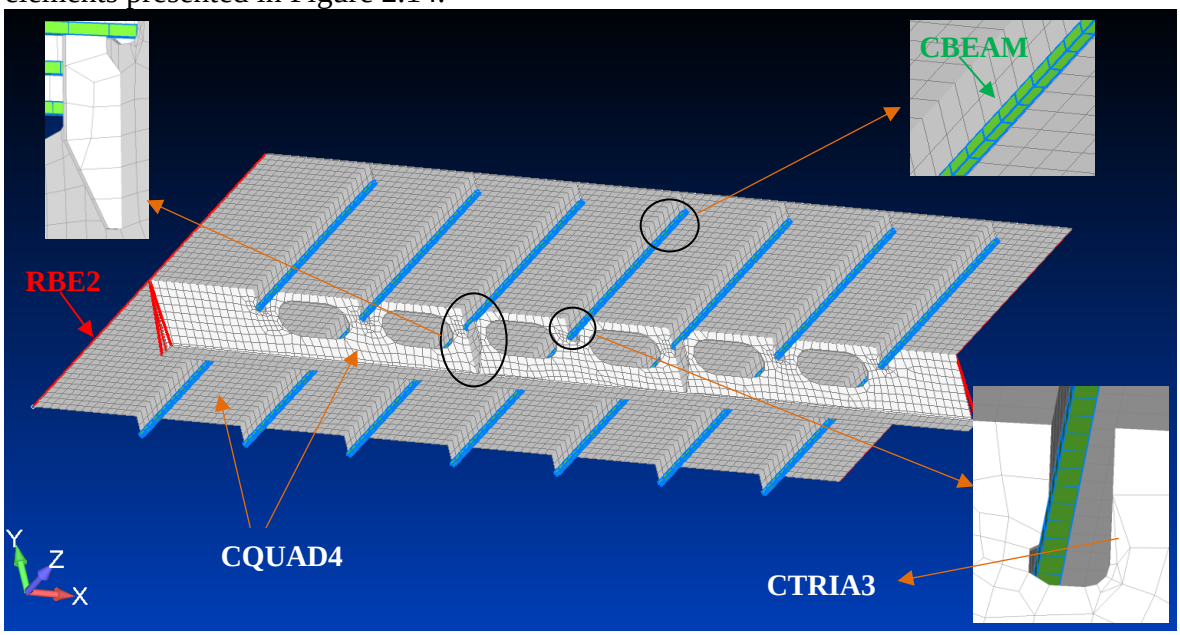

Figure 2.14: Elements in FE-models.

The nonlinear static analysis (SOL 106 NLSTATIC) performed in NX Nastran. The nonlinear properties are defined by nonlinear material data. In the following study investigated T-beams assigned with a structural steel grade S355. The plastic strain value for the following nonlinear analysis is based on stress-strain curve displayed in Figure 2.15.

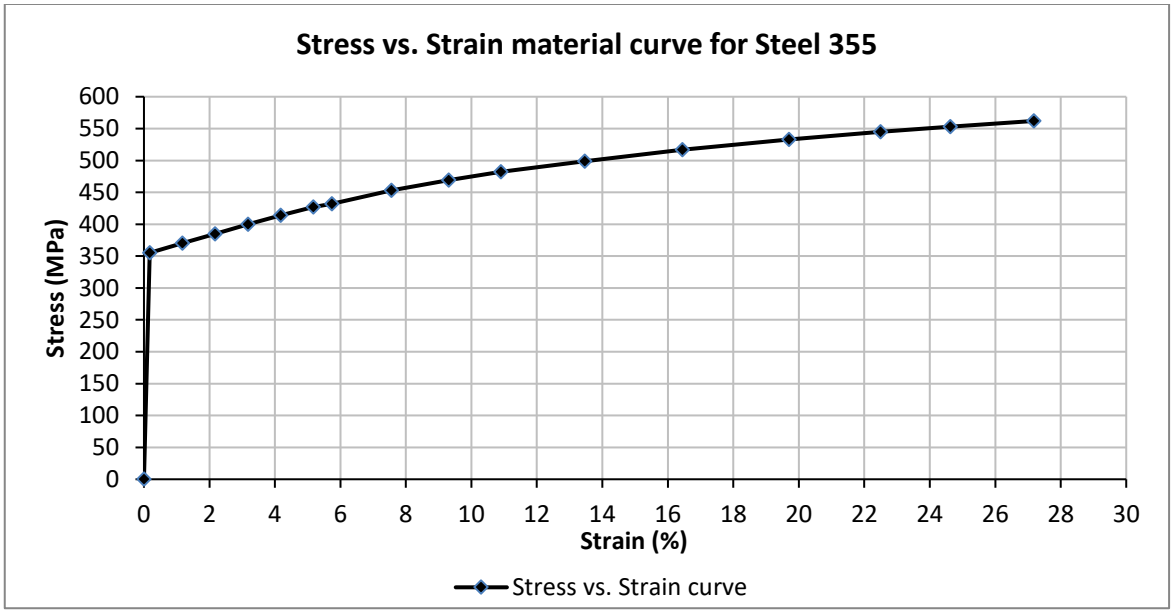

Figure 2.15: Material curve steel S355.

The nonlinear analysis is performed according to full Newton-Raphson solution algorithm, Figure 2.16. Nodal increment f^n - f^{n-1} is applied then using tangential stiffness matrix K_{T0}^n the iterative displacements δd_0^n and residual forces r_1^n are found. The tangential matrix K_{T1}^n is evaluated and iterative displacements δd_1^n and residual forces r_2^n are calculated. The algorithm repeats until convergence is found (NAFEMS, 1992).

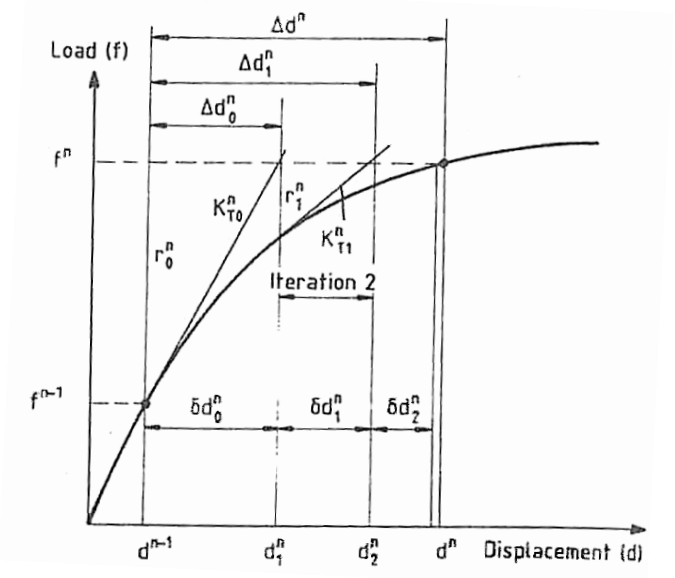

Figure 2.16: Newton-Raphson method (NAFEMS, 1992).

When the slope of nonlinear force-displacement curve changes the sign during the loading path, Figure 2.17, Newton-Raphson algorithm may fail. The main reasons why nonlinear

curve changes the sign are: plasticity work softening, snap-through or bifurcation behavior. More sophisticated Arc-Length solutions are proposed by (Riks, 1979) and (Crisfield, 1980) for solving such problems.

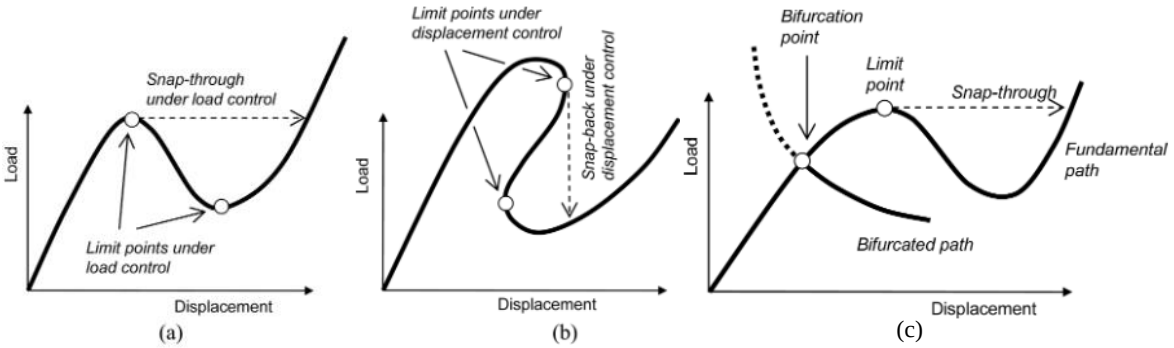

Figure 2.17: Typical instabilities of a system under load control - snap-through (a), displacement control - snap-back (b) and bifurcation behavior (c) (Leahu-Aluas & Abed-Meraim, 2011).

The Arc-Length methods find equilibrium by modifying both displacement and load increments during the iteration. This allows the solution to follow entire force-equilibrium path, including the areas where both displacement and load are decreasing (Bashir Ahmed Memon & Xiaozu Su, 2004; Degenhardt, et al., 2004). However, in this thesis the load is controlled by prescribed displacements and rotations. Therefore, arc-length method cannot be used and Newton-Raphson method with displacement control is applied. In this way, displacement will be forced to continuously increase allowing it to remain on the equilibrium curve, Figure 2.18.

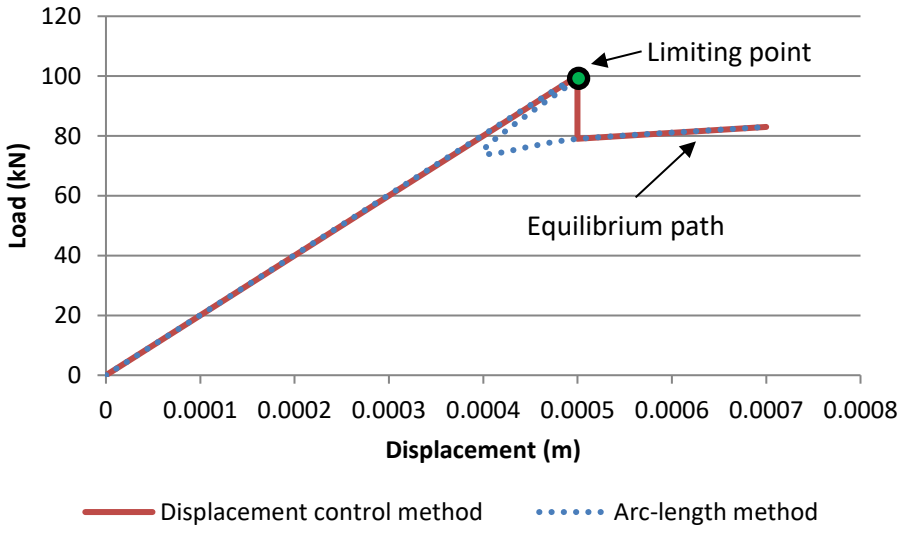

Figure 2.18: Schematic comparison between Newton-Rapson with displacement control and arc-length methods.

The main varied parameters in the nonlinear analysis are the number of increments/time steps and the maximum number of iterations per step. To choose appropriate parameters for the further nonlinear calculations the sensitivity analysis is performed. Axial compression and rotation in hogging were chosen as case studies for a sensitivity analysis. These cases cause the highest non-linearity in the structure due to plate buckling as well as that of the web-frame.

First, the total number of steps is varied from 50 to 450 while iterations per step were automatically set in FEMAP. Then, the same analysis is repeated with fixed maximum

iterations per step. The obtained results can be seen in Table A.1 in Appendix A. In some cases, the failure point is not determined accurately in FEMAP, due to poor ratio between the number of steps and number of iteration points in the analysis. These crash cases are marked with red color in Table A.1. The typical output from non-linear FEA for compression and rotation in hogging can be found in Figure A.1 & Figure A.2 and Figure A.3 & Figure A.4 respectively.

The main concern is difference in plastic range and post buckling behavior of the structure under compression when the number of steps per analysis is equal to 150, 300 or 450. The second issue is a scatter for ultimate load in case of rotation in hogging. The main reason for that is buckling mode (deformed shape) of attached deck plate as FEA minimizes the potential energy with a shape, Figure A.5.

Based on results from Table A.1 and post buckling behavior curves, it is decided to perform further calculations with the following parameters: 250 steps per analysis and 75 iterations per step. The applied parameters ensure acceptable calculation time per run. During compression, selected parameters allow to track the worst post buckling response. In rotation in hogging same parameters overestimate ULS by 4,5 % compared to analysis (with more powerful computer) with 1000 steps. In the scope of this thesis the following phenomena is not studied further due to the time limitations. The selected parameters are considered to be acceptable with 4,5% uncertainty.

2.3 Stress (yielding) criteria

The stress criteria can be verified by comparing the actual local stress levels with yielding strength of the material under uniaxial compressive or tensile loading case. In T-beam web plates length and height are much greater compared to width. For such structures under two principal stress components σ_1, σ_2 (i.e. corresponding to normal stresses in x- and y-directions $\sigma_{x,}\sigma_{y,}$ and shear τ_{xy} stresses in x-y plane), three stress criterion are applied: maximum principal-stress-based criterion, maximum shear-stress-based criterion and Mises-Hencky criterion. The last two are applicable for steel and other ductile materials, while the first one is suitable for brittle materials. The Mises-Hencky criterion can be written as following (Paik & Thayamballi, 2003):

$$\sigma_{eq} = \sqrt{\sigma_x^2 - \sigma_x\sigma_y + \sigma_y^2 + 3\tau_{xy}^2} \tag{1}$$

$$\sigma_{eq} = \sqrt{\sigma_1^2 - \sigma_1\sigma_2 + \sigma_2^2} \tag{2}$$

When the equivalent stress σ_{eq} gets to a critical point of yielding strength σ_Y, material yields. If both sides of the equation 2 are squared, then yielding criteria can be shown in graph as an ellipse, Figure 2.19. In case of normal stresses in x- and y-directions are equal to zero, the shear yield stress τ_Y is determined with the following formula:

$$\tau_Y = \frac{\sigma_Y}{\sqrt{3}} \tag{3}$$

The Tresca criterion, Figure 2.19, represents the case when maximum shear stress in the structure reaches the maximum shear at yielding τ_Y.

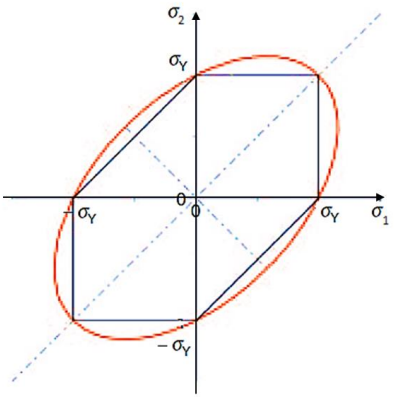

Figure 2.19: Failure criterion surface (von Mises - red curve, Tresca - black curve) (Abrate, 2008).

According to DNV GL rules, for all structure, stress in plates should be checked at its center of mid-plane. The maximum von Mises stress should not exceed the acceptance stress criteria. However, the local stress exceedance over the yielding point is not ultimately leading to a severe problem. In some cases, it can result in a better redistribution and adjustment of the stress concentration over the structure (Brubak & Hellesland, 2008).

It is decided to introduce several stress criteria. The first criterion developed for linear FE-analysis, while second and third applied for nonlinear analysis. The first criterion is calculated when applied load causes material to yield. Then, the maximum allowed load ($F_{allowed}$) is defined according to the following formula:

$$F_{allowed} = \frac{\sigma_{max}}{\sigma_Y} * F_{init} \quad (4)$$

where σ_{max} is a maximum stress value obtained with linear FE analysis, σ_Y material yield stress, F_{init} is initially applied load.

A second criterion defines the first yielding in a web plate during nonlinear FE-analysis. Basically, when the first local yield is reached then the design limit has met. However, the approach is very depended on a mesh quality. The better mesh might change the stiffness of the elements in the model. As the result, first yielding might take place in an earlier or later time step. Moreover, in some cases, Figure 2.20, captured yielding occurs quite local and does not affect the strength of the structure. The following figure represents the relevant and irrelevant capture of the first yielding point in web plate during nonlinear FE-analysis.

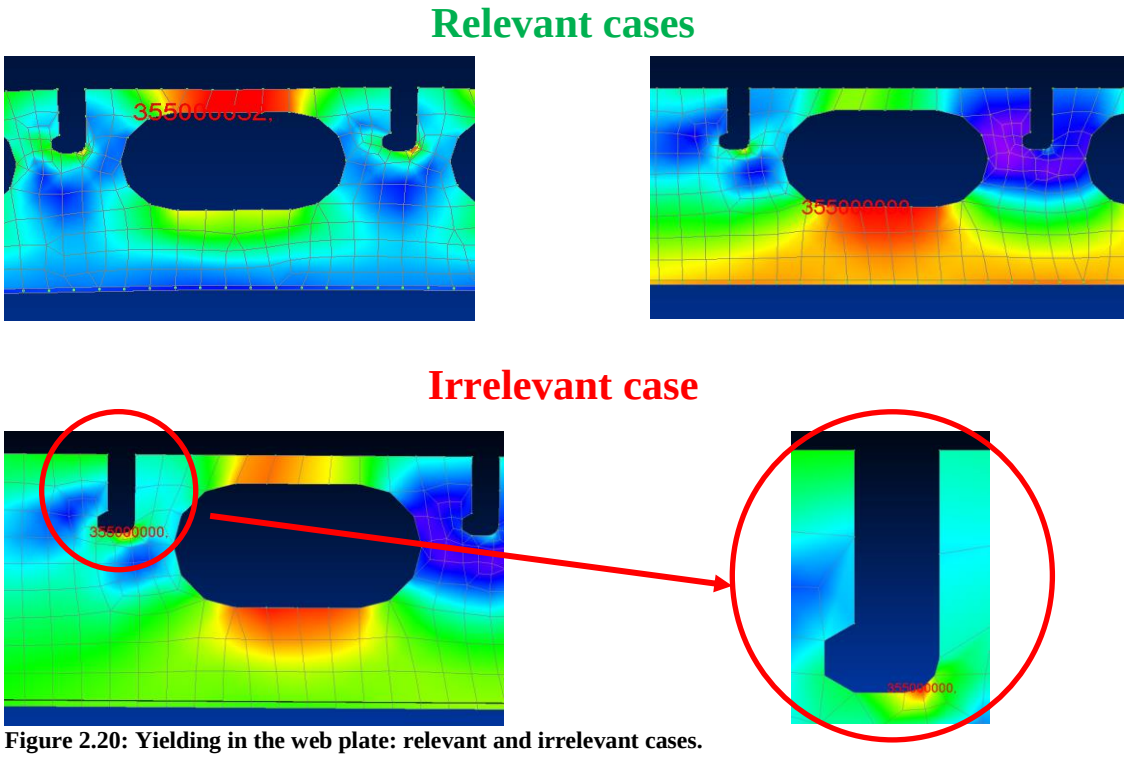

Figure 2.20: Yielding in the web plate: relevant and irrelevant cases.

Thus, it is decided to introduce third criterion in nonlinear FEA - yielding in a flange, Figure 2.21. Basically, when the first fiber of the flange yields the design maximum is reached. The chosen criteria is considered more relevant in terms of strength assessment, since the yielding in flange is more hazardous than a local yielding of a web plate.

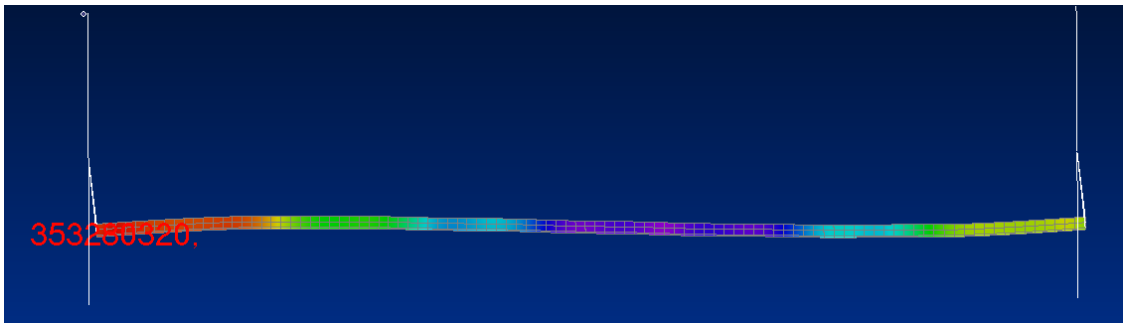

Figure 2.21: First yielding in the flange.

It should be noted that yielding criterion is calculated based on top Von Mises stress. The bottom and top Von Mises stresses produce the same result due to the small thickness of the structure. In several cases, the difference between the stresses reaches 4 %, however for the following work the accuracy is sufficient.

2.4 Buckling and post buckling criteria

Buckling of T-beam can be divided to local and global scale. Due to the high height to thickness ratio the local buckling analysis of the web plate is required. The global buckling is triggered when the flange of the T-beam buckles in a tripping mode.

The main principle of DNV GL rules is an acceptable elastic buckling. The design allows pre- and post-buckling structural behavior while yielding is not permitted, Figure 2.22. After stress is released the structure restores to its original form avoiding permanent deformations. Thus, yielding criteria also covers allowable buckling.

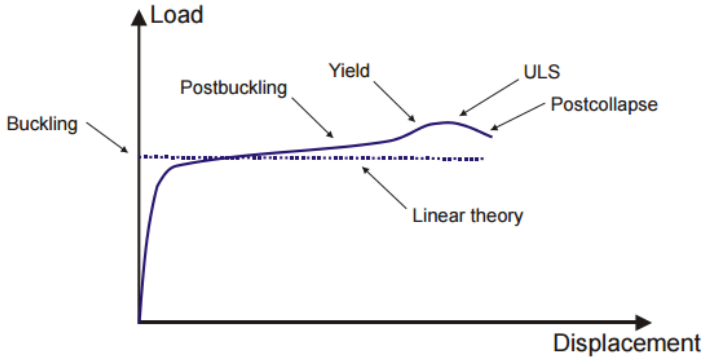

Figure 2.22: Buckling concept of load-deflection curve (Brubak, 2016).

In the study, T-beams are loaded with prescribed displacements and rotations. The technique allows evaluation between local yielding of the web plate and global buckling of T-beam. After ULS is reached, the load bearing capacity of the structure is decreasing. The loss of capacity can happen in rapid or slow manner. Rapid loss of stability causes quick load redistribution to adjusted structural members: deck and deck's stiffeners. Due to the rapidness of the process extreme stress distribution patterns occur. Slow loss of stability allows the structure to detain stress redistribution resulting in better stress distribution patterns and post collapse load bearing capacity.

To evaluate the rapidness of stability loss, post buckling parameter is introduced, Figure 2.23. Ultimate limit state is met before generic loading (displacements/rotations) reaches its prescribed value. Post buckling point captures the total constraint moment when generic load has reached prescribed value. Thus, it is possible to evaluate the rapidness of stability loss by comparing total constraint moment at ULS and post buckling stages.

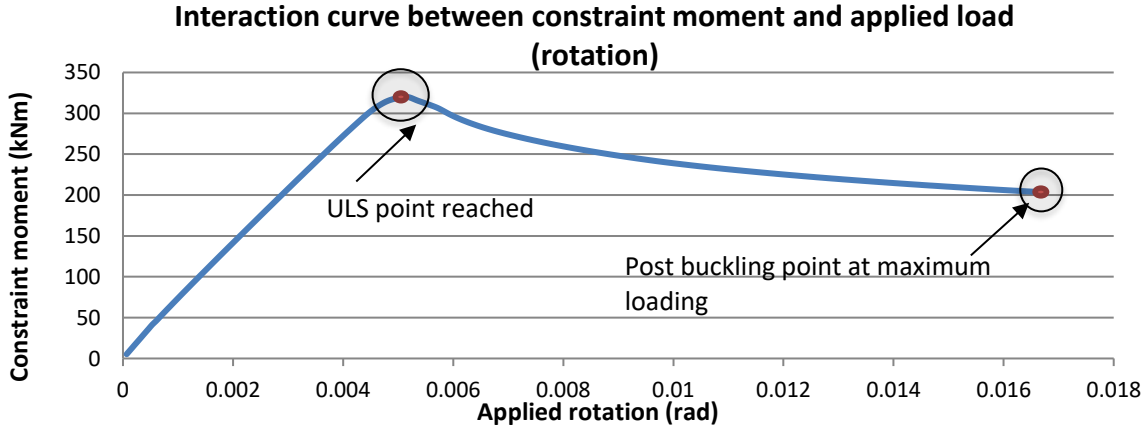

Figure 2.23: Post buckling point at maximum loading.

3 Realistic loads of a cruise ship

The investigated ship is about 110000 GT cruise vessel from the Meyer Shipyard base. Transverse orientated webs located on decks 7-15 are considered in the study, Figure 3.1. The length of the webs is restrained by the distance between two pillars (pillar spacing).

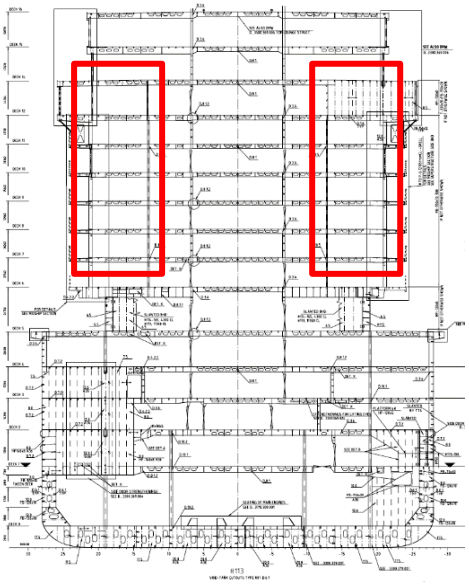

Figure 3.1: Location of investigated T-beam webs.

3.1 Global still water and wave loads

The main loading components in passenger ship are wave-induced loading moment and still water bending (Mantere, 2007). Therefore, the following study mostly considers global loads.

Shear force that occurs as a result of hull girder deflection considered to be a quite significant issue for a present-day cruise ships. The main two reasons for that are relevantly low ratio between the length and height of the vessels and low shear to bending stiffness relation. Typical value for length to height for the passenger ship is around 6. The shear problem can be neglected if the length is more than 10 times the height. Hence, the global shear deflections are included in the following work (Naar, 2006). Global loads are modeled into global FE-model, Figure 3.3, as a load distribution that results into fulfillment of bending moment and shear force distribution as given by DNV GL, Figure 3.2.

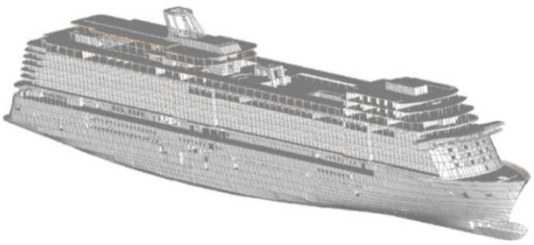

Figure 3.3: Global FE-model.

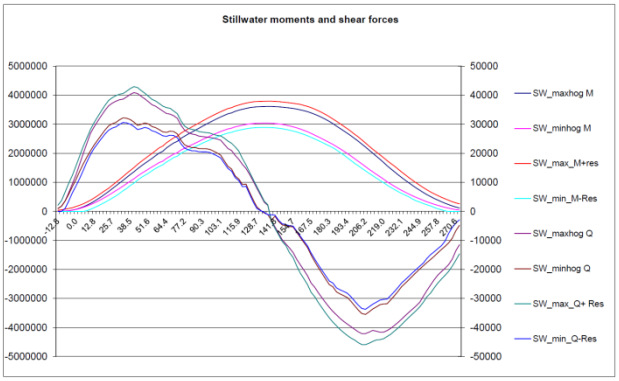

Figure 3.2: Typical bending moment distribution

Sagging and hogging loading cases are considered in relation to investigated T-beam webs. Hogging condition results in decks tension, while in sagging decks are compressed under deformed hull girder, Figure 3.4 (Romanoff, 2016). Depending on the location, webs can experience significant transverse compression in sagging and hogging. For example, transverse webs that are located next to the big deck openings can experience high compressive stress up to 40 MPa. Typical deformations during sagging and hogging can be seen in Figure 3.5.

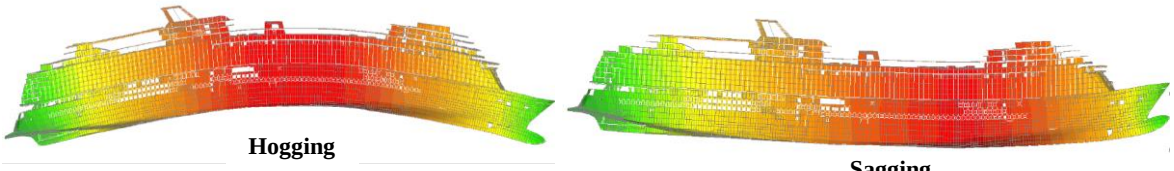

Figure 3.4: Global deformation in hogging and sagging conditions.

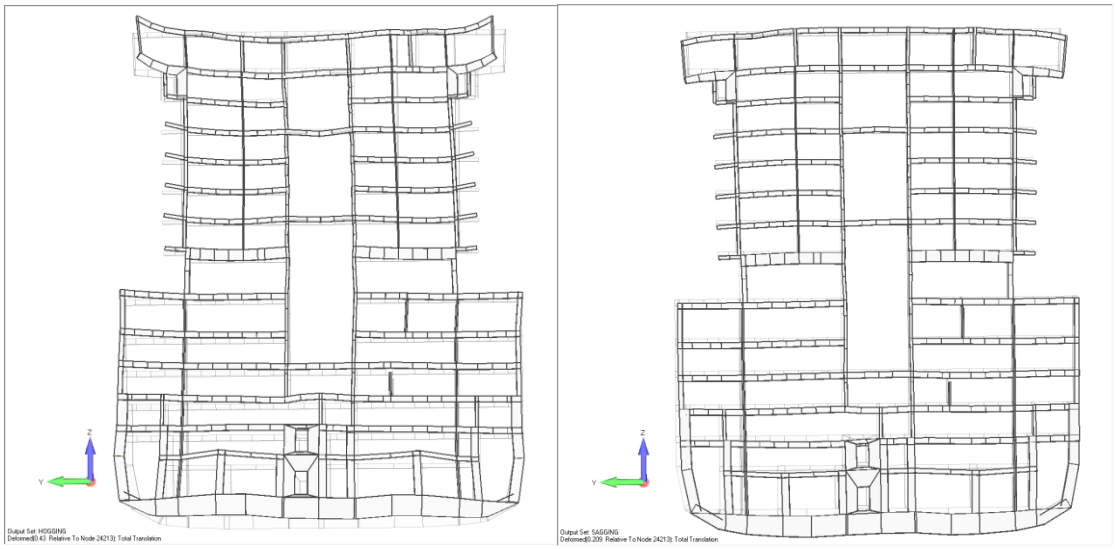

Figure 3.5: Section deformations in hogging (left) and sagging (right).

In addition, racking loading is simulated in order to verify transverse strength of T- beam webs. Racking can be described as a condition, where ship model is heeled and balanced with a distributed pressure at submerged bottom of the hull and gravity forces, Figure 3.6. The racking analysis usually required by classification societies when direct strength assessment is performed (Det Norske Veritas, 2006; Lloyd's Register, 2012).

Figure 3.6: Racking induced deformation.

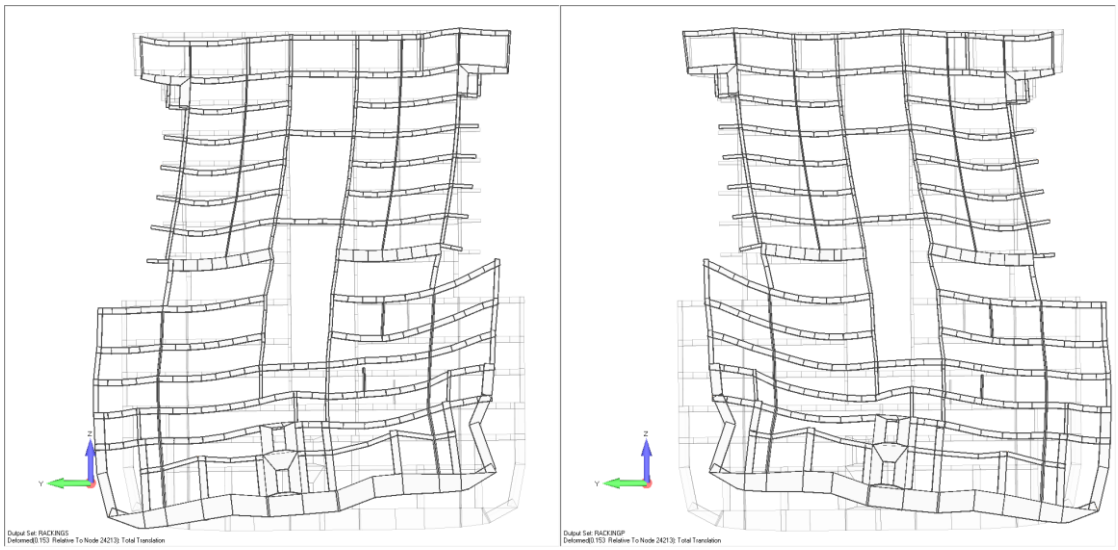

Figure 3.7: Section deformations in racking.

3.2 Global response

The global response is calculated with global finite element model. Transversal web plates are usually not investigated separately from the rest of the neighboring structure in global analysis. Unlike longitudinals, transverse structure has lighter loading conditions which do not cause extreme stress concentrations. Global FE-model does not include modeling of openings nor tripping brackets. It should be noted that global FE-model in sagging and hogging does not include steel weight of the structure; while in racking, it is considered due to the presence of gravity forces.

Global response is considered through rotations and displacements at the edge points of the web plates from global finite element model. Displacement and rotation responses of the edge node points for each web are outputted from a global model for all investigated cases on decks 7-15. Global loads are considered to be 2D problem, i.e. out of plane loads are not included in the study.

The obtained data sets are transferred to excel and sorted by x- and y-coordinates so that the nodes on the same side of the ship with the same x-coordinate are separated from the nodes on the other side of the ship. Schematically node's locations can be found in Figure 3.8. Short edge is located closer to a midship line, while the long edge is located closer to a ship's side near balconies.

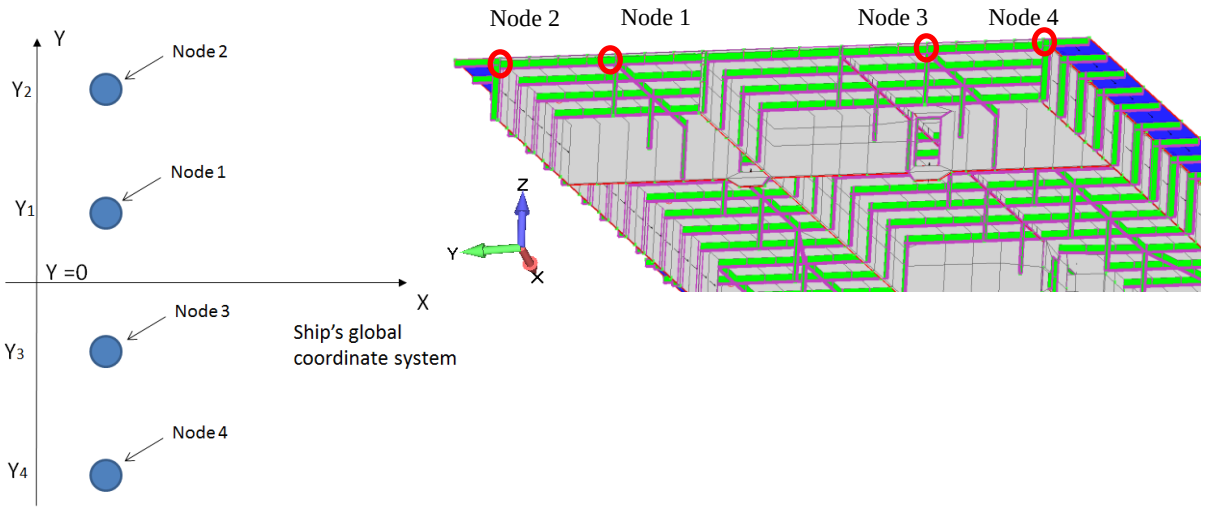

Figure 3.8: Node's locations.

All the webs were assigned with loading case based on the following algorithm, Table 3.1, where T_{y1}, T_{y2}, T_{y3}, T_{y4} are translations in y-direction for nodes 1,2,3,4 respectively and R_{x1}, R_{x2}, R_{x3}, R_{x4} are rotations around x-axis for nodes 1,2,3,4 respectively.

Table 3.1: Algorithm for global response.

Compression/ Tension	Conditions	Calculated value	Resulting load case
Y_1 , $Y_2 > 0$	If T_{y1} , $T_{y2} > 0$ $T_{y1} > T_{y2}$	-ABS(T_{y1} - T_{y2})	Compression
	If T_{y1} , $T_{y2} > 0$ $T_{y1} < T_{y2}$	ABS(T_{y1} - T_{y2})	Tension
	If T_{y1} , $T_{y2} < 0$ $T_{y1} > T_{y2}$	-ABS(T_{y1} - T_{y2})	Compression
	If T_{v1} , $T_{v2} < 0$ $T_{y1} < T_{y2}$	ABS(T_{y1} - T_{y2})	Tension
	If $T_{y1} > 0$, $T_{y2} < 0$ $T_{y1} > 0$, $T_{y2} < 0$	-ABS(T_{y1} - T_{y2})	Compression
	If $T_{y1} < 0$, $T_{y2} > 0$ $T_{y1} < 0$, $T_{y2} > 0$	ABS(T_{y2} - T_{y1})	Tension
Y_1 , $Y_2 < 0$	If T_{y4} , $T_{y3} > 0$ $T_{y4} > T_{y3}$	-ABS(T_{y4} - T_{y3})	Compression
	If T_{y4} , $T_{y3} > 0$ $T_{y4} < T_{y3}$	ABS(T_{y4} - T_{y3})	Tension
	If T_{y4} , $T_{y3} < 0$ $T_{y4} > T_{y3}$	-ABS(T_{y4} - T_{y3})	Compression
	If T_{y4} , $T_{y3} < 0$ $T_{y4} < T_{y3}$	ABS(T_{y4} - T_{y3})	Tension
	If $T_{y4} > 0$, $T_{y3} < 0$ $T_{y4} > 0$, $T_{y3} < 0$	-ABS(T_{y4} - T_{y3})	Compression
	If $T_{y4} < 0$, $T_{y3} > 0$ $T_{y4} < 0$, $T_{y3} > 0$	ABS(T_{y3} - Ty_4)	Tension
Rotation	Conditions	Calculated value	Resulting load case
Y_1 , $Y_2 > 0$	If R_{x1} , $R_{x2} > 0$	-ABS(R_{x1}-R_{x2})/2	Rotation towards short edge
	If $R_{x1} < 0$, $R_{x2} > 0$	ABS(R_{x1} - R_{x2})/2	Rotation in sagging
	If $R_{x1} > 0$, $R_{x2} < 0$	-ABS(R_{x1} - R_{x2})/3	Rotation in hogging
	If R_{x1} , $R_{x2} < 0$	ABS(R_{x1}-R_{x2})/2	Rotation towards long edge
Y_1 , $Y_2 < 0$	If R_{x4} , $R_{x3} > 0$	ABS(R_{x4}-R_{x3})/2	Rotation towards long edge
	If $R_{x4} < 0$, $R_{x3} > 0$	ABS(R_{x4} - R_{x3})/2	Rotation in sagging
	If $R_{x4} > 0$, $R_{x3} < 0$	-ABS(R_{x4} - R_{x3})/3	Rotation hogging
	If R_{x4} , $R_{x3} < 0$	-ABS(R_{x4}-R_{x3})/2	Rotation towards short edge

The load conditions are grouped accordingly to loading types introduced in chapter Generic loading. The obtained result can be seen in Figures 3.9, 3.10 and 3.11. Each dot in the figures represents load in one individual web frame. Global sagging condition causes the tension in transverse T-beams while global hogging causes compression. Racking causes both compression and tension load. Overall, in most the cases global loads force T-beams to bent in sagging or rotate both ends in the same direction.

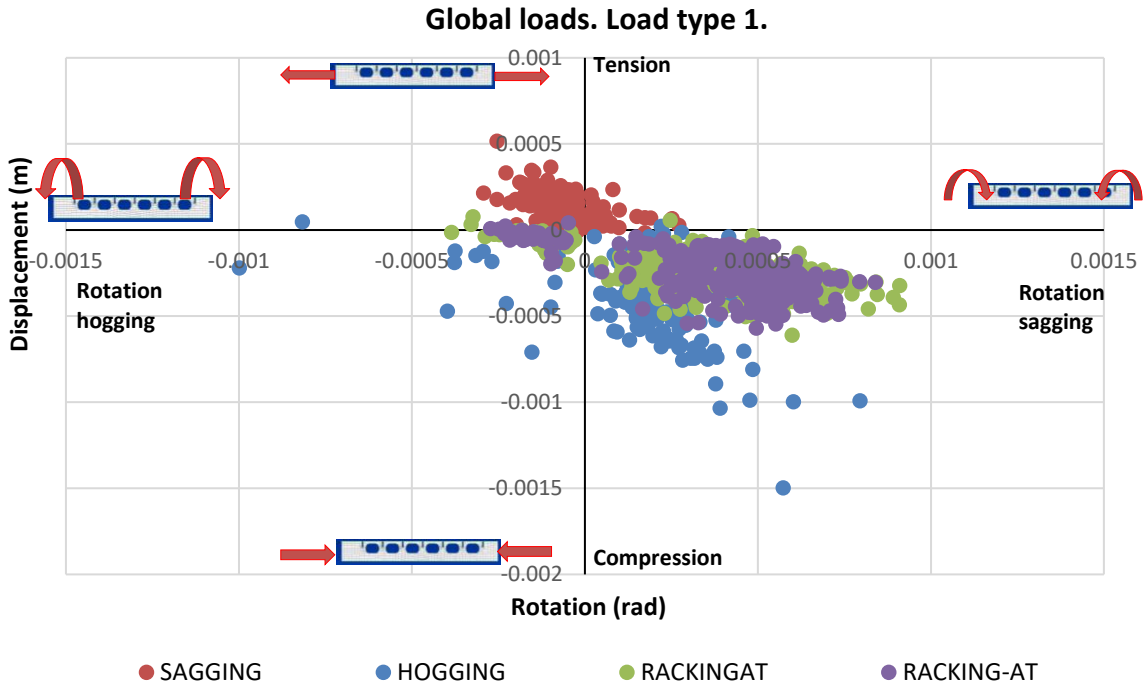

Figure 3.9: Global loads plotted in load type 1 figure.

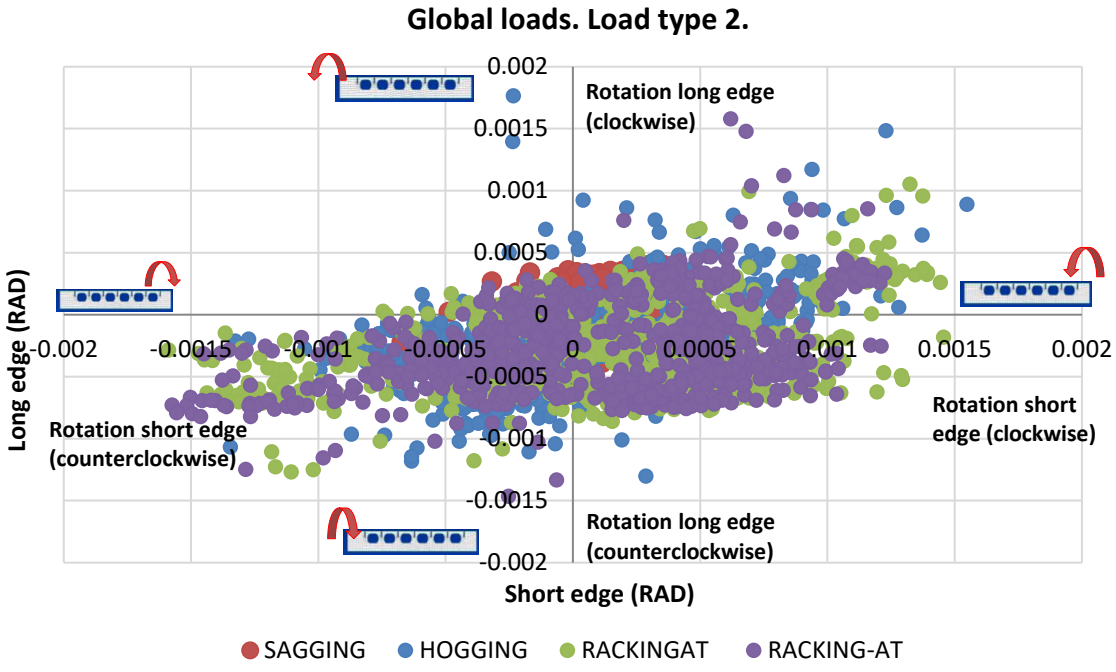

Figure 3.10: Global loads plotted in load type 2 figure.

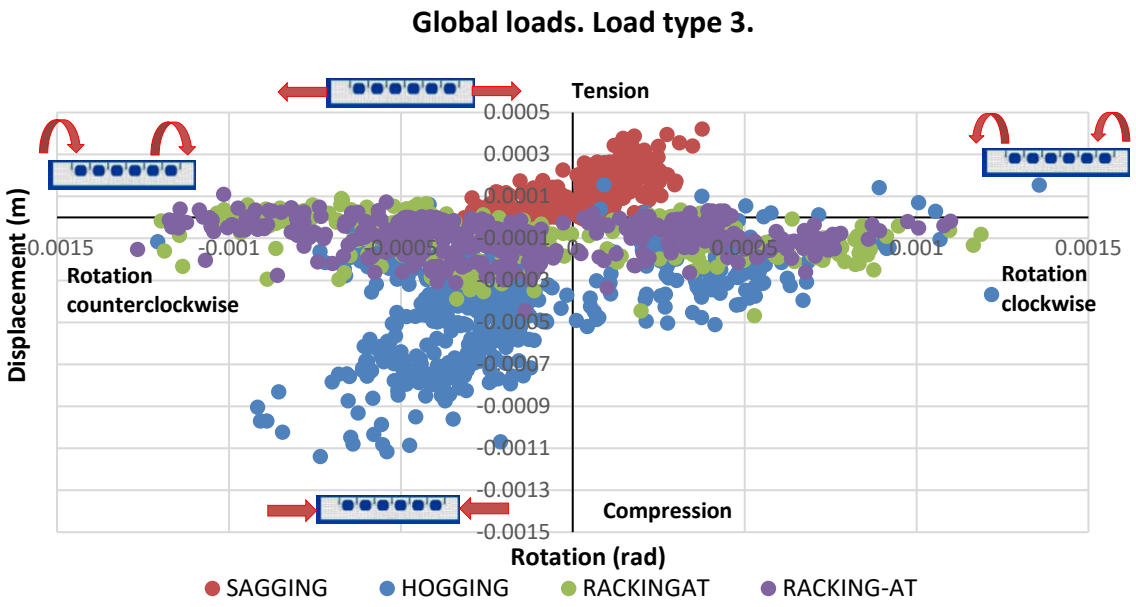

Figure 3.11: Global loads plotted in load type 3 figure.

It should be noted that some peak points are the result of additional rotation caused by the presence of intermediate bulkhead. Basically, in some rare cases bulkheads are located in the middle of the T-beams, Figure 3.12.

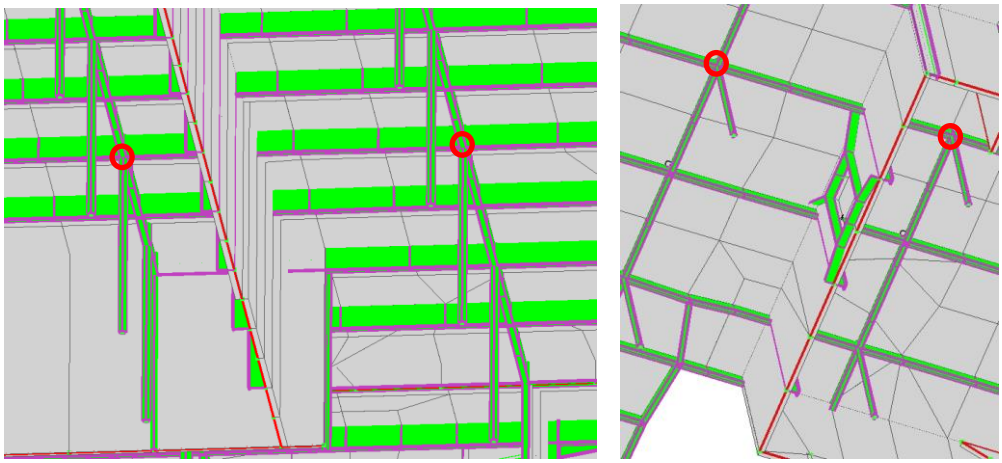

Figure 3.12: Intermediate bulkhead in the middle of the web frame.

3.3 Local deck pressure

The static pressure on non-exposed decks is the only local load that is considered in the study. According to GNV GL the minimum value for a static pressure is 2,5 kN/m^2 (DNV GL, 2017). Taking into consideration that weight of the steel is not considered in sagging and hogging, due to the absence of gravity forces in FE analysis, and no dynamic pressure is applied, it is decided to use conservative value of 5 kN/m^2 for the deck pressure load.

The load is applied to all laminate deck plate elements on decks 7-15 in a global FE-model. Typical example of modeling can be seen in Figure 3.13. The boundary conditions with entirely fixed bottom can be seen in Figure 3.14. Selected boundary conditions are conservative since the bottom of the ship is never entirely straight during the operation. Moreover, the load distribution where all the decks simultaneously subjected to distributed load of 5 kN/m^2 is doubtful to occur. Thus, the obtained design has additional safety against local load.

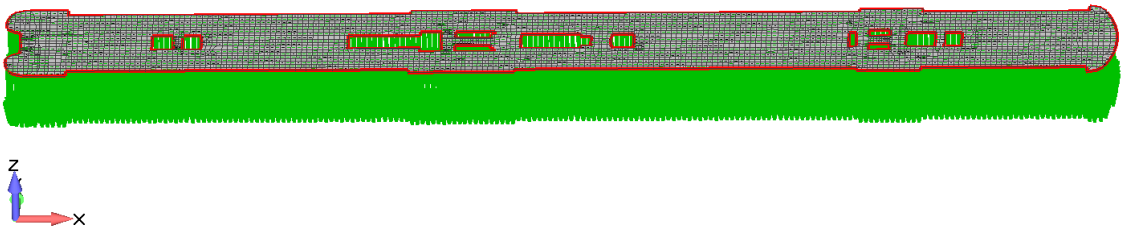

Figure 3.13: Modeling of the deck pressure (green arrows pointed down).

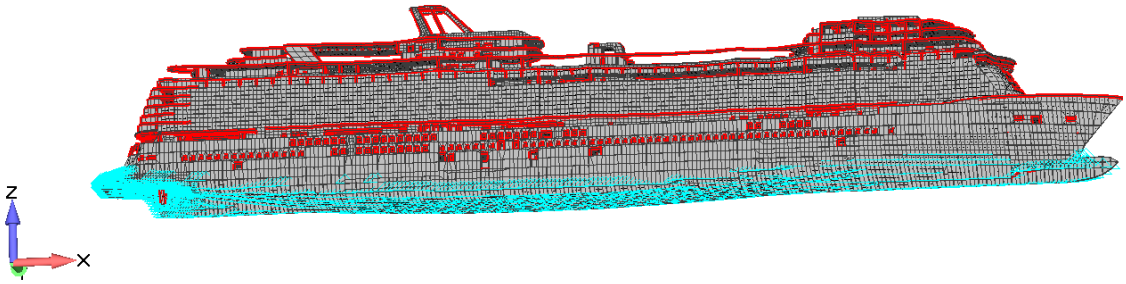

Figure 3.14: Boundary condition for a deck pressure load (bottom fixed).

3.4 Local response

Similarly to global response, local response is considered through rotations and displacements at the edge points of the web plates caused by the deck pressure load.

The obtained results are grouped accordingly to the loading types presented in Generic loading chapter. The obtained results in Figures 3.15, 3.16 and 3.17 show that deck pressure causes only sagging or same way rotation condition for transverse webs. The only exception is a single case of rotation in hogging caused by intermediate bulkhead is in a middle of the web.

Overall, rotations caused by the deck pressure has the same order of magnitude as global response, however displacements caused by compression/tension are significantly smaller.

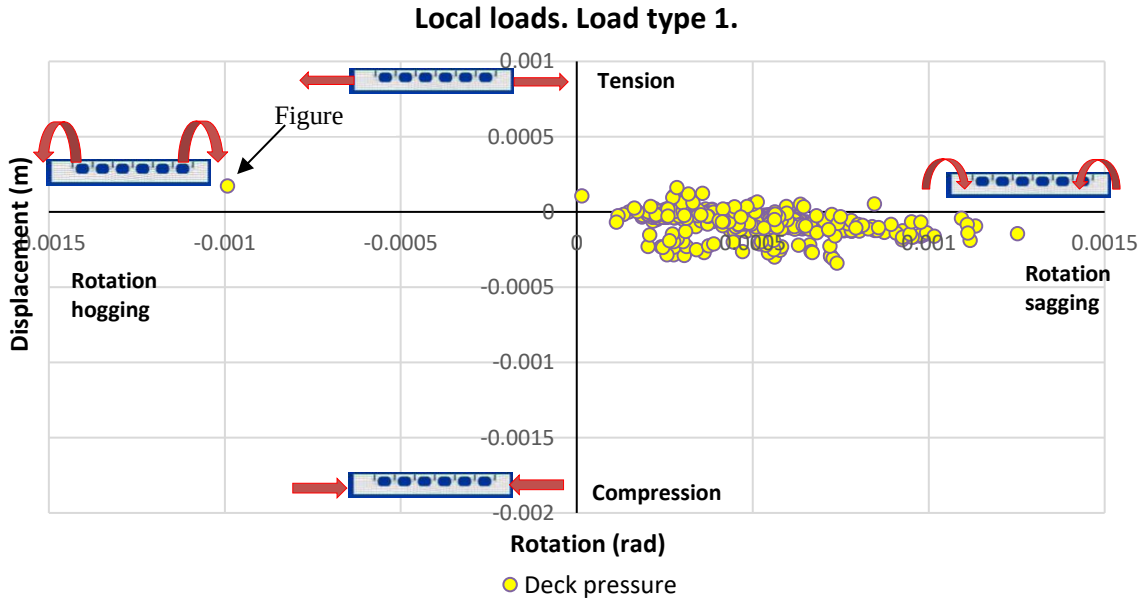

Figure 3.15: Local loads plotted in load type 1 figure.

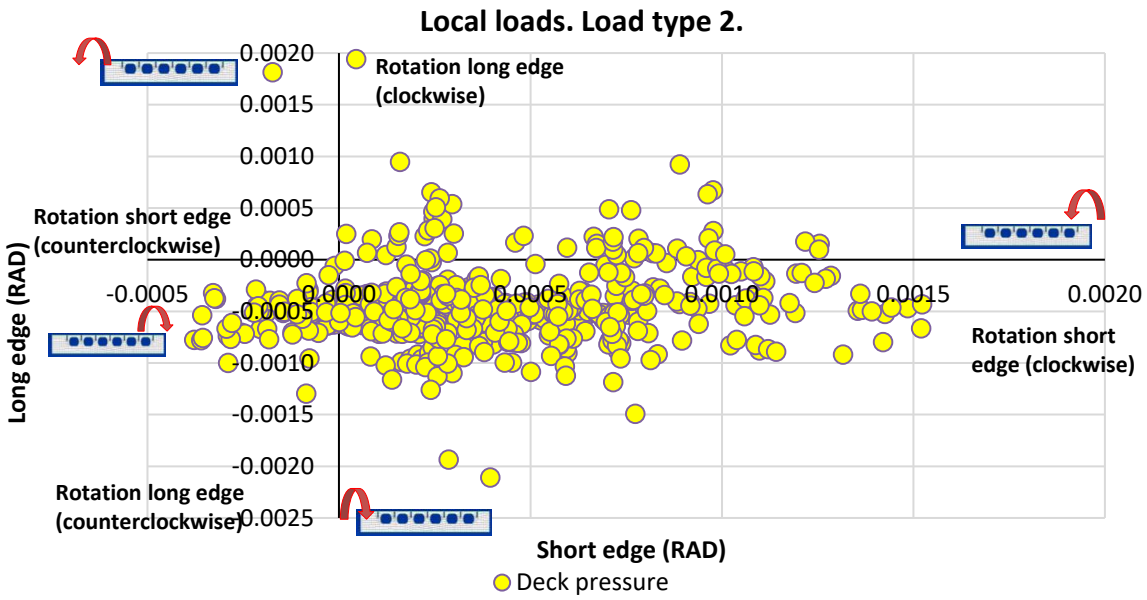

Figure 3.16: Local loads plotted in load type 2 figure.

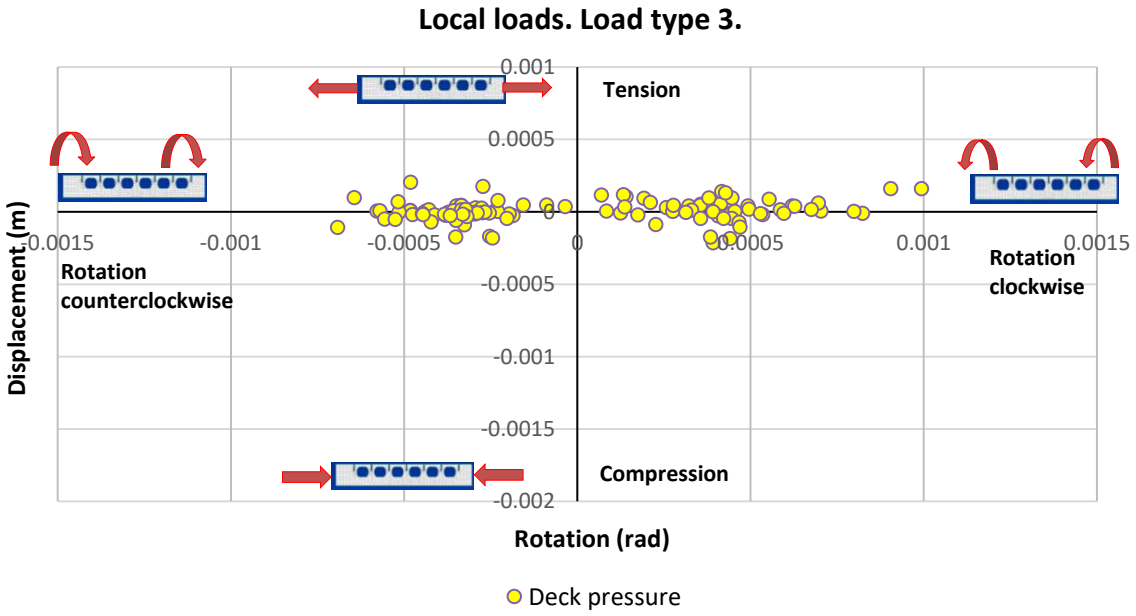

Figure 3.17: Local loads plotted in load type 3 figure.

3.5 Production loads: Block lifting

Hull production is based on block building method. Ship's hull and superstructure composed from small parts, i.e. blocks. During the production when the block is ready it is transported to a building dock and then welded to the rest of the blocks (Remes, 2015).

Lifting is required to deliver heavy blocks to the building dock. During lifting phase blocks are hanging in the air without sufficient support. Under the own weight and lifting acceleration blocks are exposed to heavy deformations. The following chapter shows two separate case studies of block lifting. Main block parameters can be found in Table 3.2.

Table 3.2: Block main dimensions.

Block	Length (m)	Breadth (m)	Max height (m)	Weight (t)
Case A	42	33	9,2	407
Case B	33,34	31	12,7	340

In both cases during the FEM modeling body acceleration load of 9,81 m/s^2 is applied. The models are entirely free to move in z-direction, whereas one corner of the block is restrained in x-, second in y- and third in both x-, y-directions, Figure 3.18.

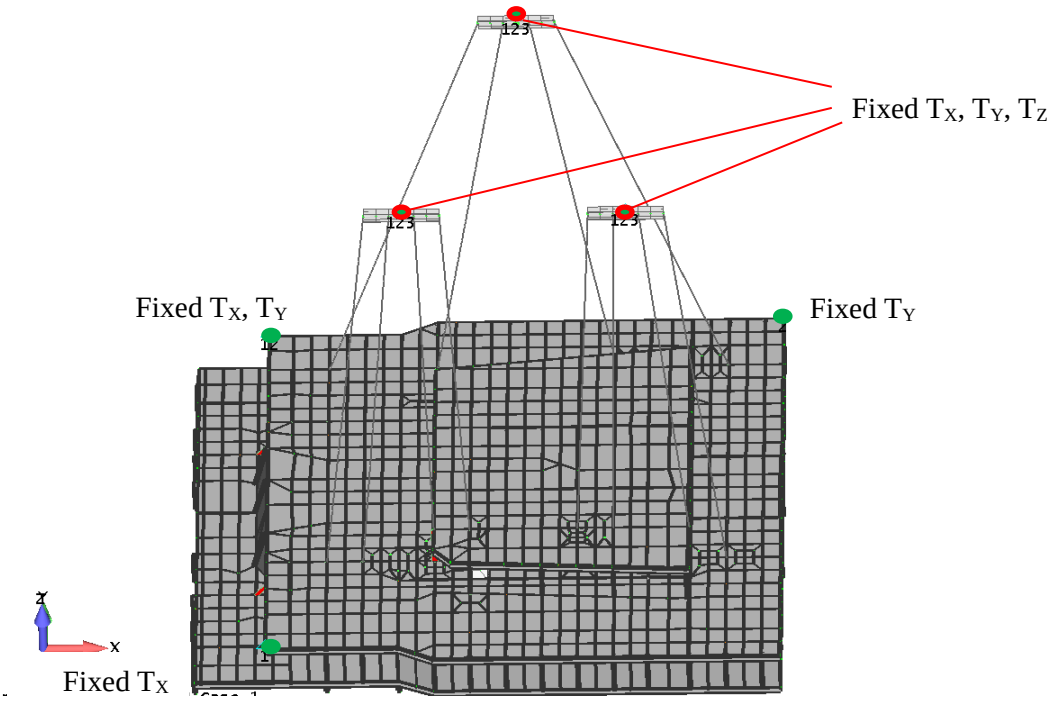

Figure 3.18: Case A: boundary conditions for block lifting load.

The block deformations during the lifting phase are presented in Figures 3.19 and 3.20.

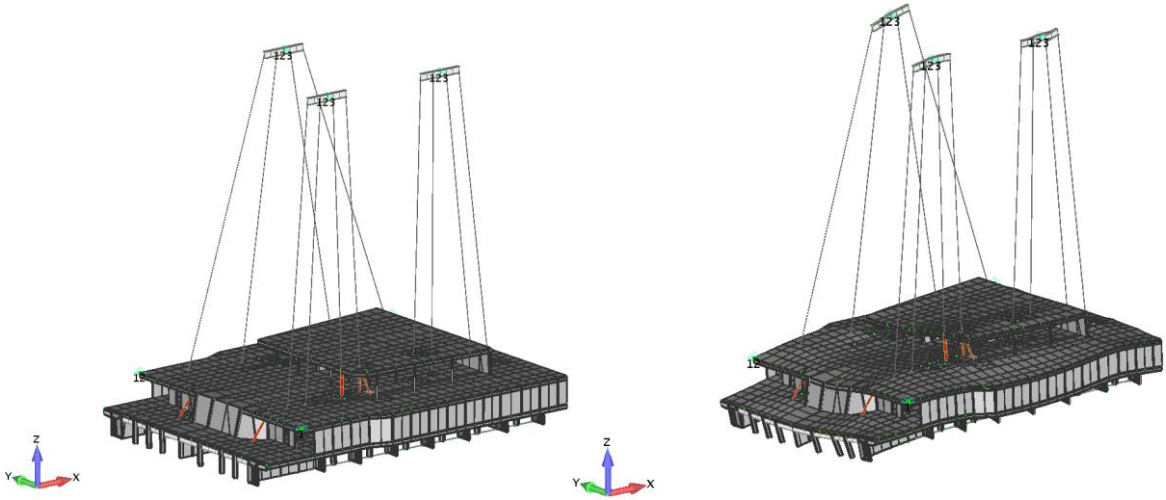

Figure 3.19: Case A: undeformed (left) and deformed (right) block lifting model in FEM.

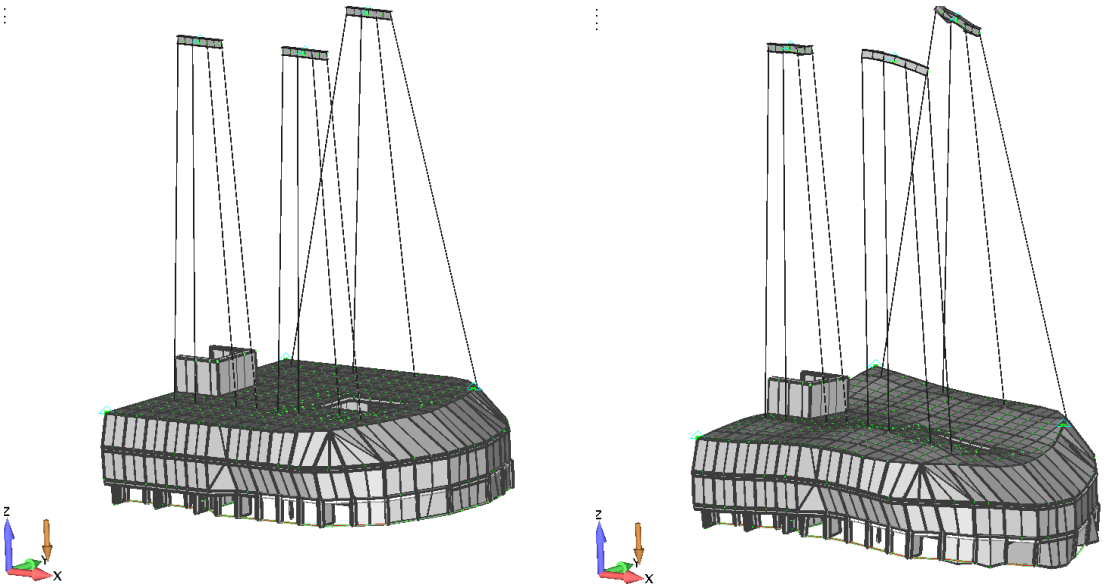

Figure 3.20 Case B: undeformed (left) and deformed (right) block lifting model in FEM.

3.6 Block lifting response

Block lifting response, similarly to global and local responses, is considered through rotations and displacements at the edge points of the web plates caused by the lifting phase.

The obtained results were grouped accordingly to the loading types presented in Generic loading chapter. The obtained results Figures 3.21, 3.22 and 3.23 show that block lifting causes only hogging or same way rotation condition for transverse webs. Rotations caused by the lifting load has the same order of magnitude as in global and local responses, however displacements caused by compression/tension load is significantly smaller compared to global response.

Figure 3.21: Block lifting plotted in load type 1 figure.

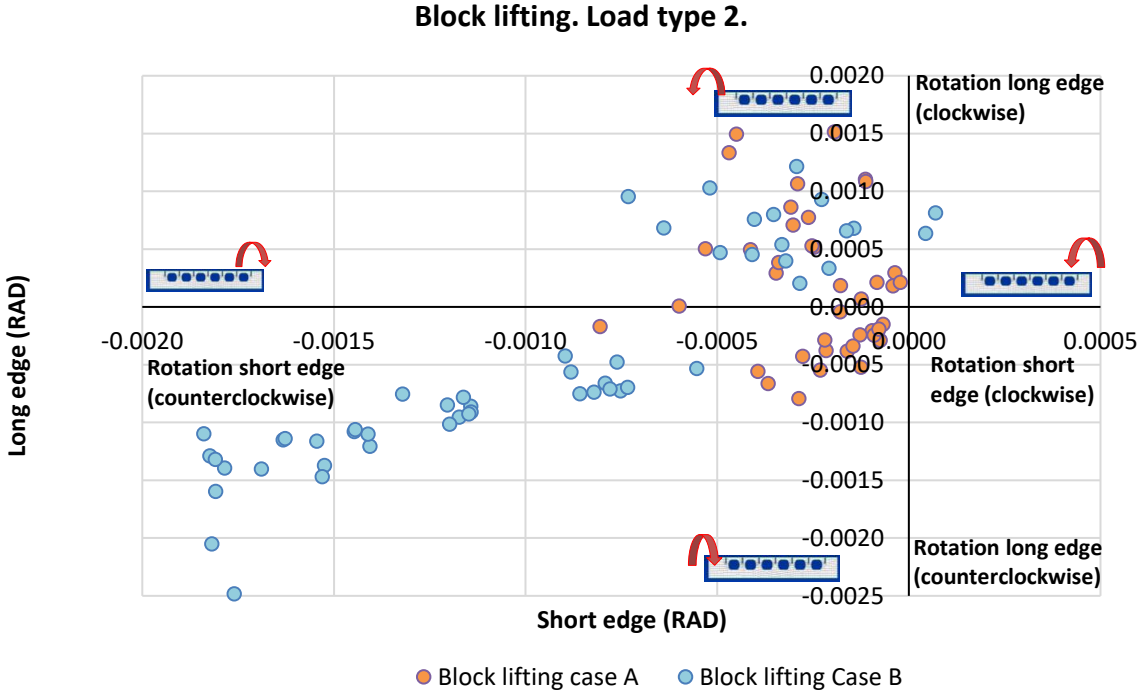

Figure 3.22: Block lifting plotted in load type 2 figure.

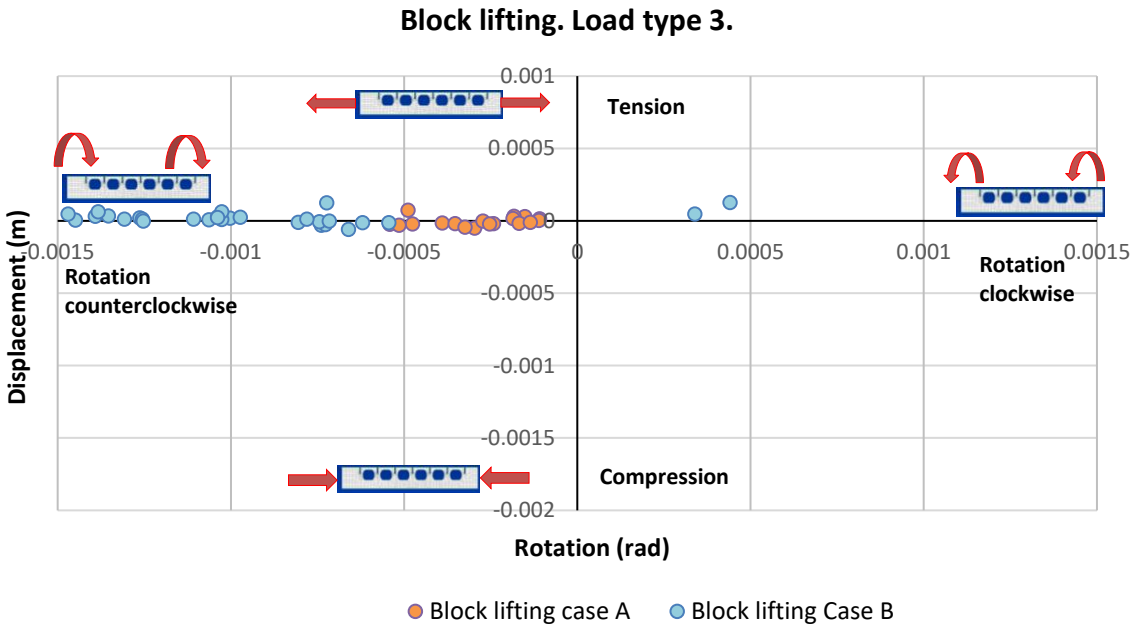

Figure 3.23: Block lifting plotted in load type 3 figure.

4 Case study 1: Effect of the tripping brackets

4.1 Studied geometry

The developed strength assessment method is applied to three web frame configurations. The main varied parameter in configuration 1, 2 and 3 is a number of Tripping Brackets (TB). The difference in load-carrying capacity between configurations is shown in the chapters Strength results and Post buckling.

The first model, Figure 4.1, includes 6 web openings, flange, deck and longitudinal deck's stiffeners. The deck thickness is 5,5 mm. Stiffeners profile is HP-120x7. The overall length of the model is 5,01 meters, while the breadth of attached deck plate is equal to web-frame spacing of 2,6 meters.

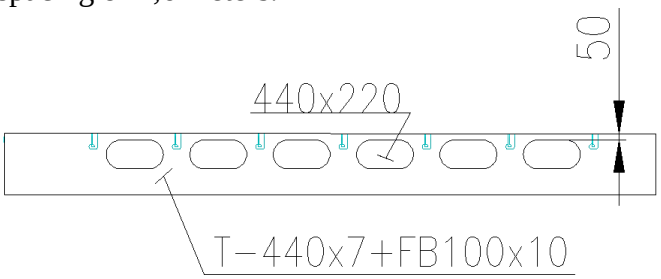

Figure 4.1: Dimensions of the web configuration without tripping brackets.

The finite element model of presented configuration can be found in Figure 4.2. There are 7457 active elements in the discretized model: 7091 shell elements (CQUAD elements - 7020, CTRIA3 elements - 71), 364 beam elements and 2 rigid elements. The average size of the elements is 50x50 mm resulting in 9 elements in web plate height, 2 elements in stiffener's web height and 2 elements in width of the web flange.

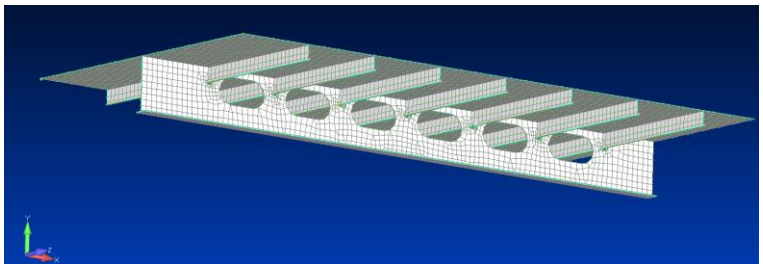

Figure 4.2: FE model of T-beam web without tripping brackets.

Second model, Figure 4.3, has the same dimensions as configuration one. The only difference is the presence of two tripping brackets. It should be noted that the following configuration currently used in modern passenger ships build by Meyer Turku Shipyard.

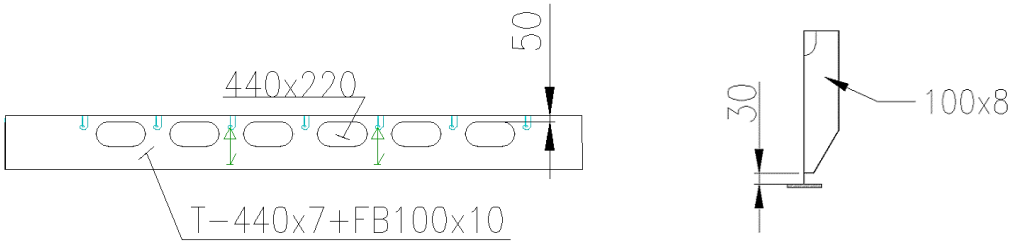

Figure 4.3: Dimensions of web configuration with 2 tripping brackets (left), tripping bracket dimensions (right).

The finite element model can be found in Figure 4.4. There are 7477 active elements in the discretized model: 7111 shell elements (CQUAD elements - 7038, CTRIA3 elements - 73),

364 beam elements and 2 rigid elements. The average size of the elements is 50x50 mm resulting in 9 elements in web plate height, 2 elements in stiffener's web height and 2 elements in width of the web flange.

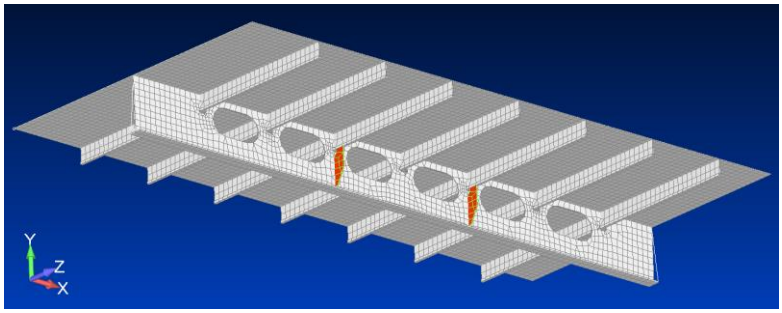

Figure 4.4: FE model of a T-beam web with 2 tripping brackets (red).

Third model, Figure 4.3, has the same dimensions as previous configurations. The only difference is the presence of a single tripping bracket, located under the middle longitudinal stiffener.

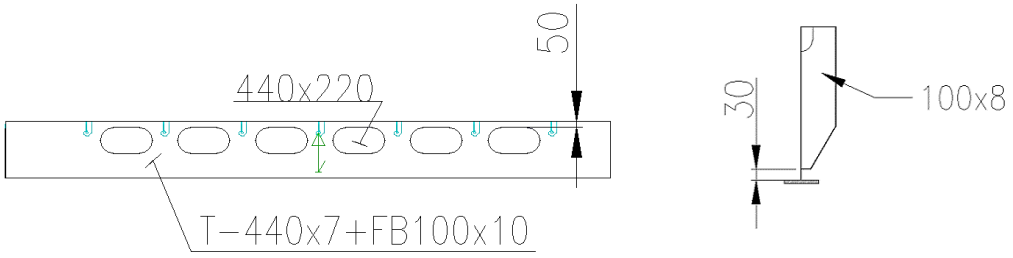

Figure 4.5: Dimensions of the web configuration with 1 tripping bracket (left), tripping bracket dimensions (right).

The finite element model can be found in Figure 4.4. There are 7494 active elements in the discretized model: 7128 shell elements (CQUAD elements - 7056, CTRIA3 elements - 72), 364 beam elements and 2 rigid elements. The average size of the elements is 50x50 mm resulting in 9 elements in web plate height, 2 elements in stiffener's web height and 2 elements in width of the web flange.

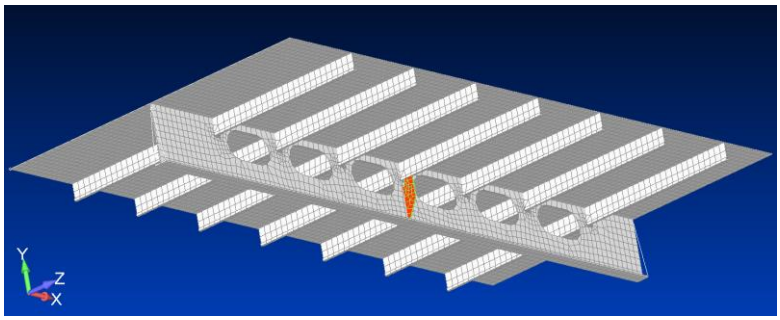

Figure 4.6: FE model of a T-beam web with 1 tripping bracket (red).

4.2 Strength results

The comparison between first yielding design curves in linear and nonlinear analysis shows:

Load type 1: axial compression / tension and equal rotations in opposite directions, **Figure 4.7.** The capacity of the web in quadrant IV is overestimated with linear analysis, where in other quadrants the capacity is almost always underestimated.

Load type 2: independent rotations at the ends, Figure 4.8. The first yielding design curve in linear analysis gives underestimation in buckling capacity in all quadrants compared to nonlinear study. However, in quadrants II and IV results match very closely.

Load type 3: axial compression / tension and equal rotations in the same direction, Figure 4.9. The first yielding design curve in linear analysis underestimate the load-carrying capacity of the structural in all four quadrants compared to nonlinear study.

The secondary x- and y-axis show the resulting strain from applied rotations and axial displacements respectively. Negative strain shows that T-beam is under compression whereas positive strain represents tension case.

Based on the results it is clear that linear analysis is not appropriate tool for identifying first yielding criteria for investigated T-beams.

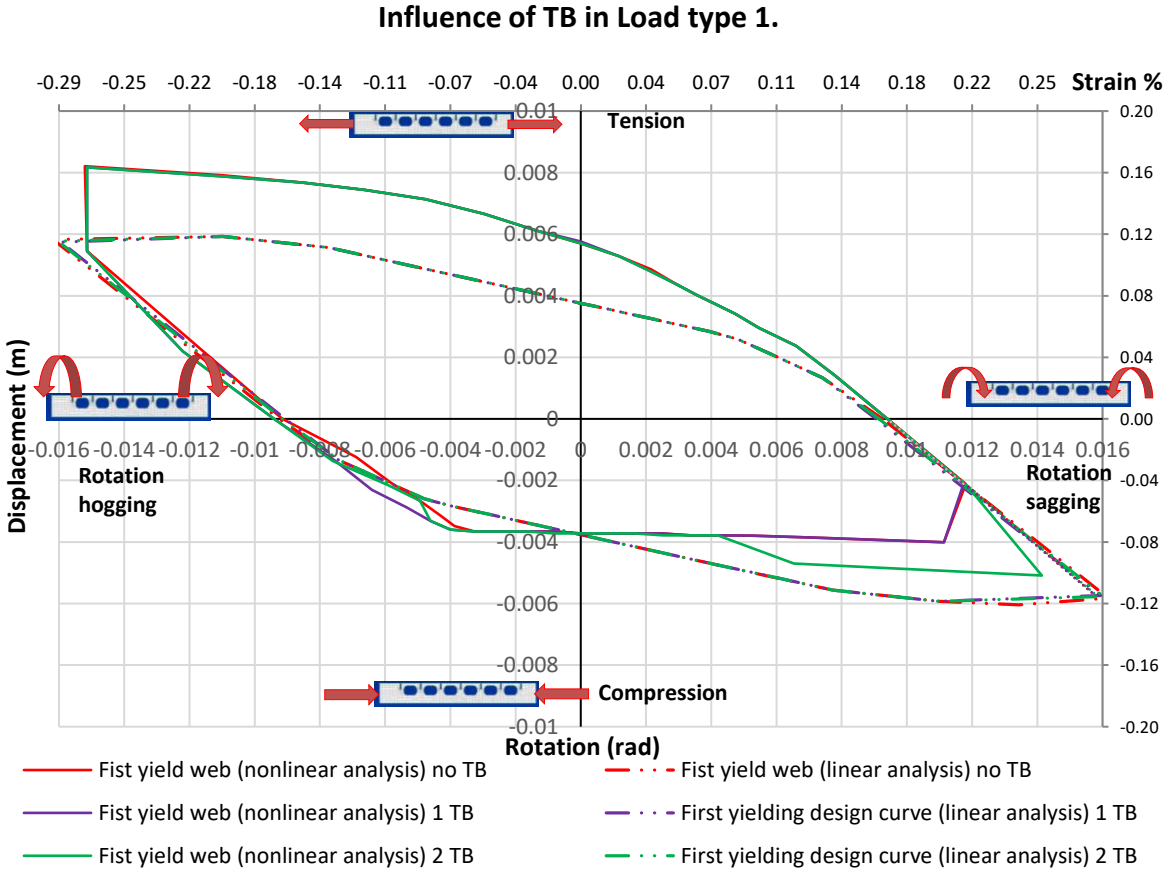

Figure 4.7: First yield in linear and nonlinear analysis plotted in load type 1 figure.

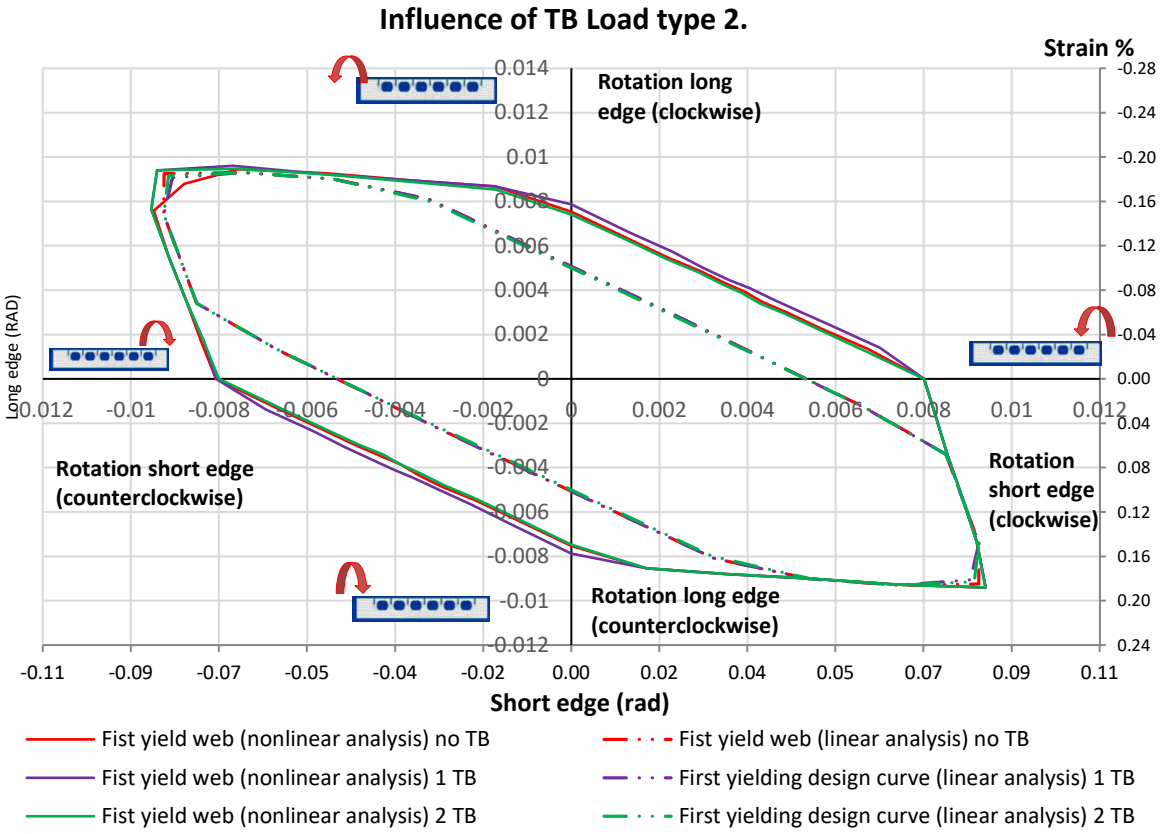

Figure 4.8: First yield in linear and nonlinear analysis plotted in load type 2 figure.

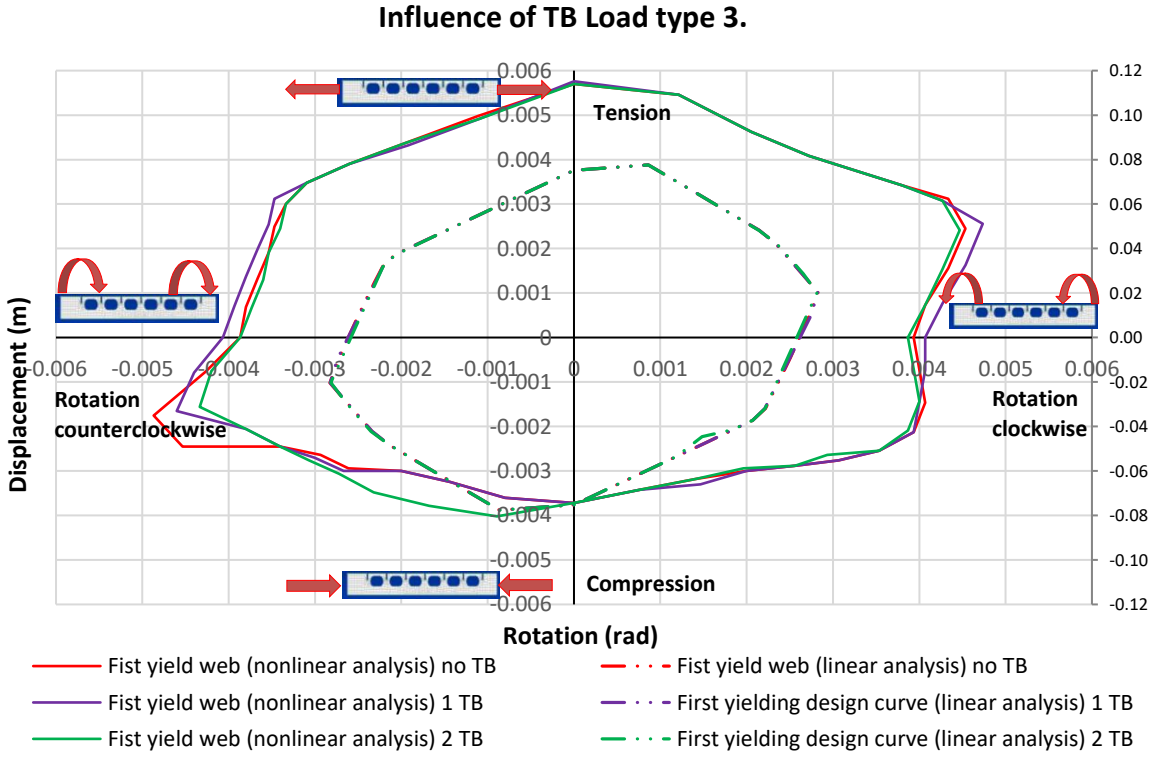

Figure 4.9: First yield in linear and nonlinear analysis plotted in load type 3 figure.

The comparative analysis between ULS and nonlinear yielding criteria in web and flange shows that ULS is reached when the T-beam flange buckles in a tripping mode. Failure mechanism can be split into two stages: first, the yielding occurs in a web plate and local buckling is initiated, then first yielding occurs in flange and finally the flange buckles in a tripping manner. Moment diagrams in case of flange tripping under the axial compression and bending in hogging presented in Figure B.1.

In the majority of cases the failure of the structure happens by yielding alone, no flange tripping. First, the deck reaches the yield limit, afterwards the web plate yields. Such failing mechanism prevents structure from sudden global (flange) buckling. Thus, the moment diagrams in Figures B.2 and B.3 do not show sudden drop in constraint moment. However, in some cases the web buckled in a tripping manner occurred after the local yielding.

The comparison between stress (yielding in web and flange) design curves and ULS obtained from nonlinear analysis shows:

Load type 1: axial compression / tension and equal rotations in opposite directions, **Figure 4.10**. The ULS is only recorded when sudden drop in the moment is present: quadrant III and several cases in quadrant II and IV. The ULS limit is almost coincide with first yielding in flange in compression/hogging case, Quadrant 3. The first yield in flange is not reached in all cases in quadrants II and IV.

Load type 2: independent rotations at the ends, Figure 4.11. The ULS is only recorded when sudden drop in the moment is present: quadrant II and several cases in quadrant I and III. The structure has an additional capacity between first yielding in web/flange and ULS. In quadrants I & III, flange yields significantly later than web plate, whereas in quadrants II and IV flange yield almost immediately after the web reaches yield limit.

Load type 3: axial compression / tension and equal rotations in the same direction, Figure 4.12. The ULS is only recorded when sudden drop in the moment is present: quadrants III and IV. In all cases, except single case in tension and clockwise rotation, first yielding in flange initiated significantly later than in web plate. In axial compression case ULS has a quite close match with first yielding in flange; while moving away from pure axial load the difference is increasing.

Overall, the ULS capacity of T-beam with two TB is higher compared to configuration with single TB and zero TB cases. The first yielding in the flange is initiated almost simultaneously in all cases regardless from number of TB while first yield in web has minor difference depending on the loading conditions. It should be reminded that the difference in web plate yielding is very much affected by the quality of the mesh as mentioned in the chapter Stress (yielding) criteria.

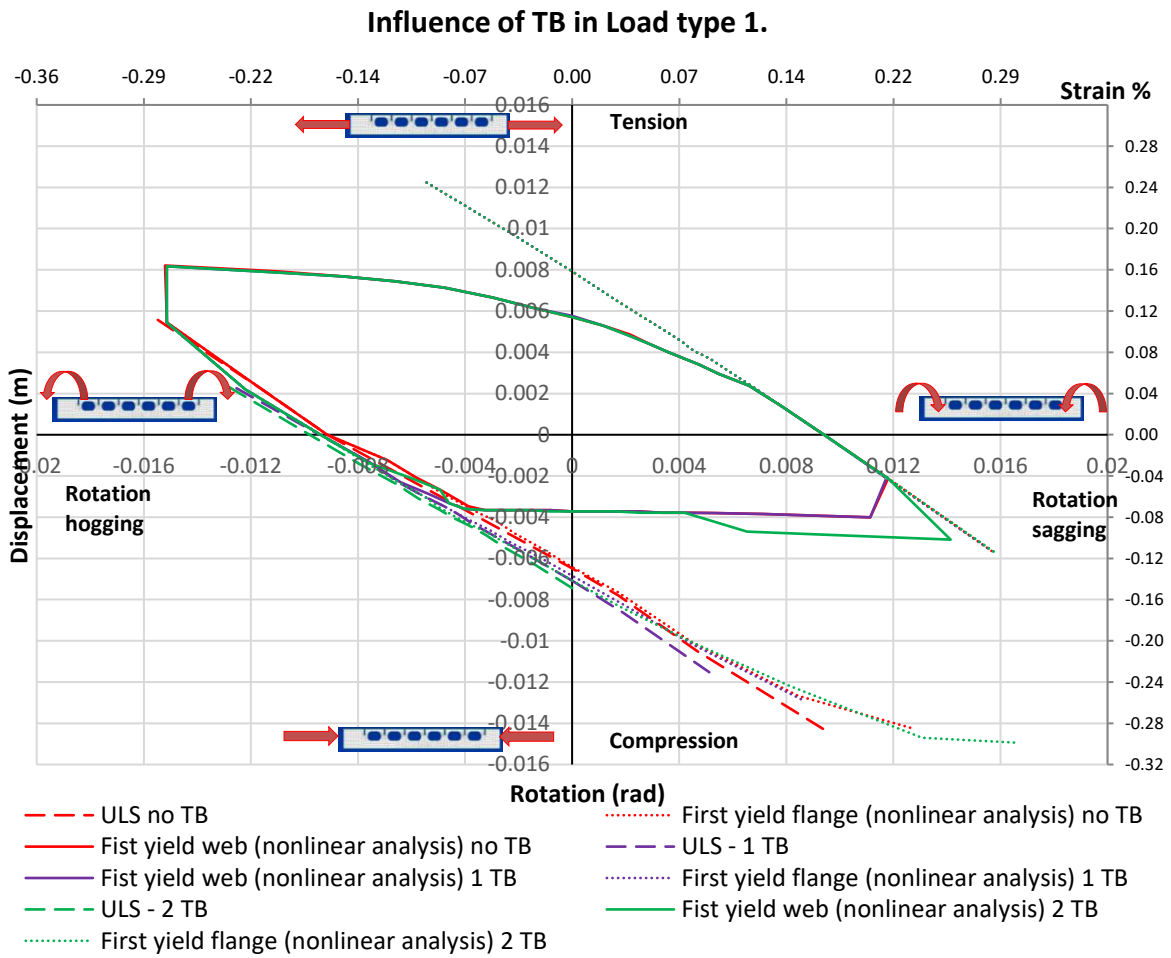

Figure 4.10: ULS, first yielding in web and flange plotted in load type 1 figure.

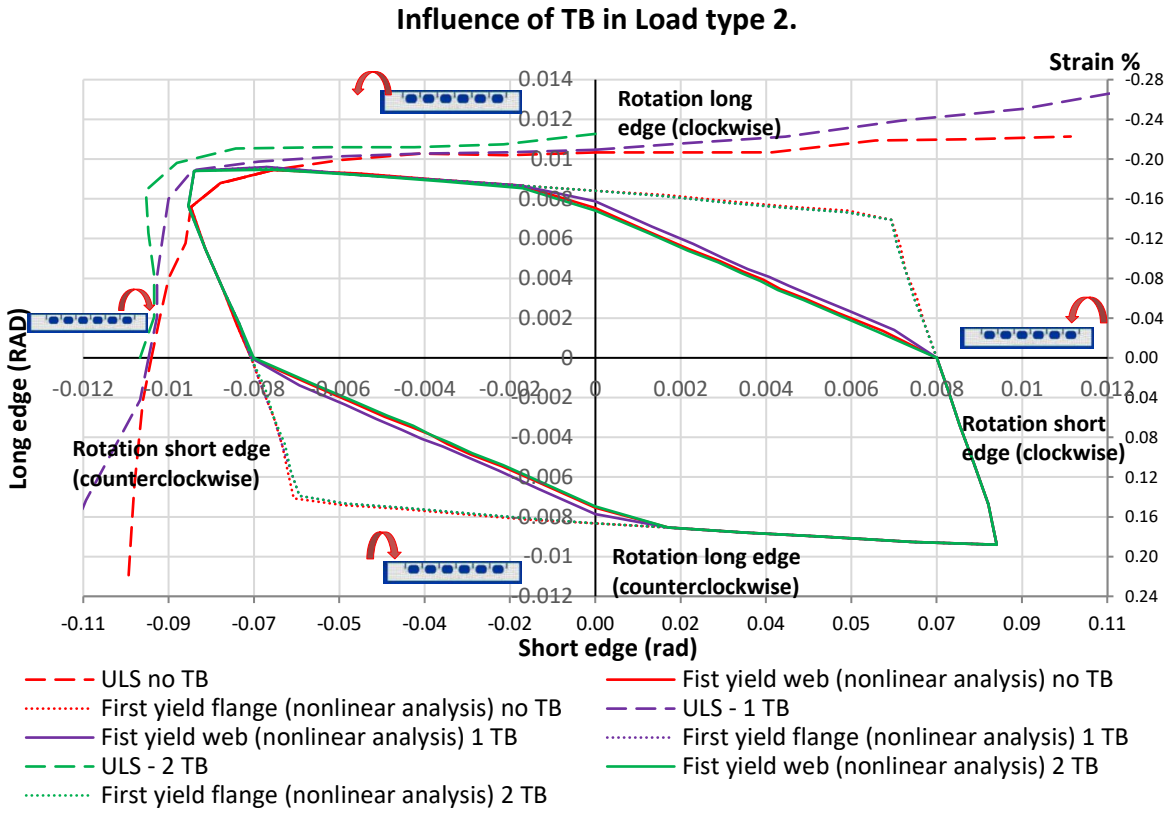

Figure 4.11: ULS, first yielding in web and flange plotted in load type 2 figure.

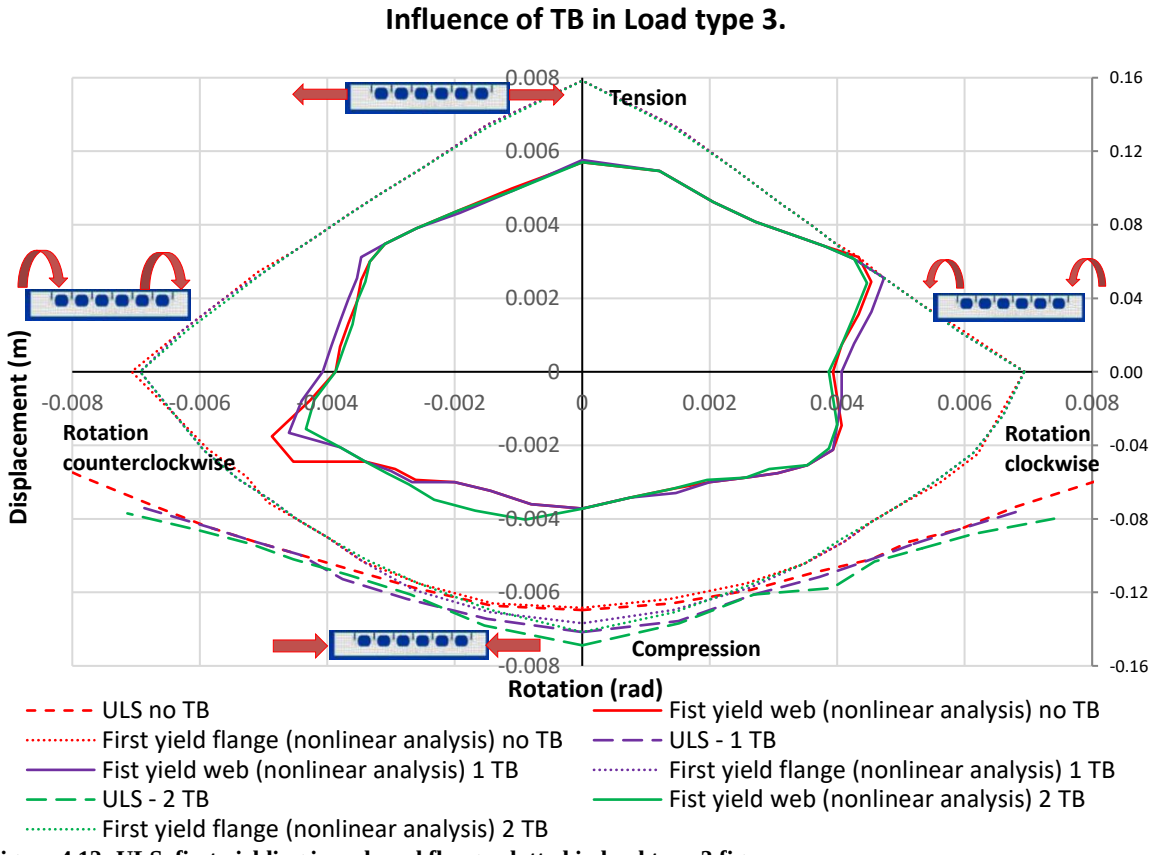

Figure 4.12: ULS, first yielding in web and flange plotted in load type 3 figure.

4.3 Post buckling

To evaluate the rapidness of stability loss, post buckling parameter is introduced. The post buckling point, Figure 4.13, captures the total constraint moment when prescribed rotation and displacement (generic load) reach maximum value.

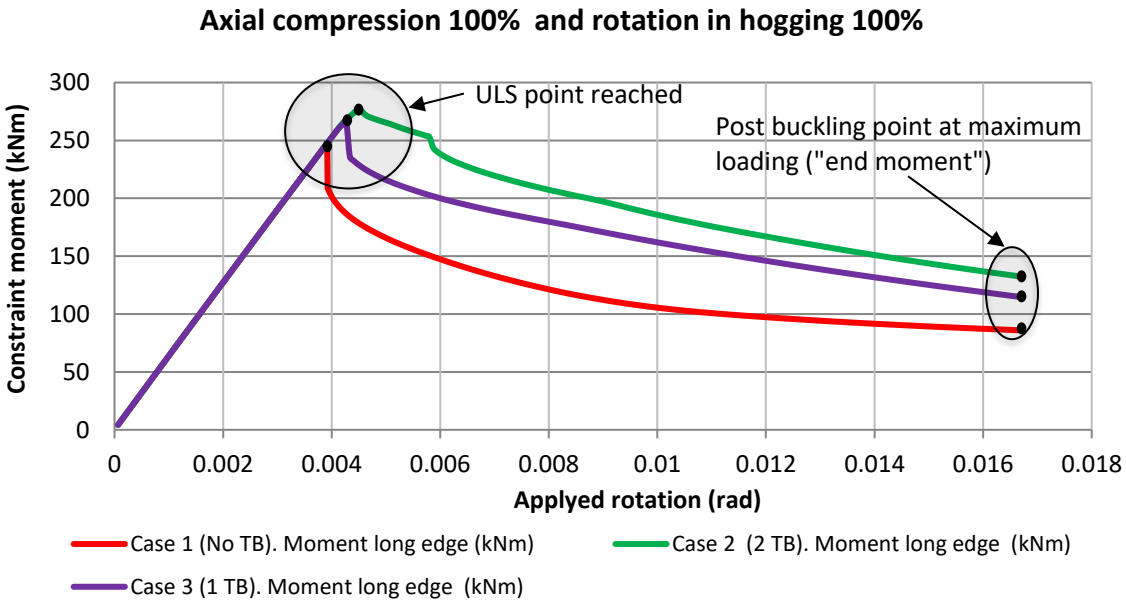

Figure 4.13: Ultimate limit state and post buckling parameter.

The numerical results for ULS and post buckling behavior can be found in Figures C.1, C.2, C.3 and C.4. The average difference in percentage between ULS and post buckling capacities in case of 0, 1 and 2 TB can be seen in Table 4.1.

Table 4.1: Average difference in ultimate limit state and post buckling between cases with 0, 1 and 2 TB.

Case	Average difference in ULS (max) and post buckling (end) capacities							
	Max (ULS) moment long %	End moment long %	Max (ULS) force %	End Force %	Max (ULS) moment short %	End moment short %	MAX (ULS) Moments and Force combined	END Moments and Force combined
Load type 1, Quadrant III. Axial compression and Rotation in hogging								
2 TB	11,57	76,23	7,71	32,50	11,92	86,44	10,40	65,06
1 TB	8,77	40,19	6,54	22,58	8,89	36,17	8,07	32,98
0 TB	0	0	0	0	0	0	0	0
Load type 2, Quadrant II. Clockwise and counterclockwise rotation								
2 TB	6,10	78,85	-	-	8,51	42,88	7,30	60,87
1 TB	3,71	46,56	-	-	3,22	19,11	3,47	32,84
0 TB	0	0	0	0	0	0	0	0
Load type 3, Quadrant III. Axial compression and Rotation counterclockwise								
2 TB	10,80	79,70	3,60	16,65	2,25	32,10	5,55	42,82
1 TB	3,42	34,58	-0,10	9,74	1,81	14,13	1,71	19,48
0 TB	0	0	0	0	0	0	0	0
Load type 3, Quadrant IV. Axial compression and Rotation clockwise								
2 TB	1,84	46,11	4,24	16,32	6,66	73,00	4,25	45,14
1 TB	0,80	17,91	2,27	9,20	2,87	40,02	1,98	22,38
0 TB	0	0	0	0	0	0	0	0

The overall average difference among all load cases shown in Table 4.2. ULS with 2 TB is 7% higher compared to case without TB, while the capacity with single TB is increased only by 4 %. In contrast, post buckling capacity when TB is present is significantly higher

compared to unstiffened web configurations. Resulting post buckling capacity increases by 27% in case of single TB and by 53% in case of two TB.

Table 4.2: Overall average difference in ULS and post buckling capacity between cases with 0, 1 and 2 TB.

Average difference between case studies (all loading cases)		
Case	ULS Moments and Force combined	END Moments and Force combined
2 TB	6,88	53,47
1 TB	3,80	26,92
0 TB	0	0

The main difference in post buckling behavior is caused by the initiated buckling modes, Figure C.5. In case of 0 TB the whole flange buckles in a tripping mode, while in configuration with a single TB buckling of the flange is split into two half-waves creating an S-shape buckling. In case of 2 TB the buckling of the flange mostly occurs locally between two tripping brackets. Presence of TBs significantly reduces plastic deformations; thus, the greatest deformations occur in unstiffened T-beams.

5 Case study 2: Magnitude of production loads

5.1 Cumulative production load

Cumulative production load considers the potential effects from construction phase. Steel structure often gets deformed during the construction phase due to frequent impacts, welding, assembling procedures, transportation, excessive inner stress, post heating treatment, block assembly, etc. Each phase in production causes imperfections and eccentricities in steel elements (European Commission, Directorate-General for Research and Innovation, 2012). As a result of cumulative production load the defects rarely occur in production phase, Figure 5.1.

Production defects are usually corrected by a thermal technique, i.e. frame straightening. The process is complicated and well established only for a limited number of basic geometries. Flame straightening of the deck plate can cause additional stress in T-beams. Therefore, the accuracy and quality of flame straightening is highly dependent on knowledge and experience of operator (European Commission, Directorate-General for Research and Innovation, 2012). Flame straightening procedures are often required during shipbuilding process since the actual magnitude and types of production load are not well known.

Figure 5.1: Production phase: defects in T-beams.

Based on production reports from Meyer Turku shipyard T-beams with flange 100x10 mm and 2 TB were subjected to buckling during the production phase, Figure 5.1. However, T-beams with wider flange 150x10 mm have never been reported to buckle. Thus, the range of cumulative production load can be found by performing comparison analysis of ULS between two above mentioned T-beam configurations.

5.2 Studied geometry

The configuration of T-beam with 2 TB and flange 150x10 has the same dimensions as 2 TB model presented in Case study 1: Effect of the tripping brackets, except of the wider flange. Dimensions of the model and tripping brackets can be found in Figure 4.3.

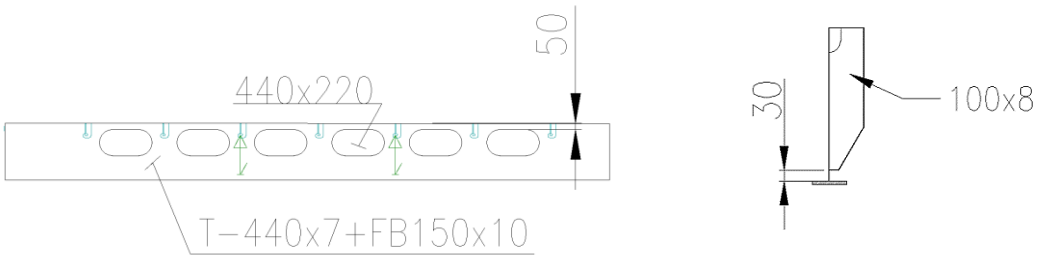

Figure 5.2: Dimensions of the web configuration with 2 tripping brackets (left), tripping bracket dimensions (right).

The finite element model of presented configuration can be found in Figure 4.4. There are 7477 active elements in the desacralized model: 7111 shell elements (CQUAD elements - 7038, CTRIA3 elements - 73), 364 beam elements and 2 rigid elements. The average size of the elements is 50x50 mm resulting in 9 elements in web plate height, 2 elements in stiffener's web height and 2 elements in width of the web flange.

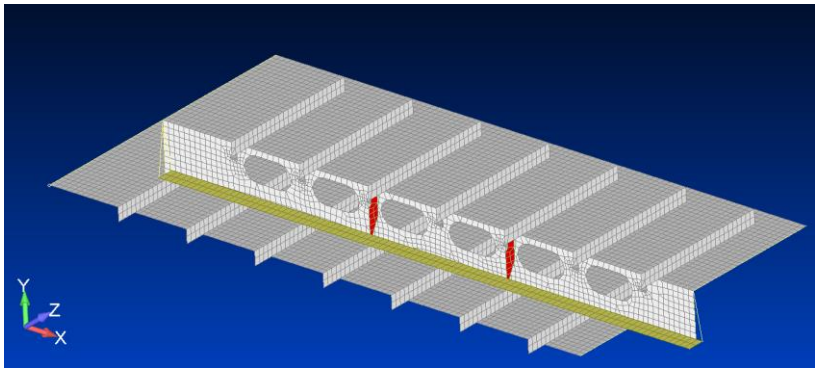

Figure 5.3: FE model of a T-beam web with 2 tripping brackets (red) and flange 150x10 mm (yellow).

5.3 Results

The obtained results show the cumulative production load range, Figures 5.4, 5.5 and 5.6. In case of axial compression and tension and rotation in sagging and hogging the capacity of ULS in not increased considerably. However, in case of clockwise/counterclockwise rotation and axial compression/ tension and rotation clockwise /counterclockwise the increase in buckling capacity is significant.

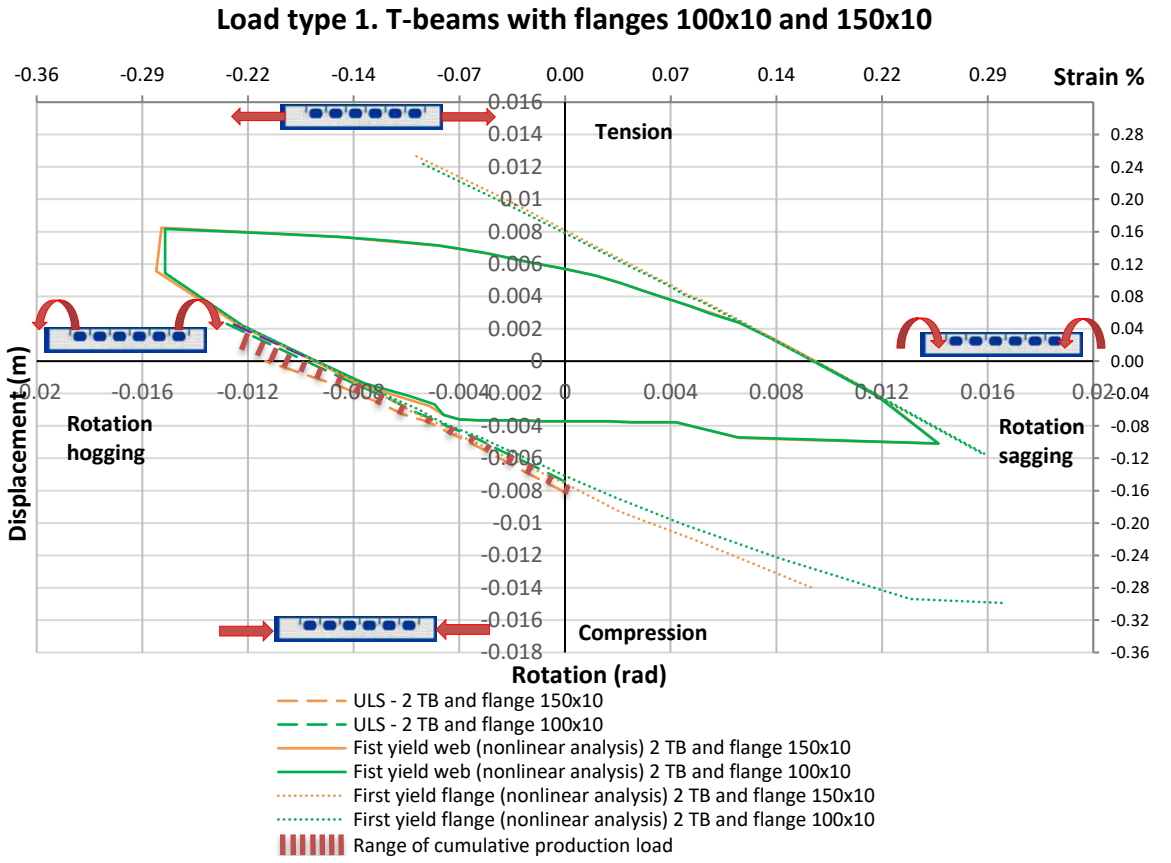

Figure 5.4: Capacity of T-beams with flanges 100x10 and 150x10 plotted in load type 1 figure.

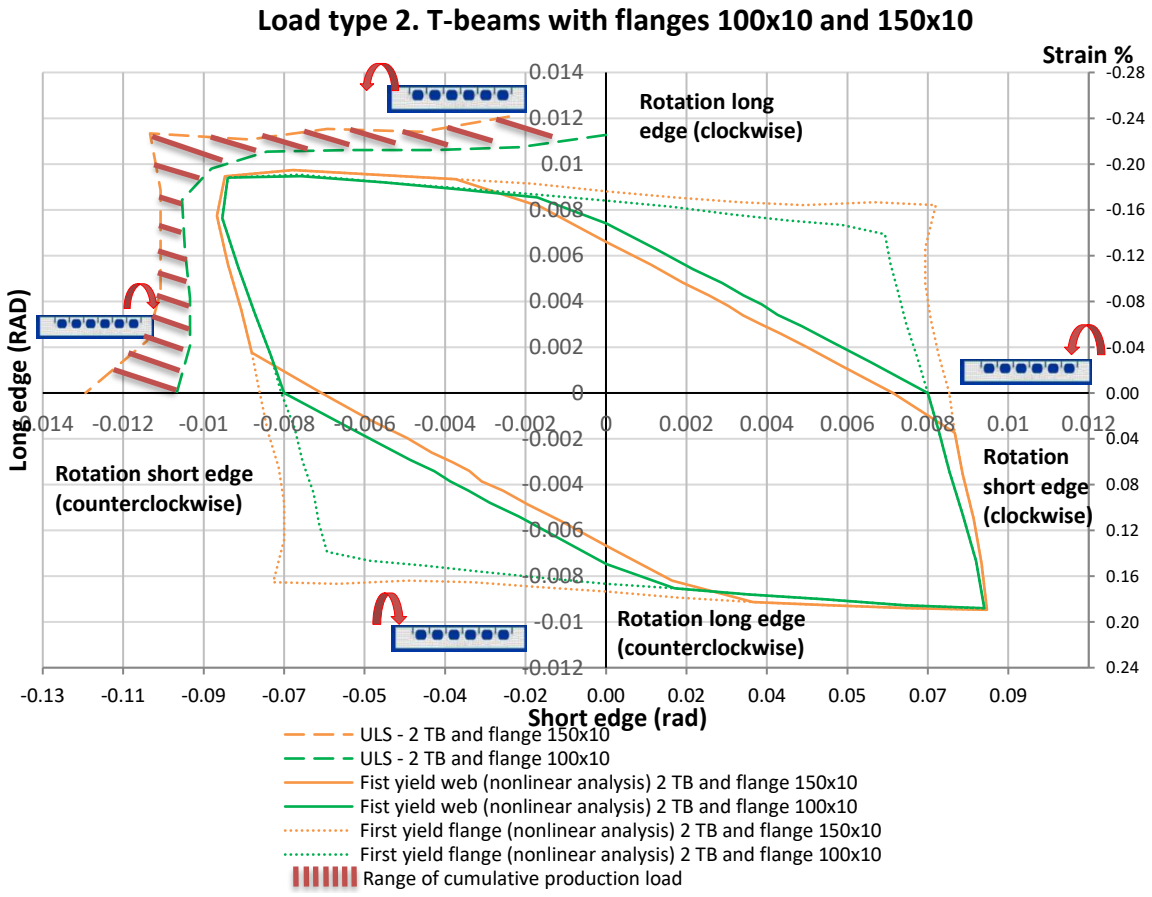

Figure 5.5: Capacity of T-beams with flanges 100x10 and 150x10 plotted in load type 2 figure.

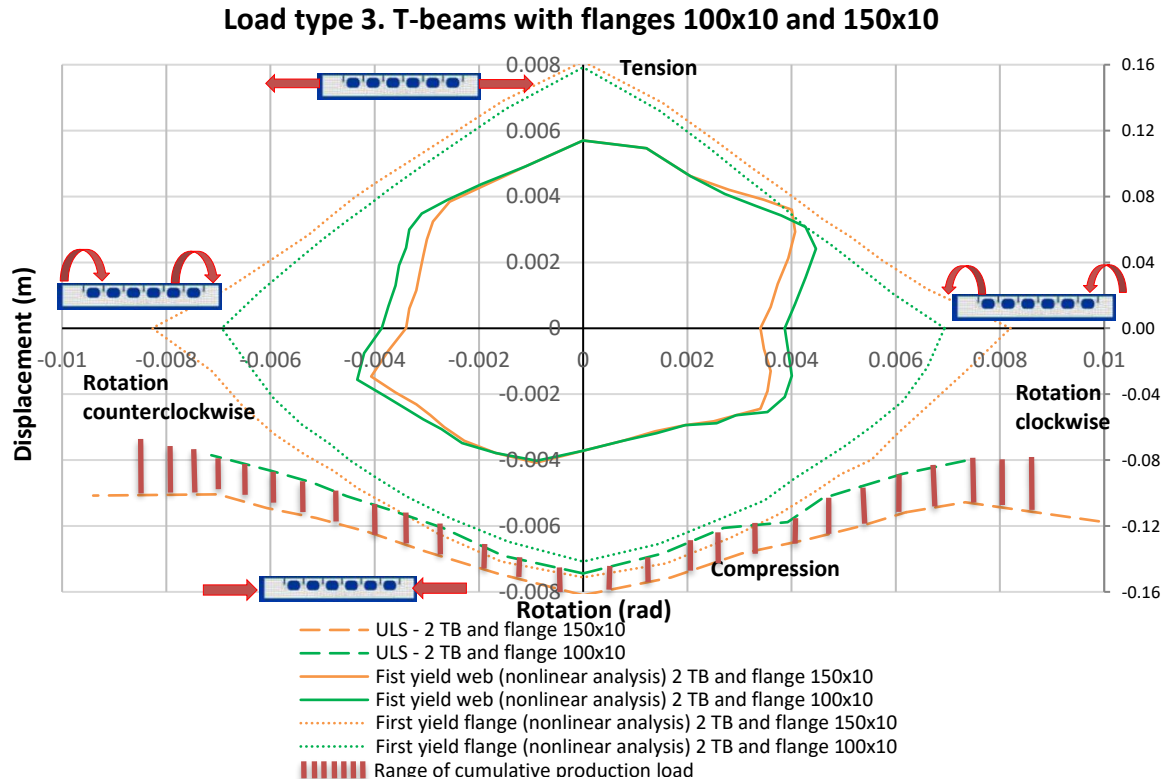

Figure 5.6: Capacity of T-beams with flanges 100x10 and 150x10 plotted in load type 3 figure.

The numerical results for ULS and post buckling behavior for all load cases can be found in Figure D.1. The average difference between ULS and post buckling capacities in case of wider flange can be seen in Table 5.1.

Table 5.1: Average difference in ultimate limit state and post buckling capacities in case of wider flange 150x10 mm.

Case	Average difference in ULS (max) and post buckling (end) capacities							
	Max (ULS) moment long %	End moment long %	Max (ULS) force %	End Force %	Max (ULS) moment short %	End moment short %	MAX (ULS) Moments and Force combined	END Moments and Force combined
Load type 1, Quadrant III. Axial compression and Rotation in hogging								
2TB flange 150x10	31,34	58,79	15,01	17,27	31,56	58,95	25,97	45,00
2TB flange 100x10	0	0	0	0	0	0	0	0
Load type 2, Quadrant II. Clockwise and counterclockwise rotation								
2TB flange 150x10	62,70	39,28	-	-	88,17	80,71	75,43	60,00
case 2TB flange 100x10	0	0	0	0	0	0	0	0
Load type 3, Quadrant III. Axial compression and Rotation counterclockwise								
2TB flange 150x10	45,91	49,73	10,00	10,25	26,56	33,41	27,49	31,13
2TB flange 100x10	0	0	0	0	0	0	0	0
Load type 3, Quadrant IV. Axial compression and Rotation clockwise								
2TB flange 150x10	25,50	46,62	12,04	13,28	81,84	46,02	39,79	35,31
2TB flange 100x10	0	0	0	0	0	0	0	0

The overall average difference among all load cases is presented in Table 5.2. Both ULS and post buckling capacity are increased, in case of wider flange compared to 100x10 mm flange, by 42% and by 43% respectively.

Table 5.2: Overall average difference in ULS and post buckling capacity between the cases with flanges 100x10 mm and 150x10mm.

Average difference between case studies (all loading cases)		
Case	ULS Moments and Force combined	END Moments and Force combined
2TB flange 150x10	42,17	42,86
2TB flange 100x10	0	0

The main difference in post buckling behavior is caused by the initiated buckling modes, Figure D.2. T-beam with 150x10 mm flange is only subjected to a local buckling, whereas T-beam with 100x10 mm flange is exposed to a higher plastic deformations inducing tripping buckling mode.

6 Design safety against realistic loads

The applied strength assessment showed that the realistic loads occurred during operation in sagging, hogging and racking are significantly lower than capacity of transversal T-beam webs. Although, one should understand that deck pressure, global still water and wave load may act simultaneously during the operation. Thus, it is decided to compare combined contribution from global and local loads against ULS.

The obtained results in Figures 6.1, 6.2 and 6.3 show that the most severe combined contribution from global and local loads is still several times smaller than the critical load which causes yielding in a web plate. However, the cumulative production load can may be higher than capacity of the T-beams with 0, 1 and 2 TBs.

Considering the fact that cumulative production load can be so high, the T-beam webs might already be at post buckling stage during the operation. The consequences in such case may lead to significant reduction in load carrying capacity of T-beams.

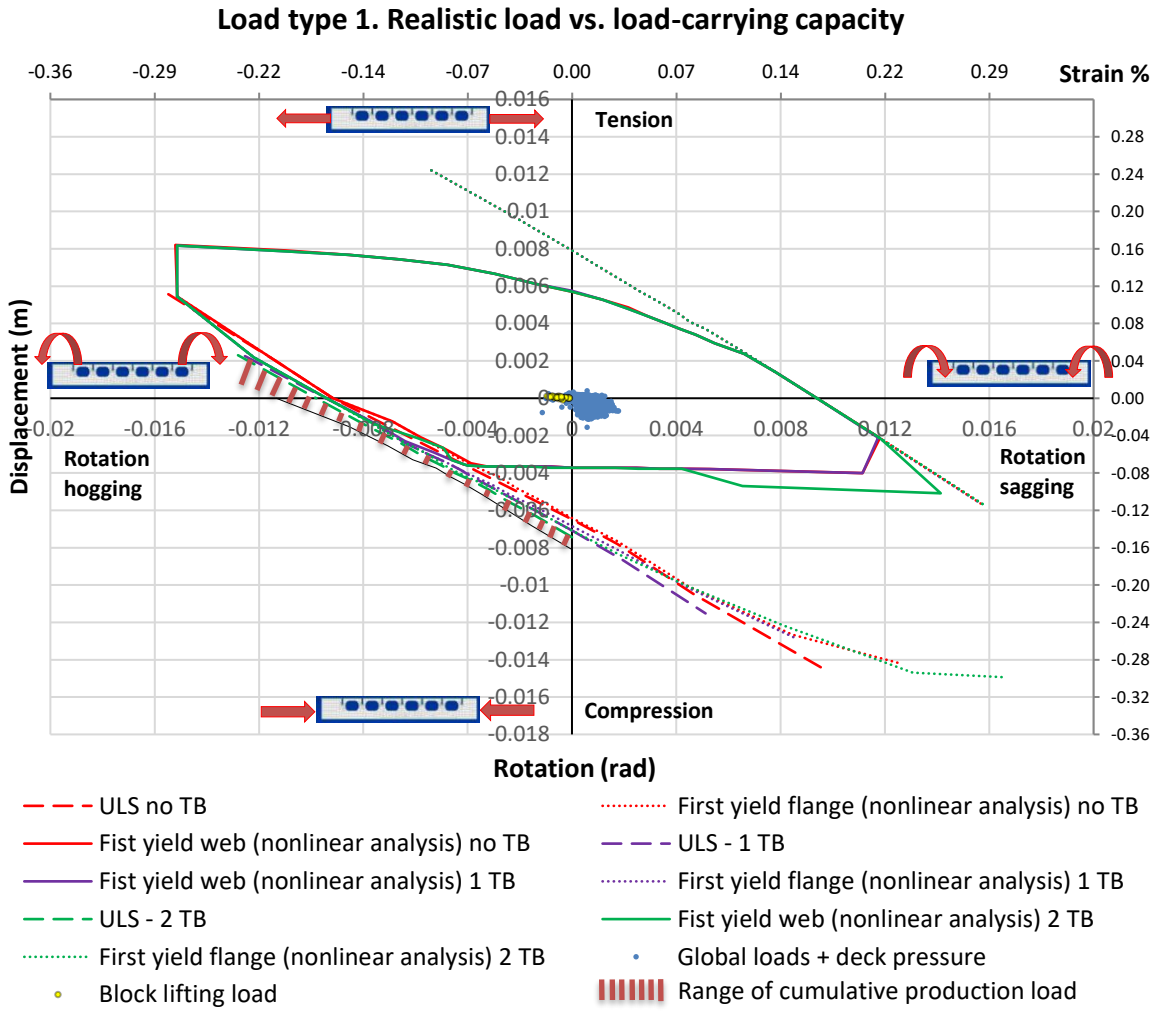

Figure 6.1: Realistic load and load-carrying capacity plotted in load type 1 figure.

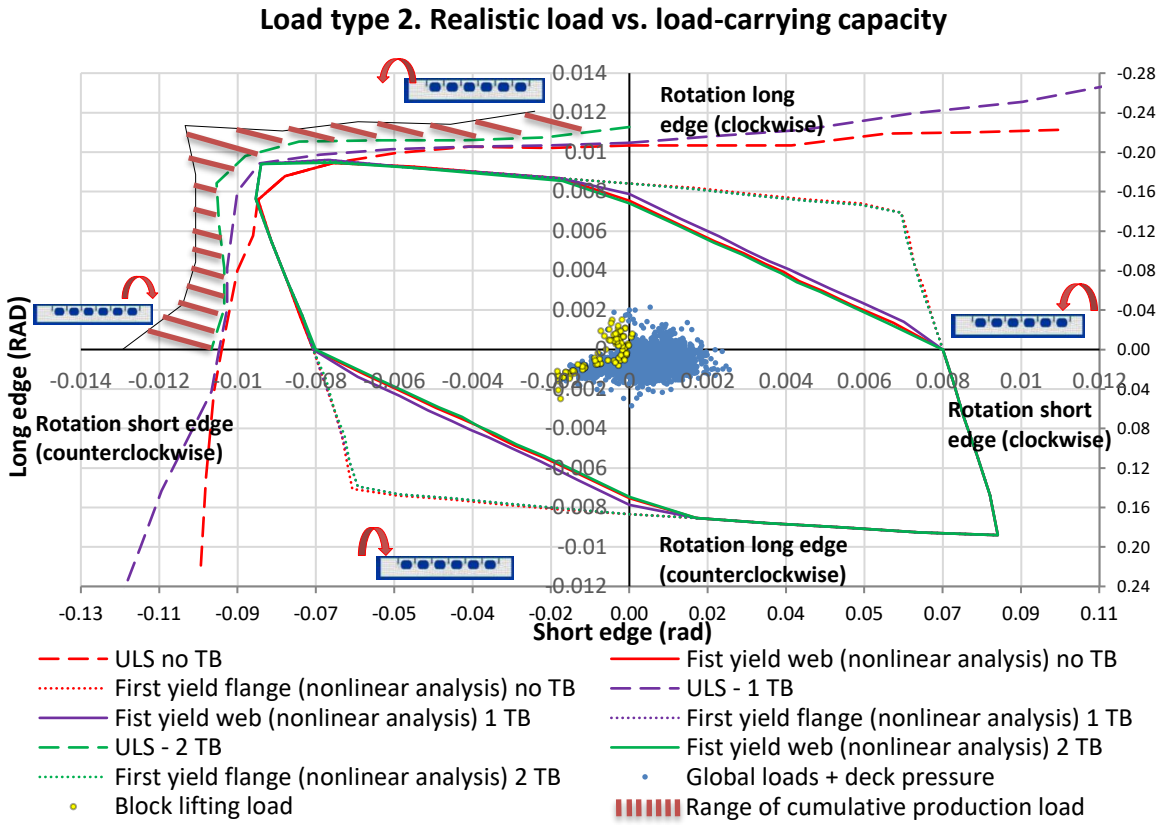

Figure 6.2: Realistic load and load-carrying capacity plotted in load type 2 figure.

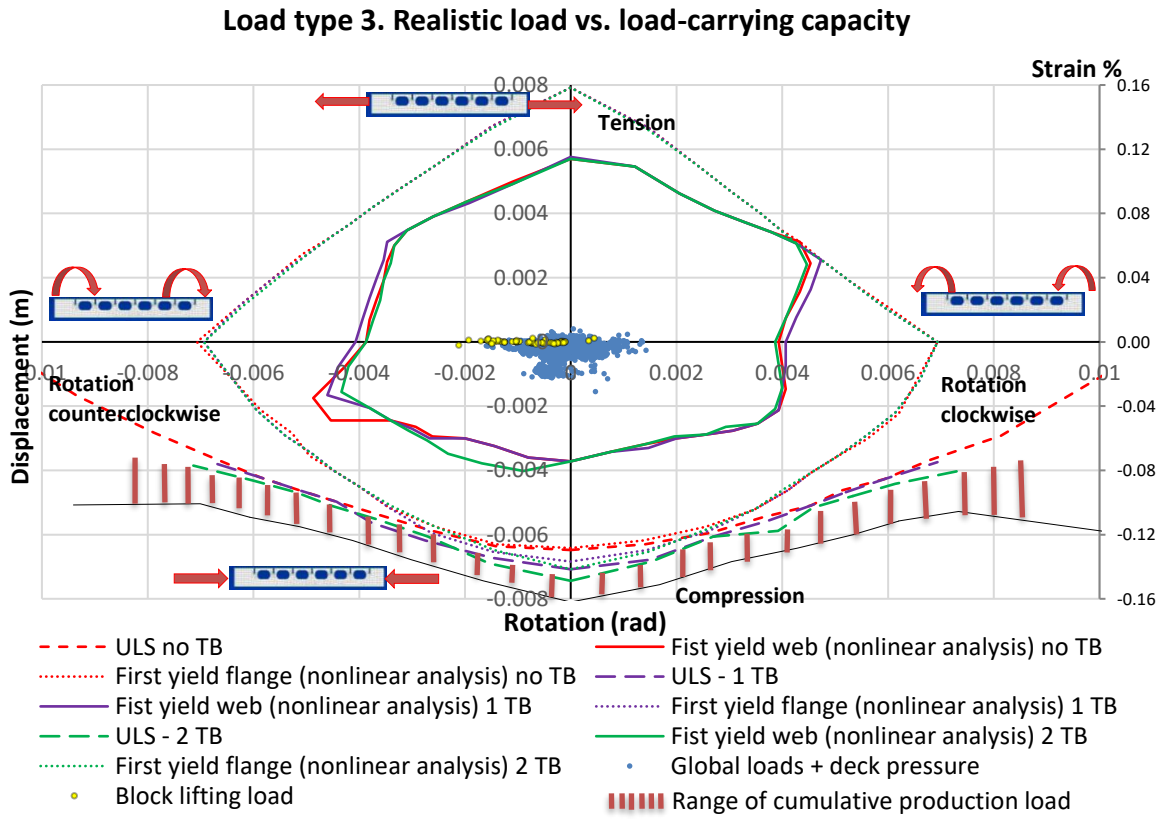

Figure 6.3: Realistic load and load-carrying capacity plotted in load type 3 figure.

7 Discussion

During the operation, ship is exposed to global still water and wave loads, deck pressure and other minor local loads. The main assumption regarding the loads in the study is to neglect out of plane loads, i.e. realistic loads are considered as 2D problem. However, there might be some cases where out of plane loads make considerable contribution to obtained loads.

The presented method is based on nonlinear study with limited number of steps per analysis and iterations per step. The accuracy of obtained result is strongly depended on chosen parameters for nonlinear FEA. Based on the sensitivity analysis the most appropriate parameters to provide the best accuracy/time ratio were chosen. Future studies might involve more time consuming and accurate parameters for the analysis.

The presence of initial imperfections and residual stresses is omitted in the work. The welding of tripping brackets and flange to a web leads to an increase in residual stress concentrations. The combined effect of stiffeners and welding residual stress was studied by (Smith & Kirkwood, 1977) and later by (Fujikubo & Yao, 1999; Gannon, et al., 2010). It was discovered that in some cases the buckling strength of stiffened panels in bulk carriers have almost the same buckling strength as simply supported plate without residual stress. In some cases, the expected increase in the buckling strength due to stiffening was counteracted by arise of residual stresses. The long span plates under tripping mode have less buckling capacity compared to simply supported panels. However, the presence of tensile residual stress next to the flange welds (area of maximum horizontal displacement) may improve buckling strength.

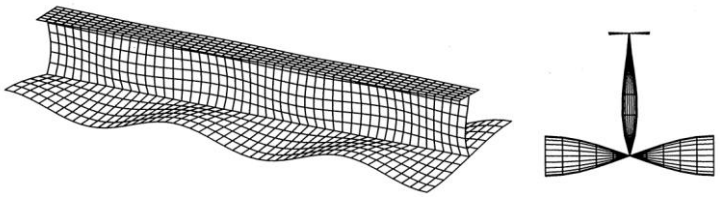

Figure 7.1: Tripping mode of a stiffener with tee profile (Fujikubo & Yao, 1999).

Possible future improvement of the presented strength assessment method is to consider the production load more thoroughly. The study requires monitoring systems on web plates at the initial phase of production. This approach will allow capturing entire production load range at each phase: cutting out web openings, welding of the flange, welding of tripping brackets, welding to the deck, block lifting, block balancing, grand block assemble and deck straightening.

8 Conclusion

Increasing manufacturing automation and reducing the number of structural parts would help increasing productivity at shipyards. Potential target for the improvements is the design of transversal T-beams. This thesis presents strength assessment method for evaluation transversal T-beam webs in cruise ships.

The method is based on nonlinear finite element analysis and includes calculation of 120 individual loads. The loading types consist of three sets: axial compression / tension and equal rotations in opposite directions, independent rotations at the ends (i.e. shear case), and axial compression / tension and equal rotations in the same direction.

The method is applied to a several web configurations in case study one. The aim is to compare the effect of the tripping brackets. Ultimate limit state capacity is reached when the flange of the T-beams buckles in a tripping mode. Both ULS and yielding strength criteria had a good match in all investigated cases regardless from the number of TB. In contrast, post buckling behavior showed more difference among the cases with 0, 1 and 2 tripping brackets.

In case study two, cumulative production load from transportation, welding, blocks balancing, block lifting etc. is studied. The order of magnitude of production load was found by comparing the ULS of buckled and unbuckled web configurations. Currently, there is no practical approach on how to model and consider loads at all stages of production in strength assessment.

The main realistic loading conditions of ship operation were presented. Realistic loading is compared against strength criteria in yielding and buckling obtained by generic load. The presented strength assessment method showed that cumulative production load can be significantly higher than combined contribution from global and local realistic loads.

References

European Commission, Directorate-General for Research and Innovation, 2012. *Optimisation and improvement of the flame straightening process (Optistraight).* s.l.:European Union.

Lloyd's Register, 2012. Ro-Ro Ships Direct Calculation Procedure. In: *Primary Structure of Ro-Ro Ships.* s.l.:s.n.

Abrate, S., 2008. Criteria for Yielding or Failure of Cellular Materials. *Journal of Sandwich Structures and Materials,* Volume 10.

Bashir Ahmed Memon & Xiaozu Su, 2004. Arc-length technique for nonlinear finite element analysis. *Zhejiang University Science,* 5(5), p. 618–628.

Brubak, L., 2016. *Advanced Buckling & Panel Ultimate Limit State (PULS). Technical Seminar. DNVGL AS.*. s.l.:s.n.

Brubak, L. & Hellesland, J., 2008. Strength criteria in semi-analytical, large deflection analysis of stiffened plates in local and global bending. *Thin-Walled Structures,* Issue 46, pp. 1382-1390.

Chow, F. Y. & Narayanan, R., 1984. Ultimate capacity of uniaxially compressed perforated plates. *Thin-Walled Structures,* pp. 241-264.

Crisfield, M. A., 1980. *Incremental/iterative solution procedures for nonlinear structural analysis.*. Swansea, Pineridge Press.

Degenhardt, R., Rohwer, K., Wagner, W. & Delsemme, J., 2004. *Postbuckling and collapse analysis of CFRP stringers stiffened panels – a GARTEUR activity. Procs. Forth Int. Conf. Thin- Walled Str.*. Loughborough, IOP Publishing Ltd.

Det Norske Veritas, 2006. *Classification notes No. 31.2 Strength Analysis of Hull Structure in Roll on/Roll of Ships and Car Carriers.* s.l.:s.n.

DNV GL AS, 2016. *DNVGL-CG-0128: Class Guideline – Buckling.* s.l.:s.n.

DNV, 2009. *Det Norske Veritas. Rules for classification of ships, Pt.3, Ch.1, Sec.13 Buckling Control.*. Hovik, Norway: DNV.

DNV GL, 2017. *Rules for classification: Ships — DNVGL-RU-SHIP Pt.3 Ch.6.* s.l.:DNV GL AS.

El-Sawy, K. M., Nazmy, A. S. & Martini, M. I., 2004. Elasto-plastic buckling of perforated plates under uniaxial compression. *Thin-Walled Structures,* Issue 42, pp. 1083-1101.

Fujikubo, M. & Yao, T., 1999. Elastic local buckling strength of stiffened plate considering plate/stiffener interaction and welding residual stress.. *Marine Structures,* Issue 12, pp. 543-56.

Gannon, L., Liu, Y., Pegg, N. & Smith, M., 2010. Effect of welding sequence on residual stress and distortion in flat-bar stiffened plates. *Marine Structures,* Issue 23, p. 385–404.

Garbatov, Y., Saad-Eldeen, S. & Guedes Soares, C., 2015. Hull girder ultimate strength assessment based on experimental resultsand the dimensional theory. *Engineering Structures,* Issue 100, pp. 742-750.

Gaspar, B., Teixeira, A. P., Guedes Soares, C. & Wang, G., 2011. Assessment of IACS-CSR implicit safety levels for buckling strength of stiffened panels for double hull tankers. *Marine Structures,* Volume 24, p. 478–502.

Guedes Soares, C. & Gordo, J., 1997. Design methods for stiffened plates under predominantly uniaxial compression. *Marine Structures,* Volume 10, p. 465–97.

Guedes Soares, C. & Soreide, T. H., 1983. Behaviour and design of stiffened plates under predominantly compressive loads.. *International Shipbuilding Progress,* Volume 30.

Hellgren, S., Hänninen, M., Valdez Banda, O. A. & Kujala, P., 2017. Modelling of a Cruise Shipbuilding Process for Analyzing the Effect of Organization on Production Efficiency. *Journal of Ship Production and Design,* Volume 32, pp. 101-121.

Hughes, O. F., 1983. *Ship structural design.* New York: Wiley.

Hughes, O., Ghosh, B. & Chen, Y., 2004. Improved prediction of simultaneous local and overall buckling of stiffened panels. *Thin-Walled Structures,* Issue 42, p. 827–850.

Komur, M. & Sönmez, M., 2008. Elastic buckling of rectangular plates under linearly varying in-plane normal load with a circular cutout. *Mechanics Research Communications,* Issue 35, pp. 361-371.

Leahu-Aluas, I. & Abed-Meraim, F., 2011. A proposed set of popular limit-point buckling benchmark problems. *Structural Engineering & Mechanics,* 38(6).

Mantere, H., 2007. *Strength analysis for the design of local ship structure in concept design. Master's Thesis.* s.l.:s.n.

Mathisen, K. M., 2016. *TMR 4190 Finite Element Methods In Structural Analysis. Lecture notes.*. s.l.:Norwegian University Of Science And Technology (NTNU).

Meyer Turku Media, 2016. *Meyer Turku enlarges investment package to 75 million euros with a new Steel Storage and Pre-Treatment Plant.* [Online] Available at: http://www.meyerturku.fi/en/meyerturku_com/media/presseticker/pressemitteilung_detailansicht_12627.jsp
[Accessed 8 Feb 2017].

Moen, C. & Schafer, B., 2009. Elastic buckling of thin plates with holes in compression or bending.;. *Thin-Walled Structures.*

Naar, H., 2006. *Ultimate Strength Of Hull Girder For Passenger Ships. Doctoral Dissertation.* Espoo: Helsinki University of Technology Department of Mechanical Engineering Ship Laboratory.

NAFEMS, 1992. *Introduction to Nonlinear Finite Element Analysis.* s.l.:NAFEMS Ltd..

NX Nastran 10, 2014. *Element Library Reference.* s.l.:s.n.

Ostapenko, A. & Yoo, D., 1988. *Tripping Of Asymmetrical Stiffeners Under Combined Loading. Final Report,* s.l.: U. S. Department of Transportation, Maritime Administration Office of Research and Development.

Paik, J. et al., 2009. *Committee III.1: Ultimate Strength. 17th International Ship and Offshore Structures Congress (ISSC).* SEOUL, ISSC.

Paik, J. K. & Kim, B. J., 2002. Ultimate strength formulations for stiffened panels under Combined axial load, in-plane bending and lateral pressure: a Benchmark study. *Thin-Walled Structures,* Volume 40, p. 45–83.

Paik, J. K. & Seo, J. K., 2009. Nonlinear finite element method models for ultimate strength analysis of steel stiffened-plate structures under combined biaxial compression and lateral pressure actions — PartII: Stiffened panels. *Thin-Walled Structures,* 47(8-9), pp. 998-1007.

Paik, J. K. & Thayamballi, A. K., 2003. *Ultimate Limit State Design of Steel-Plated Structures.* s.l.:John Wiley and Sons Ltd.

Paik, J. K., Thayamballi, A. K. & Lee, W. H., 1998. A numerical investigation of tripping. *Marine Structures,* Issue 11, p. 159–183.

Paik, J. & Thayamballi, A., 2000. Buckling strength of steel plating with elastically restrained edges.. *Thin-Walled Structures,* Issue 37, p. 27–55..

Pires, F., Lamb, T. & Souza, C., 2009. Shipbuilding performance benchmarking. *International Journal of Business Performance Management,* Issue 11.

Rahbar-Ranji, A., 2012. Elastic coupled buckling analysis in stiffened plates with T-bar stiffeners. *Mechanical Engineering Science,* Issue 227 (6), p. 1135–1149.

Remes, H., 2015. *Kul-24.4130 Shipyard Engineering.* s.l.:s.n.

Riks, E., 1979. An Incremental Approach to the Solution of Snapping and Buckling Problems. *International Journal of Solids and Structures,* Volume 15, p. 524–551.

Rockey, K. C., 1957. *Shear buckling of a web reinforced by vertical stiffeners and a central horizontal stiffener.* Zürich: s.n.

Romanoff, J., 2016. *Lecture notes. Kul-24.4140 Ship Dynamics.*. s.l.:Aalto University.

Serror, M. H., Hamed, A. N. & Mourad, S. A., 2016. Numerical study on buckling of steel web plates with openings. *Steel and Composite Structures,* Volume 22, pp. 1417-1443.

Serror, M. H., Hamed, A. N. & Mour, S. A., 2016. Numerical study on buckling of steel web plates with openings. *Steel and Composite Structures,* 22(6), pp. 1417-1443.

Shama, M., 2013. *Buckling of Ship Structures.* s.l.:Springe.

Shanmugam, N. E., Thevendran, V. & Tan, Y. H., 1999. Design formula for axially compressed perforated plates. *Thin-Walled Structures,* Issue 34.

Shufrin, I., Rabinovitch, O. & Eisenberger, M., 2008. Elastic nonlinear stability analysis of thin rectangular plates through a semi-analytical approach. *International Journal of Solids and Structures,* Volume 46, p. 2075–2092.

Smith, C. S. & Kirkwood, W., 1977. Influence of Initial Deformation and Residual Stresses in Inelastic Flexural Buckling of Stiffened Plates and Shells. *Steel Plated Structures,* pp. 838-864.

Sweedan, A. M. & El-Sawy, K. M., 2011. Elastic local buckling of perforated webs of steel cellular beam–column elements. *Journal of Constructional Steel Research,* pp. 1115-1127.

The MediTelegraph , 2016. *Korean shipyards invest In automation.* [Online] Available at: http://www.themeditelegraph.com/en/markets/regulation/2016/12/05/korean-

shipyards-invest-automation-HKHs476VgjTM03ryO0LgiJ/index.html
[Accessed 08 Feb 2017].

Timoshenko, S. & Gere, J., 1961. *Theory of elastic stability.*. 2nd ed. New York: McGraw-Hill Book Company.

Webb Institute of Naval Architecture, 1973. *Load Criteria For Ship Structural Design.* Washington, D.C.: s.n.

Yao, T. et al., 2006. *16th International Ship and Offshore Structures Congress. Report of Committee III. 1: Ultimate strength.* Southampton, UK, 16th ISSC.

Yong Hur, Weicheng Cui & Preben Terndrup Pedersen, 2004. Maintained ship hull xcgirxcder ultimate strength reliability considering corrosion and fatigue. *Marine Structures,* Issue 17, p. 91–123.

Zheng, G. & Hu, Y., 2005. Tripping of thin-walled stiffeners in the axially compressed stiffened panel with lateral pressure and end moments. *Thin-Walled Structures,* Issue 43, p. 789–799.

Appendix A: Sensitivity analysis for nonlinear finite element analysis

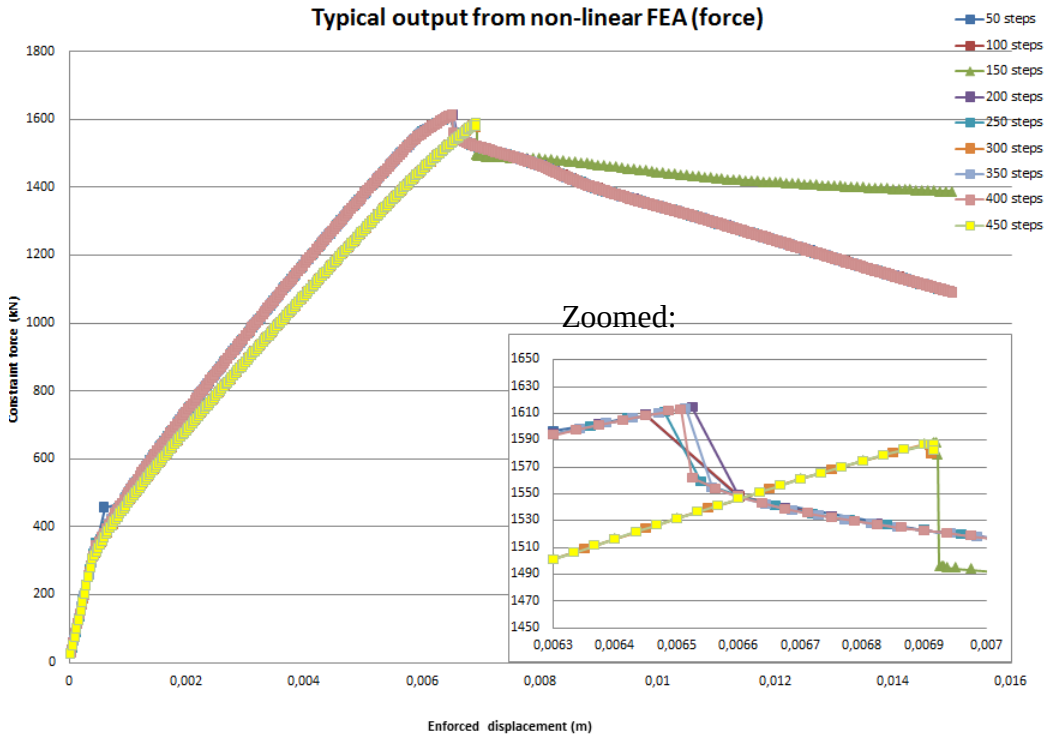

Figure A.1: Typical output from non-linear FEA in case of axial compression. Constraint force.

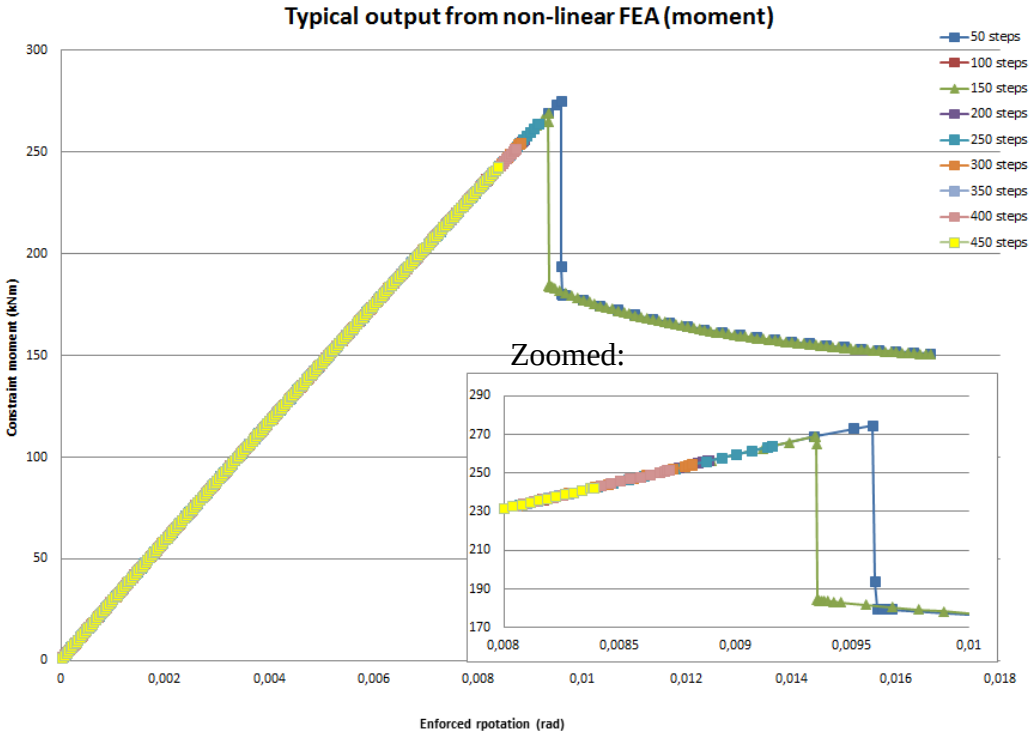

Figure A.2: Typical output from non-linear FEA in case of rotation in hogging. Constraint moment.

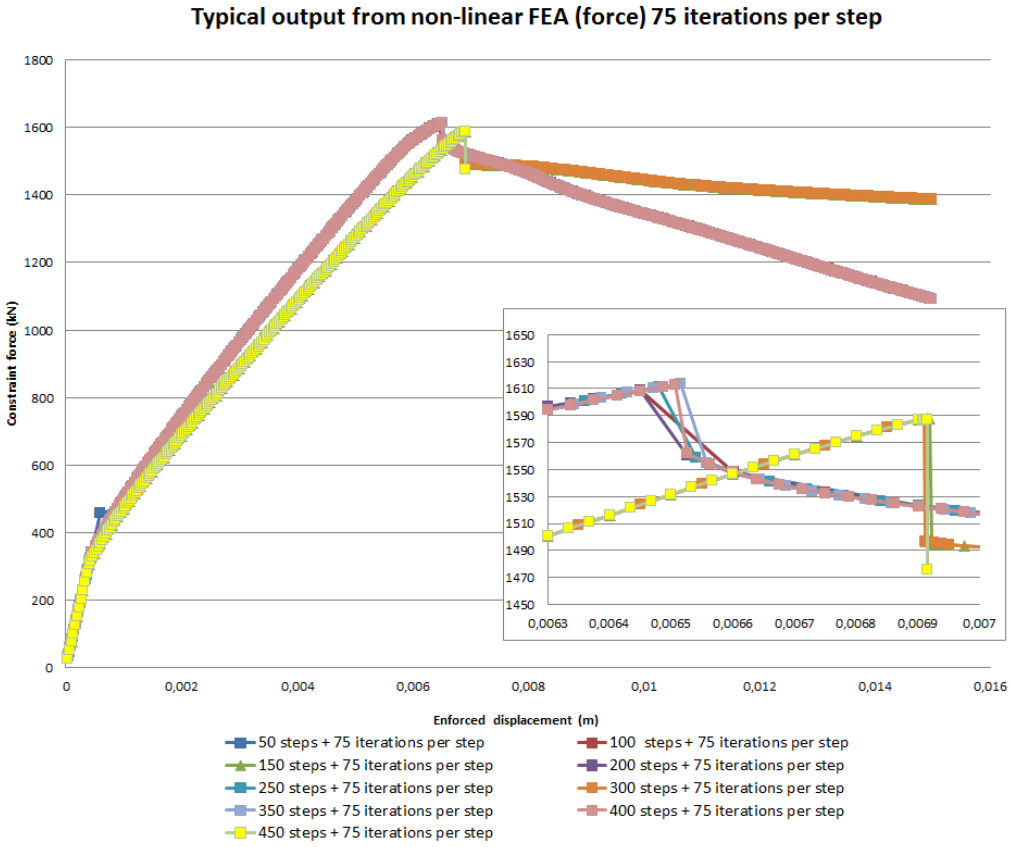

Figure A.3: Typical output from non-linear FEA in case of axial compression. Constraint force with 75 iterations per step.

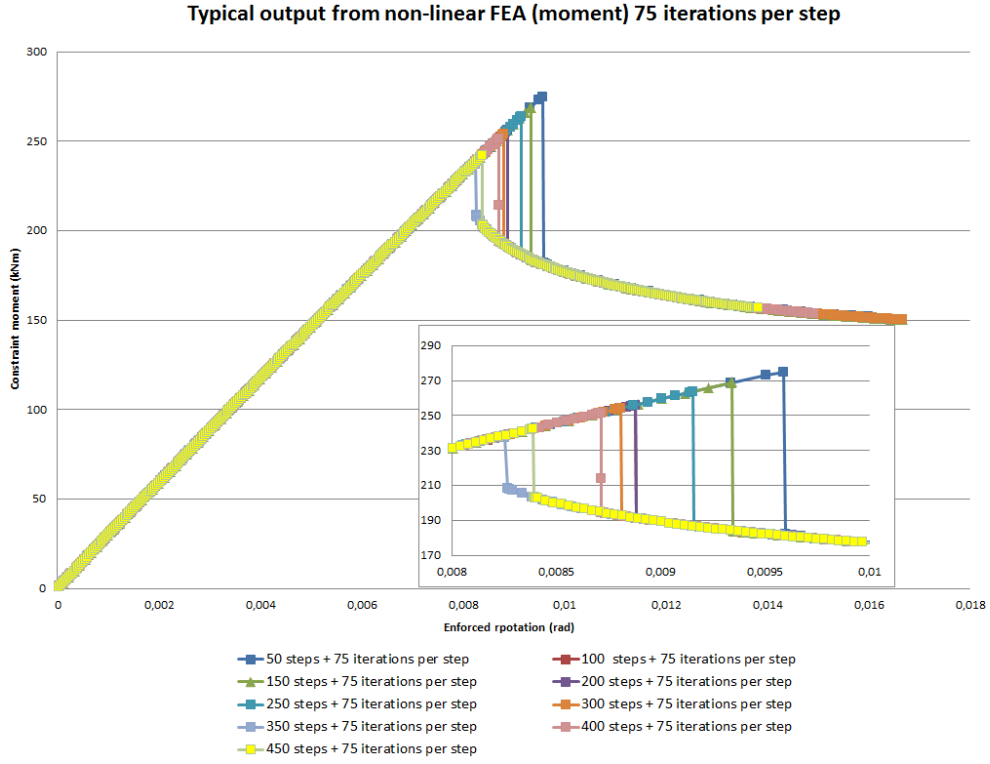

Figure A.4: Typical output from non-linear FEA in case of rotation in hogging. Constraint moment with 75 iterations per step.

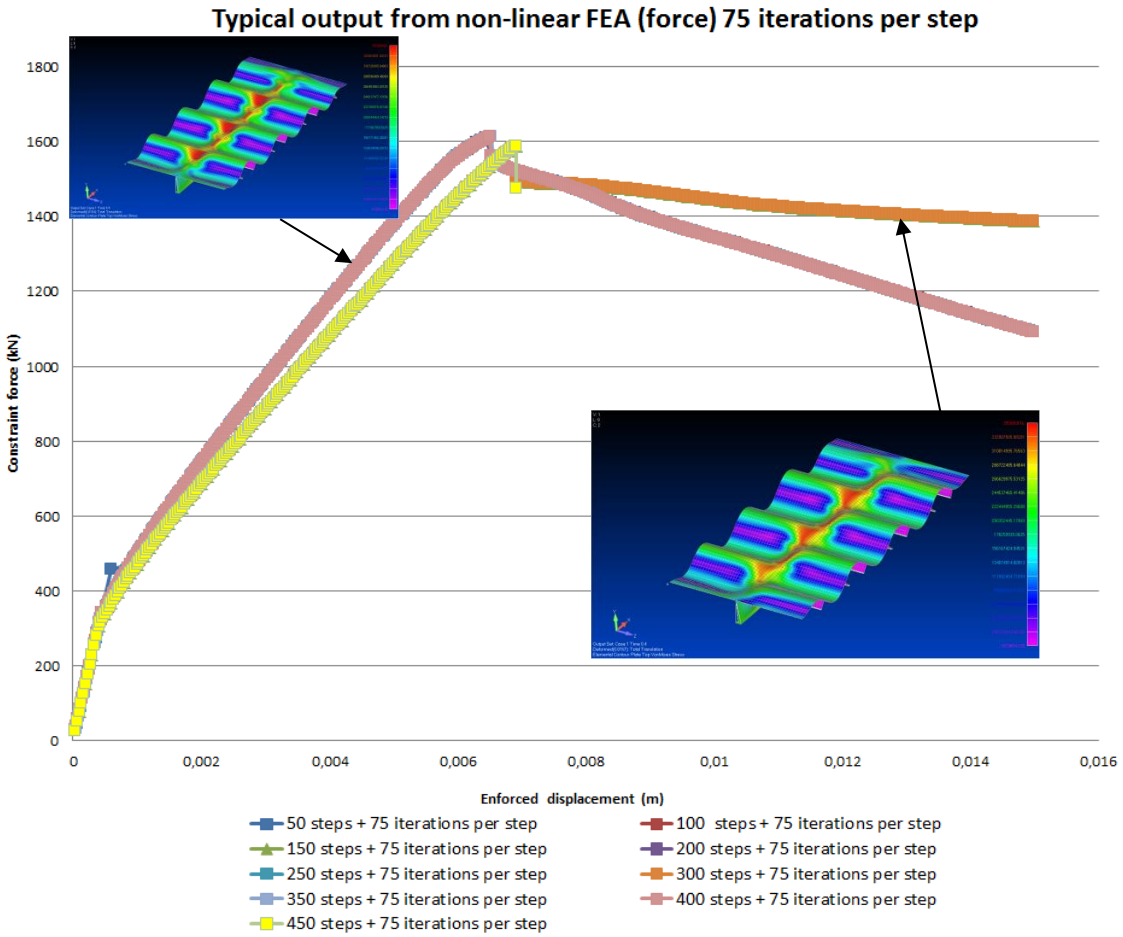

Figure A.5: Two different buckling modes of attached deck plate in in case of axial compression.

Table A.1: Sensitivity analysis for nonlinear FEA.

Applyed rotation on single edge (RAD)	Max. Moment Nm)	Max. Enforced rotation (m)	Difference (%)	Time increase	Time for analysis	**Applyed displacement (m)**	Max.Compressive force (N)	Max. Enforced displacement	Difference (%)	Time increase	Time for analysis	
0,016672844						**0,015**						
Analysis settings						Analysis settings						
50 steps	274632,72	0,009586885			0:08:28	50 steps	1608928,3	0,00645			0:06:12	
100 steps	256197,19	0,008883499	-7,92	0:02:37	0:11:05	100 steps	1608726,5	0,00645	0,00	0:04:27	0:10:39	
150 steps	268986,56	0,009340265	-2,64	0:10:22	0:18:50	150 steps	1587847,1	0,00691875	6,78	0:12:42	0:18:54	post buckling curve behaviour
200 steps	256147,09	0,008880895	-7,95	0:06:29	0:14:57	200 steps	1614688,9	0,006525	1,15	0:15:59	0:22:11	
250 steps	263816,16	0,009153391	-4,74	0:07:19	0:15:47	250 steps	1611309,3	0,00648	0,46	0:24:06	0:30:18	
300 steps	254192,17	0,008810556	-8,81	0:10:00	0:18:28	300 steps	1586895,3	0,006906251	6,61	0:09:23	0:15:35	post buckling curve behaviour
350 steps	239215,52	0,008278365	-15,81	0:12:47	0:21:15	350 steps	1613608,8	0,006514286	0,99	0:36:33	0:42:45	
400 steps	251492,88	0,008714167	-10,01	0:15:48	0:24:16	400 steps	1612837,1	0,00650625	0,86	0:34:00	0:40:12	
450 steps	242343,08	0,008388524	-14,29	0:16:41	0:25:09	450 steps	1587182	0,006914583	6,72	0:18:09	0:24:21	post buckling curve behaviour
50 steps + 25 iterations per step	274632,72	0,009586885	0,00	###########	0:08:20	50 steps + 25 iterations per step	1608928,3	0,00645	0,00	0:00:46	0:06:58	
100 steps 25 iterations per step	256197,19	0,008883499	-7,92	0:02:43	0:11:11	100 steps 25 iterations per step	1608726,5	0,00645	0,00	0:05:10	0:11:22	
150 steps + 25 iterations per step	268986,56	0,009340265	-2,64	0:10:23	0:18:51	150 steps + 25 iterations per step	1587847,1	0,00691875	6,78	0:11:52	0:18:04	post buckling curve behaviour
200 steps + 25 iterations per step	256147,09	0,008880895	-7,95	0:06:32	0:15:00	200 steps + 25 iterations per step	1614688,9	0,006525	1,15	0:15:07	0:21:19	
250 steps + 25 iterations per step	263816,16	0,009153391	-4,74	0:07:43	0:16:11	250 steps + 25 iterations per step	1611309,3	0,00648	0,46	0:23:14	0:29:26	
300 steps + 25 iterations per step	239215,52	0,008278365	-15,81	0:12:40	0:21:08	300 steps + 25 iterations per step	1586895,3	0,006906251	6,61	0:09:20	0:15:32	post buckling curve behaviour
350 steps + 25 iterations per step	239215,52	0,008278365	-15,81	0:13:26	0:21:54	350 steps + 25 iterations per step	1613608,8	0,006514286	0,99	0:38:52	0:45:04	
400 steps + 25 iterations per step	251492,88	0,008714167	-10,01	0:16:55	0:25:23	400 steps + 25 iterations per step	1612837,1	0,00650625	0,86	0:33:43	0:39:55	
450 steps + 25 iterations per step	242343,08	0,008388524	-14,29	0:15:47	0:24:15	450 steps + 25 iterations per step	1587182	0,006914583	6,72	0:19:02	0:25:14	post buckling curve behaviour
50 steps + 50 iterations per step	274632,72	0,009586885	0,00	0:00:08	0:08:36	50 steps + 50 iterations per step	1608928,3	0,00645	0,00	0:00:44	0:06:56	
100 steps + 50 iterations per step	256107,83	0,008878289	-7,98	0:13:23	0:21:51	100 steps + 50 iterations per step	1608726,5	0,00645	0,00	0:05:01	0:11:13	
150 steps + 50 iterations per step	268986,56	0,009340265	-2,64	0:19:49	0:28:17	150 steps + 50 iterations per step	1587847,1	0,00691875	6,78	0:12:08	0:18:20	post buckling curve behaviour
200 steps + 50 iterations per step	256108,25	0,008878289	-7,98	0:22:10	0:30:38	200 steps + 50 iterations per step	1609088,5	0,00645	0,00	0:16:06	0:22:18	
250 steps + 50 iterations per step	263816,16	0,009153391	-4,74	0:21:52	0:30:20	250 steps + 50 iterations per step	1611309,3	0,00648	0,46	0:19:40	0:25:52	
300 steps + 50 iterations per step	254159,94	0,008808818	-8,83	0:49:50	0:58:18	300 steps + 50 iterations per step	1586895,3	0,006906251	6,61	0:27:55	0:34:07	post buckling curve behaviour
350 steps + 50 iterations per step	237222,78	0,008253058	-16,16	0:41:17	0:49:45	350 steps + 50 iterations per step	1613608,8	0,006514286	0,99	0:28:49	0:35:01	
400 steps + 50 iterations per step	251467,81	0,008712863	-10,03	0:52:33	1:01:01	400 steps + 50 iterations per step	1612837,1	0,00650625	0,86	0:34:18	0:40:30	
450 steps + 50 iterations per step	242318,8	0,008388524	-14,29	0:22:18	0:30:46	450 steps + 50 iterations per step	1587182	0,006914583	6,72	0:22:03	0:28:15	post buckling curve behaviour
50 steps + 75 iterations per step	274632,72	0,009586885	0,00	###########	0:08:23	50 steps + 75 iterations per step	1608928,3	0,00645	0,00	0:00:15	0:06:27	
100 steps + 75 iterations per step	256107,83	0,008878289	-7,98	0:13:48	0:22:16	100 steps + 75 iterations per step	1608726,5	0,00645	0,00	0:04:17	0:10:29	
150 steps + 75 iterations per step	268986,56	0,009340265	-2,64	0:23:43	0:32:11	150 steps + 75 iterations per step	1587847,1	0,00691875	6,78	0:11:07	0:17:19	post buckling curve behaviour
200 steps + 75 iterations per step	256108,25	0,008878289	-7,98	0:23:44	0:32:12	200 steps + 75 iterations per step	1609088,5	0,00645	0,00	0:15:58	0:22:10	
250 steps + 75 iterations per step	263816,16	0,009153391	-4,74	0:24:23	0:32:51	250 steps + 75 iterations per step	1611309,3	0,00648	0,46	0:17:45	0:23:57	
300 steps + 75 iterations per step	254159,94	0,008808818	-8,83	1:17:58	1:26:26	300 steps + 75 iterations per step	1586895,3	0,006906251	6,61	0:27:55	0:34:07	post buckling curve behaviour
350 steps + 75 iterations per step	237222,78	0,008253058	-16,16	0:41:11	0:49:39	350 steps + 75 iterations per step	1613608,8	0,006514286	0,99	0:29:00	0:35:12	
400 steps + 75 iterations per step	251467,81	0,008712863	-10,03	2:26:07	2:34:35	400 steps + 75 iterations per step	1611478,4	0,0064875	0,58	0:40:39	0:46:51	
450 steps + 75 iterations per step	242318,28	0,008387367	-14,30	1:13:31	1:21:59	450 steps + 75 iterations per step	1587182	0,006914583	6,72	0:54:31	1:00:43	post buckling curve behaviour
1000 steps + 75 iterations per step CON	252658,63	0,008755327	-9,50	1:11:05	1:19:33	1000 steps + 75 iterations per step CO	1612244,6	0,00651	0,92	1:47:14	1:53:26	
						900 steps + 75 iterations per step CON	1586880,1	0,006911979	6,68			

* the analysis marked with red color have crashed, i.e. no post buckling behavior is recorded
post buckling curve behavior - sign shows that the particular run has different ultimate curve compared to the runs with the same number of iterations per step

Appendix B: Moment diagrams

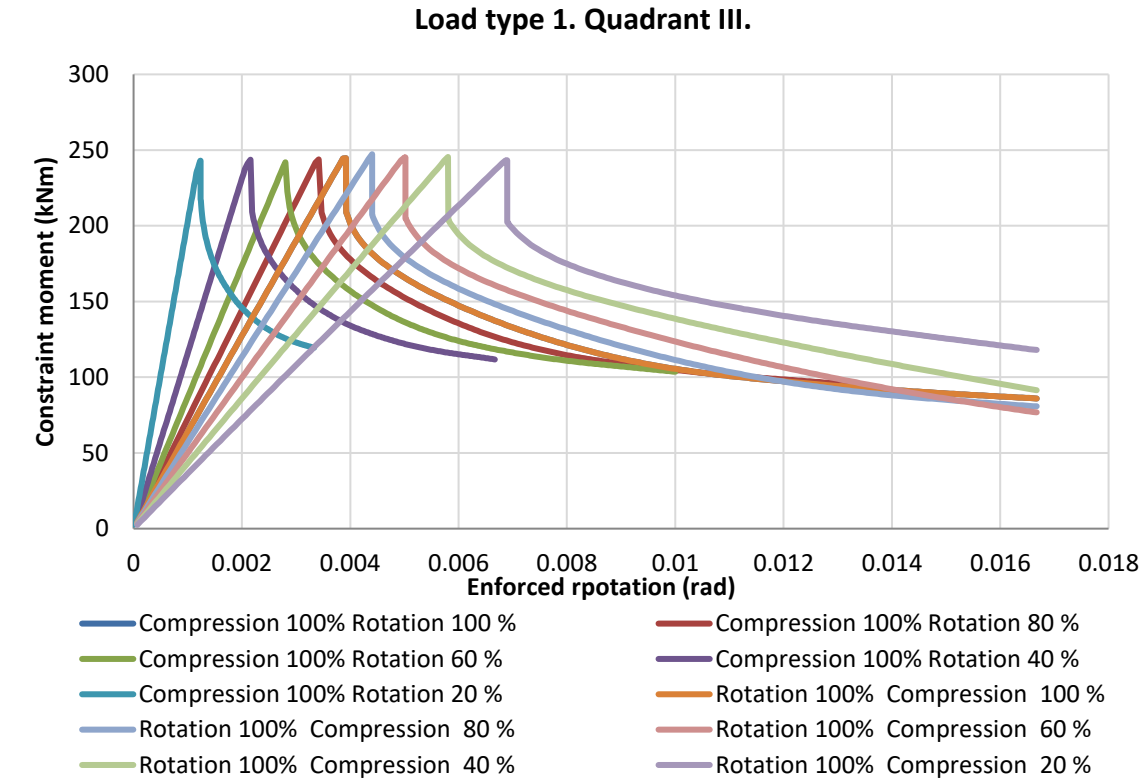

Figure B.1: Quadrant III: output from non-linear FEA (Constraint moment).

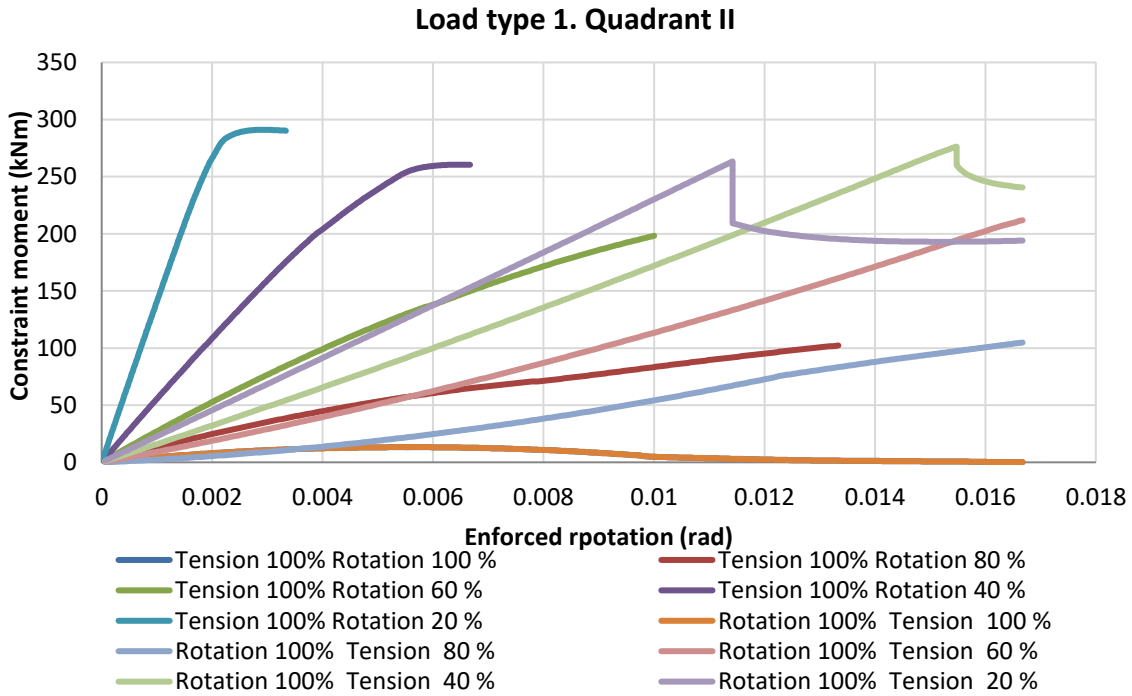

Figure B.2: Quadrant II: output from non-linear FEA (Constraint moment).

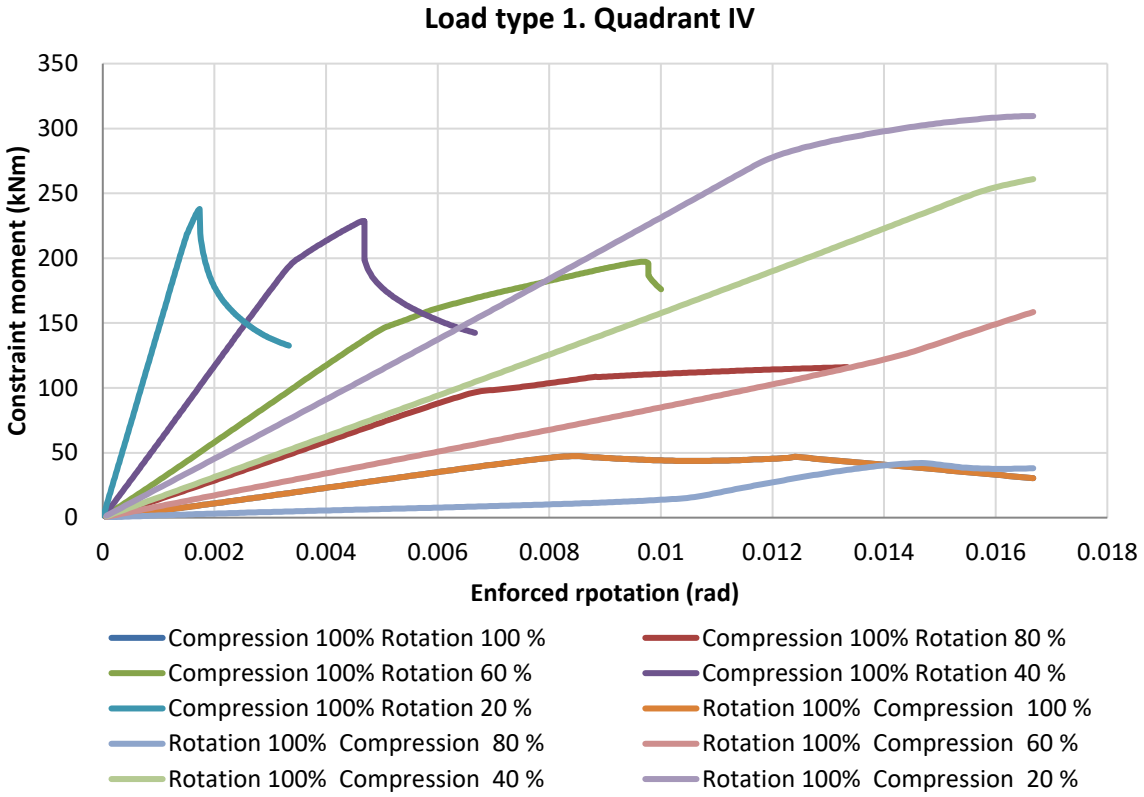

Figure B.3: Quadrant IV: output from non-linear FEA (Constraint moment).

Appendix C: Post buckling behavior and ULS

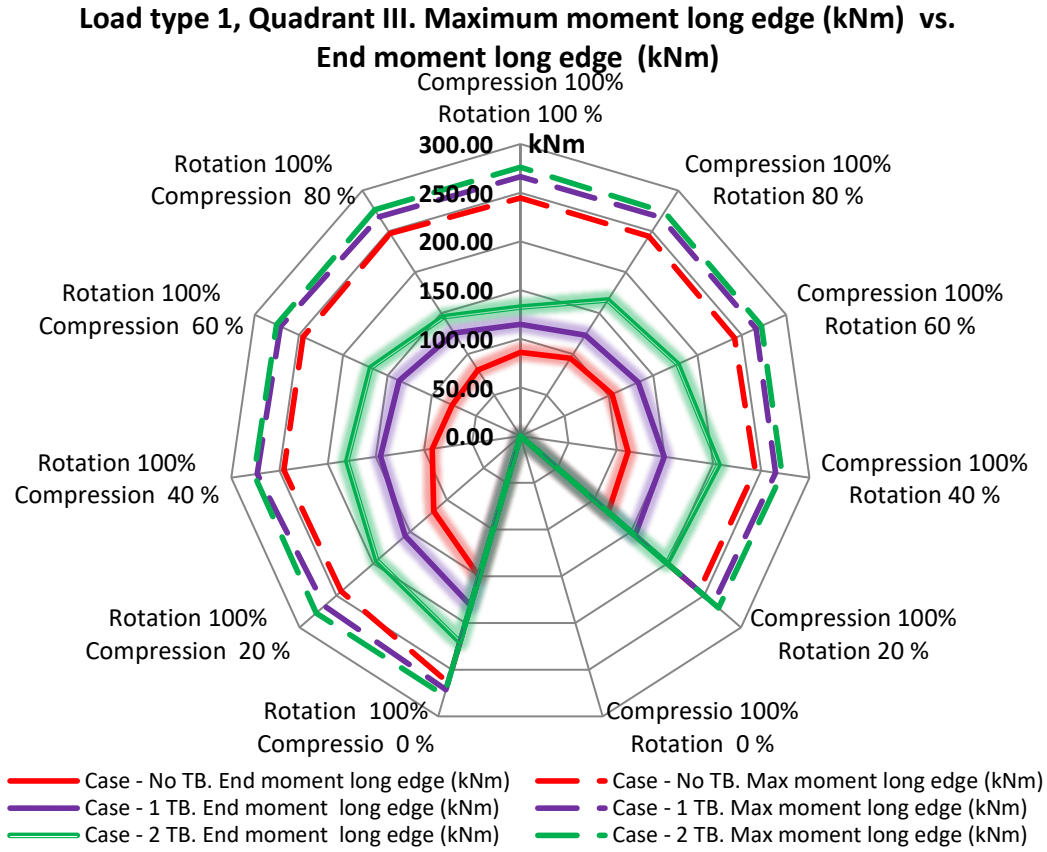

Figure C.1: Load type 1, Quadrant III. Maximum (ULS) and End moments at failure (long) edge.

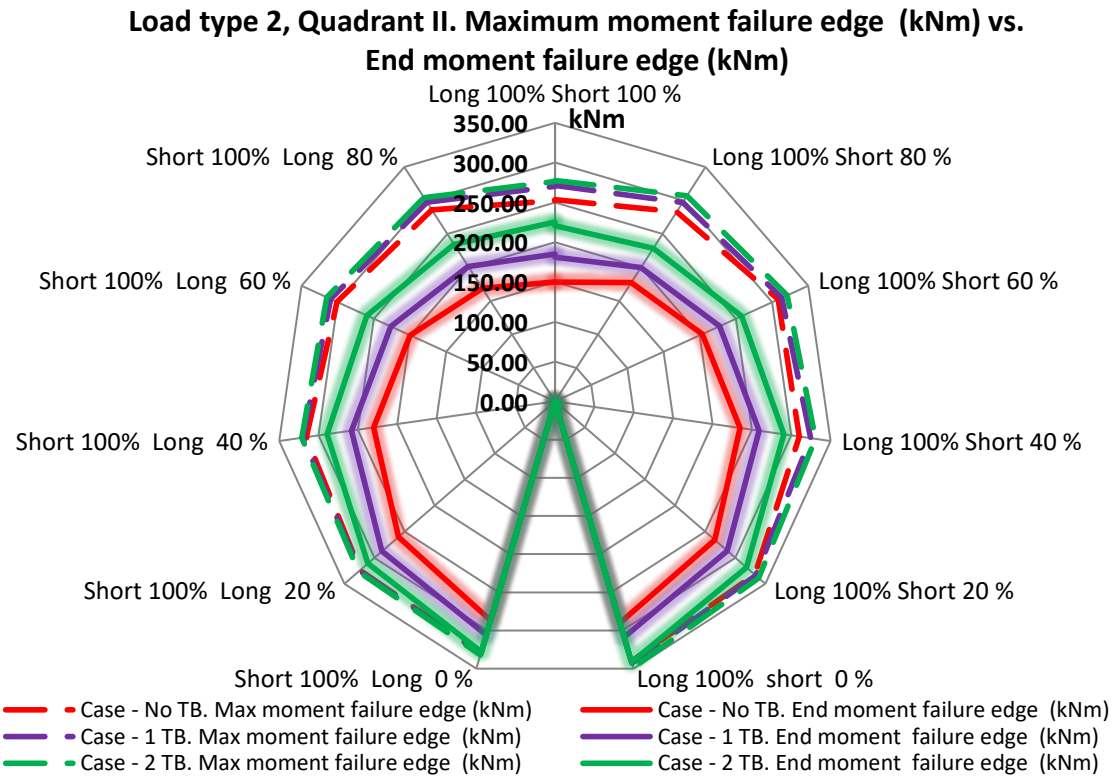

Figure C.2: Load type 2, Quadrant II. Maximum (ULS) and End moments at failure (long/short) edge.

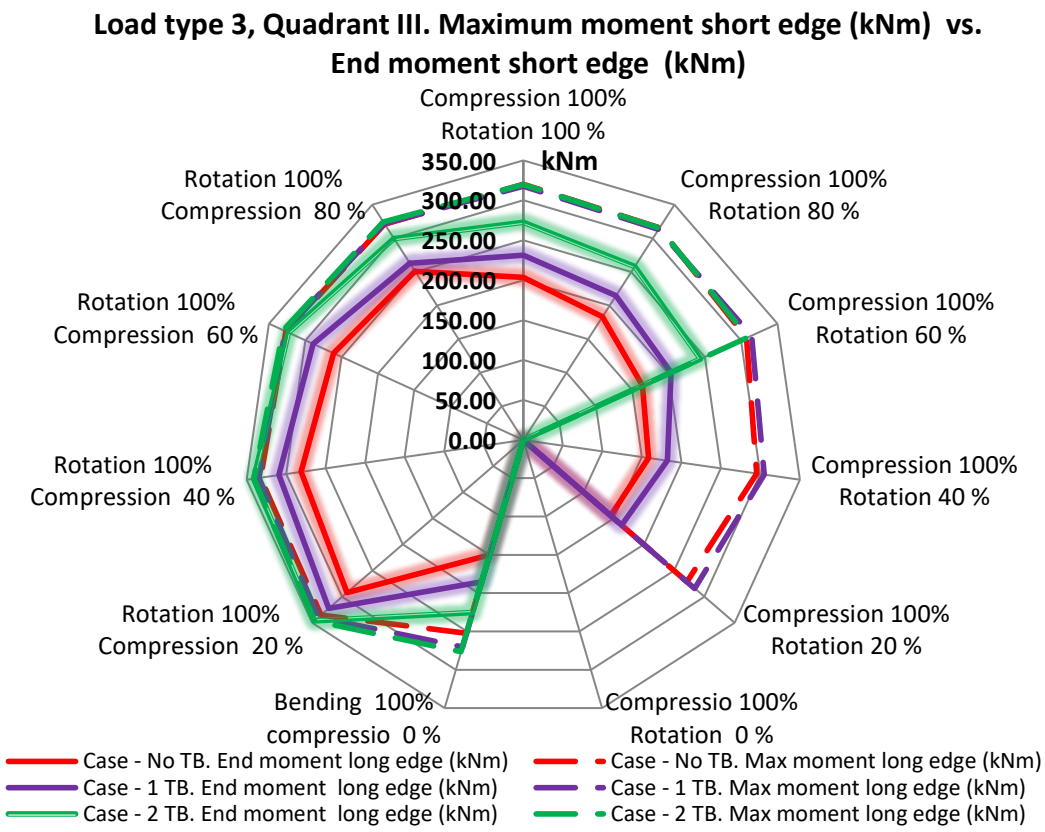

Figure C.3: Load type 3, Quadrant III. Maximum (ULS) and End moments at failure (short) edge.

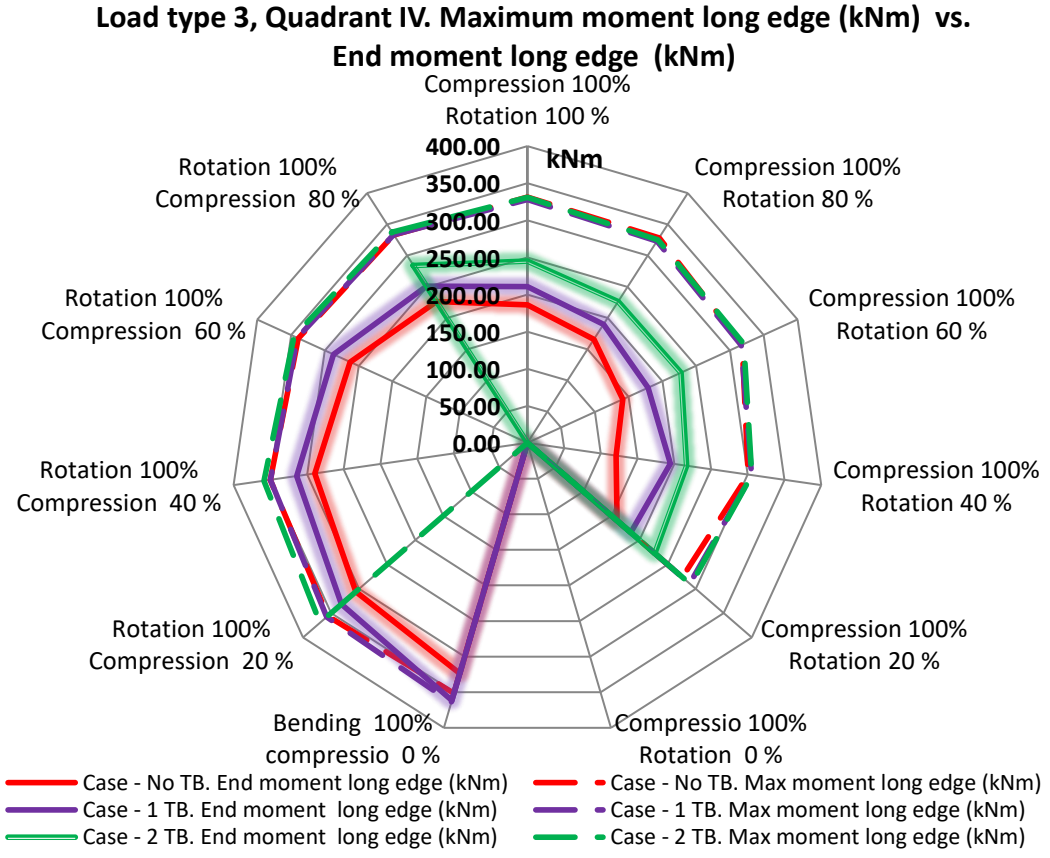

Figure C.4: Load type 3, Quadrant IV. Maximum (ULS) and End moments at failure (long) edge.

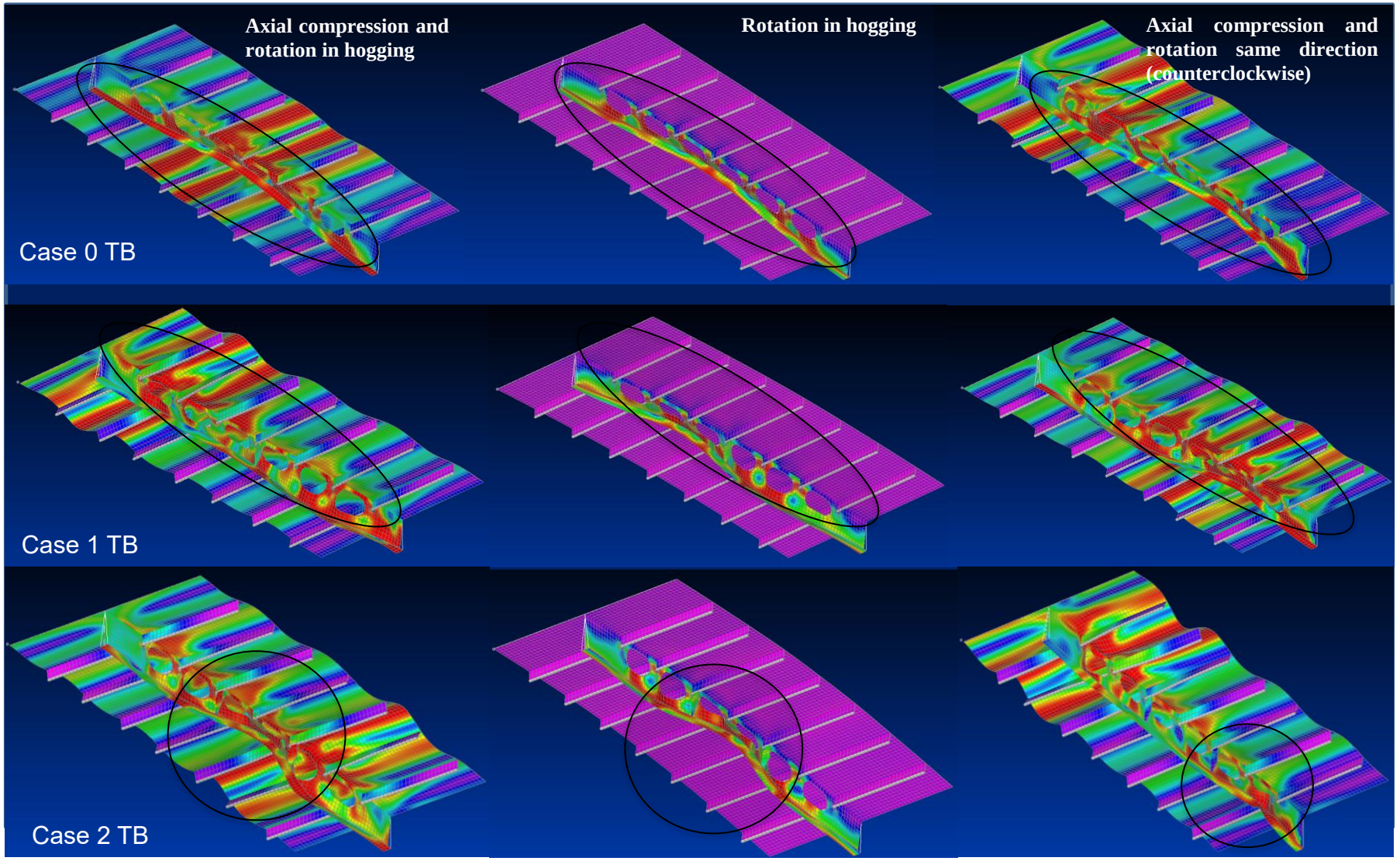

Figure C.5: Buckling modes comparison 0, 1 and 2 TB.

Appendix D: Increase in capacity with wider flange

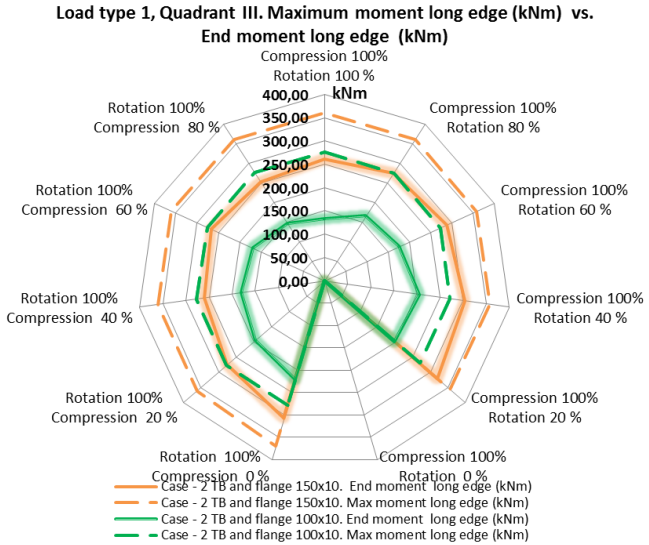

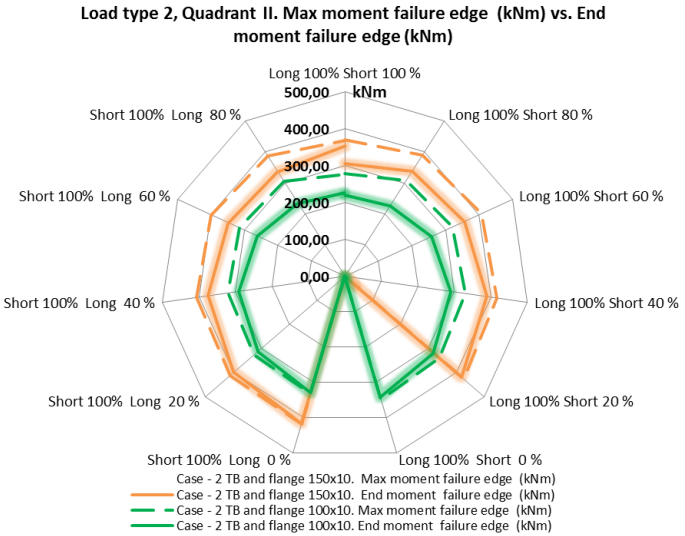

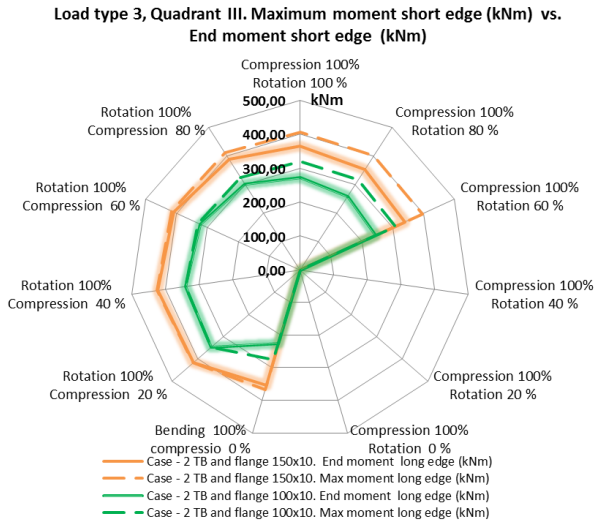

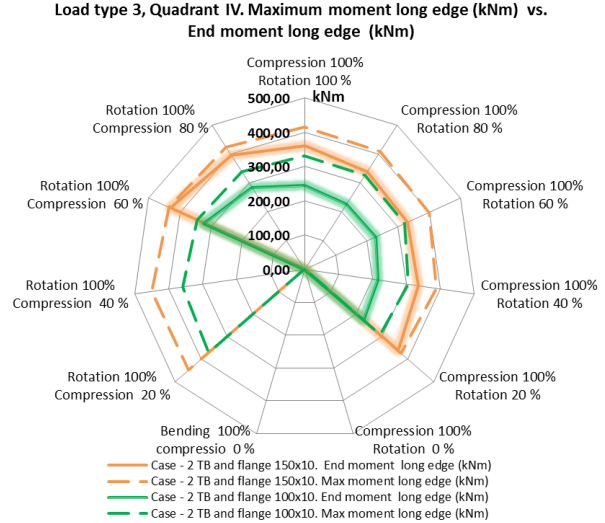

Figure D.1: ULS and post buckling criteria for cases with 2 TB and flange 100x10 & flange 150x10.

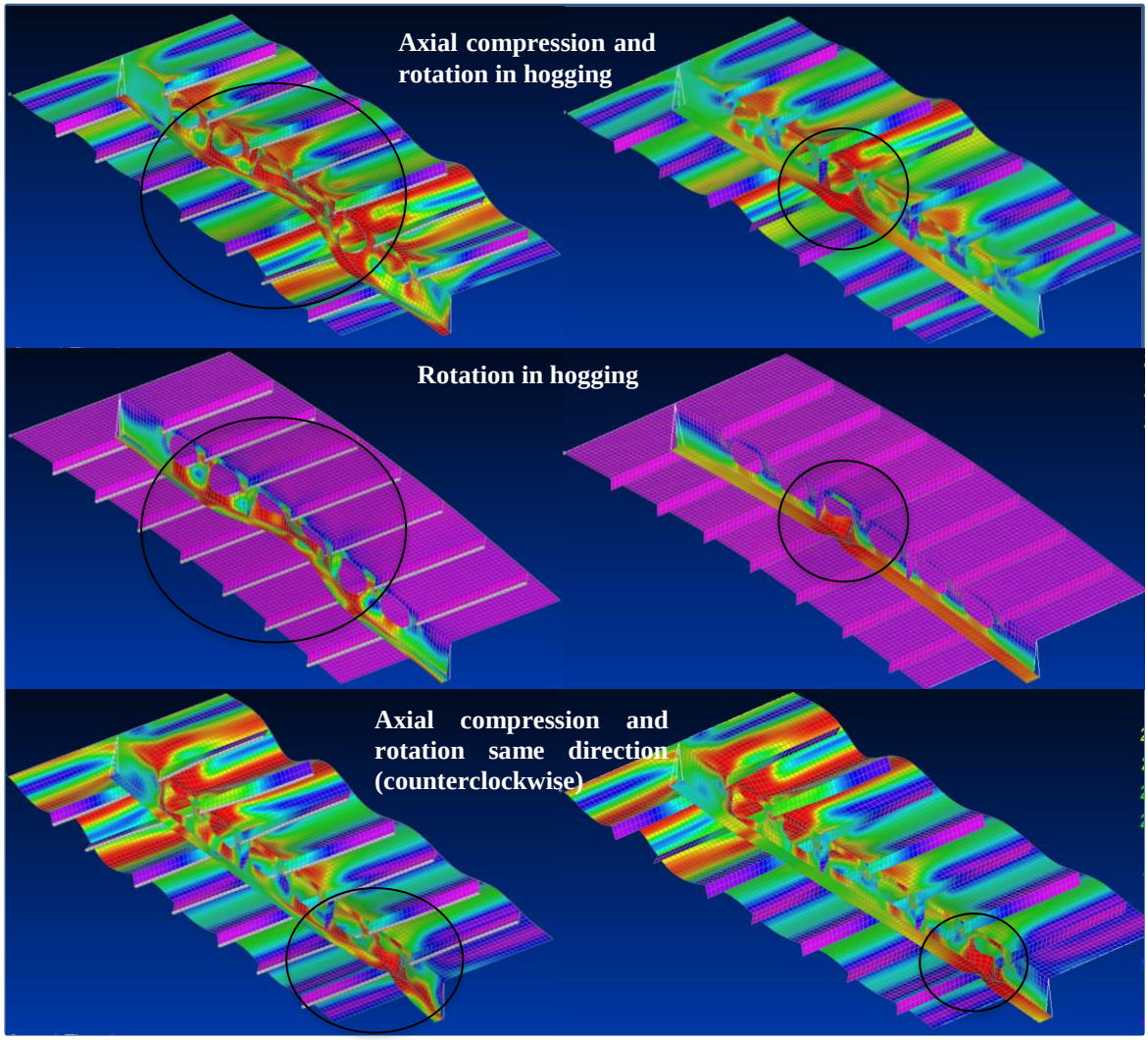

Figure D.2: Buckling modes left - flange 100x10mm, right- flange 150x10mm.